THE PREDICTION OF THE OUTERMOST TRAJECTORY OF MEDIA IN A GRINDING MILL FOR LIFTER BARS WITH ROUNDED OR WORN PROFILES

ANDREW L. MILNER

Thesis presented for partial fulfilment for the degree of

MASTER OF SCIENCE

In the Department of Mechanical Engineering

UNIVERSITY OF CAPE TOWN

November 1996

I, Andrew Leigh Milner, submit this thesis in part fulfilment of the requirements for the degree of Masters of Science in Mechanical Engineering. I claim that this is my original work and has not been submitted in this or any other form for a degree at any university.

ACKNOWLEDGEMENTS

Thanks are due to :

MINTEK for their financial support.

Dr Adrian Hinde for his support during the project.

The staff of the workshop in the Department of Mechanical Engineering for constructing the experimental equipment.

Mark Gelman for his support, ideas and help with various problems encountered during the theoretical derivations.

My Supervisor Prof. G.N. Nurick who has assisted and advised me during the thesis.

ABSTRACT

This thesis presents the analysis of the path of a ball on the inside of a ball mill for lifter bars with rounded or worn profiles. The model predicts the response of a single ball with particular reference to the balls trajectory after departure from the lifter bar and incorporates the effect of friction, mill rotational speed, lifter height as well as different lifter bar profiles. The out of plane travel of the particles are ignored and hence the system is reduced to a two dimensional problem. A set of experiments were performed on a model perspex mill in order to obtain data by which the theory could be compared.

The lifter bar is analysed using a parabolic expression which allows the shape to be changed to model various stages of lifter wear. Two possible formulations are investigated in determining the motion of the particle on the lifter bar. The first formulation assumes the ball to roll on the lifter bar until a limiting friction is reached after which the ball will slide along the lifter. The second formulation considers the ball to have a pure sliding motion on the lifter.

A set of governing equations are derived for each of the cases. These equations are solved by using a fourth order Runga Kutta numerical solution scheme. Both formulations are solved by a computer simulation program coded in Visual Basic.

Experiments were done to validate the theoretical models and to gain information on how the various operating variables effect the charge motion in the mill for a range of mill filling ratios. Three filling ratios of 40 %, 10 % and one layer of balls covering the base of the mill was investigated. The single layer case was incorporated to neglect the effect of charge motion and obtain results by which the theory could be compared. The power draw of the mill for the various operating conditions was also investigated.

The sliding model showed a good correlation with the experimental results whereas the sliding/rolling model over predicted the trajectory heights.

The experimental results illustrate that as lifter wear increases the impact angle of the outer layer of balls decreases and as the mill speed is increased the impact angle increases. The percentage fill is also found to influence the outer trajectories as a mill with a larger percentage fill has a larger charge pressure which leads to higher trajectories.

The sliding simulation illustrates that the departure angle and impact angle are a function of lifter shape, mill speed and friction conditions in the mill. The coefficient of friction has a small effect on the charge motion in relation to the shape of the lifter bar which caused a much larger variation in the charge shape. An increase in mill speed strongly influences the charge trajectories.

NOMENCLATURE

General variables

$\|A\|$	The modulus of the A value
m	Mass of the ball (kg)
g	Gravitational acceleration (9.8 m/s^2)
A	Variable defining the shape of the lifter
C	Variable defining the shape of the lifter
R	Mill radius (m)
Ω	Mill rotational speed (rad/s)
r	Distance from ball centre to mill centre (m)
θ	Angular position of the ball on the lifter (rad)
$\dot{\theta}$	Angular velocity (rad/s)
$\ddot{\theta}$	Angular acceleration of the ball (rad/s^2)
N_t	Normal force at the mill wall (N) (tangent to the lifter face)
N_n	Normal force at the lifter face (N) (normal to the lifter face)
Ω	Angular velocity of the mill (rad/s)
μ	Static friction coefficient
μ	Kinetic friction coefficient
ρ	Instantaneous radius of rotation of the ball (m)
f	Friction force at the base of the ball (N)
a	Ball radius (m)
β	Angular position of the ball from the horizontal (rad)
γ	The angular position of the lifter tangent at the contact point from the horizontal (rad)
ϕ	The mill rotation angle
(X_c, Y_c)	Centre of the ball (in global co-ordinates)
(x_c, y_c)	Centre of the ball (in local co-ordinates)
t_p	Time from departure
$a_{tangential}$	$\rho\ddot{\theta}$
a_{normal}	$\rho\dot{\theta}^2$
φ	Angular acceleration of the ball about its centre

Subscripts

0	Neutral Position (Lifter bar base is horizontal)
t	Time dependant
te	Equilibrium point
td	Departure point
i	Impact point
b	Contact point on the lifter
c	Centre of the ball
x	Local co-ordinate system
X	Global co-ordinate system

xd	x component in the local co-ordinate system at the departure point.
yd	y component in the local co-ordinate system at the departure point
r	Resultant
n	Normal component at the contact surface between the ball and the lifter bar
ne	Normal component at the equilibrium point

GLOSSARY

Shoulder of the charge	:	The uppermost part of the charge at the point of departure
Toe of charge	:	The lowest part of the charge onto which the cateracting balls impact
Critical Speed	:	The speed at which the gravitational and centrifugal forces acting on a point at the top of the mill just balance, so a small particle would theoretically centrifuge at this speed
ROM	:	Run of mine
- 25 μm	:	Particles smaller than 25 microns
Free surface	:	Surface above the cascading part of the load

CONTENTS

LIST OF ILLUSTRATIONS

Figures

1. INTRODUCTION

The South African Gold Mining industry grinds 110 Mt of ore annually to a fineness that permits a high percentage of the gold to be extracted by the cyanide-leaching process. At the nominal figure of 30 kW hours of electrical energy consumed per ton of material smaller than 75 μm produced, 2.4 million MW hours of electrical energy are utilised at a cost of 70 million rands per annum [1].In order to achieve this crushing (communition) of ore, milling plants consisting of tube mills approximately 8 meters in length and 5 meters in diameter are used. The mills are charged with steel balls and the rotary action of the mill causes the balls to grind the ore to the required particle size. Due to the extensive wear on the mill liner by this crushing action, the operating costs of the mill are substantial. It is therefore essential to optimise the crushing performance of these mills.

Gold occurs mainly in very hard, abrasive quartzitic ores. This together with the high mill speeds that are employed cause the mill liners to wear rapidly. The gross overall average wear of liners in the gold mines is 85 kg per day per mill. This results in an annual usage of 20 Kt of metal at a cost of R40 million per annum [2]. Besides the material costs, mill downtime can reduce production and cost South African mines millions of rands annually.

The South-African gold mines have in the past used a combination of primary crushers followed by rotary mills. The new trend is to use only run of mine (ROM) mills. These are large single stage mills that are fed with rock directly from underground. The ROM mills have the advantage that a lower capital investment is required and also have lower running costs. The milling also takes place in one process whereas previous milling circuits first required primary crushing and then size reduction by the secondary mills.

The ROM mills used in South Africa are horizontally aligned rotating cylinders with lengths in the range of 1.5 - 2 times the diameter. The mill is lined with mill liners (backing plates bolted onto the inside of the mill wall) to protect the outer shell. Lifter

bars are mounted on top of the liners. The lifter bars enhance the lifting effect of the system and reduce slip thereby protecting the liners from wear. The rock is fed into the mill via a feed hole and is crushed into a sandy mixture (mixture of water and very fine sand).

The ore is lifted up one side of the mill due to the rotating action. The extent of this lifting action is dependant on the friction between the wall and the balls and the shape of the lifter bars. Two types of motion may take place inside the mill due to this lifting effect. The balls may slide or roll over one another causing a cascading motion or the balls can leave the charge and follow a parabolic flight trajectory causing a cataracting motion (Figure 1.1). Cataracting is required for coarser grinding and cascading for finer grinding.

Three types of grinding action break down the ore. Impact crushing is caused by the cataracting balls landing on the toe of the charge whereas attrition and abrasion takes place in the *en masse* region of the charge due to the cascading effect. The feed rate is set to obtain a final product that produces 80 % of the particles to be smaller than 75 μm. This size particle allows for optimum bonding of the gold during the cyanide leaching process. Hydrocyclones are generally used to classify the final product into various size categories. The milling circuit allows for the oversized particles to be returned to the feed end of the mill for further crushing.

It has been reported by Bradley et al [3] that crushing tests performed on gold bearing Witwatersrand quartzite resulted in the usage of 14 kWh of electrical energy to crush one ton of rock to obtain 72% of the particles to be smaller than 75μm in size. The overall average energy required to obtain the same average grind from the mills on the gold mines is 20.2 kWh per ton. This illustrates that mills may (depending on size distribution) require approximately 40% more energy than is required for crushing tests. This illustrates the need for much improvement on the mill designs.

The life and the grinding performance of the mill are highly dependent on the shape of lifter bars. The degree of slip that exists between the milling media and the mill liner

dictates this liner life and by reducing the amount of slip that occurs the life of the liner can be extended and costs of replacement reduced. Slip can be reduced significantly by the use of optimised lifter bars. These optimised shapes should incorporate a strong keying-in action (the rock is locked into position due to the geometry of the bar) on the mill liners.

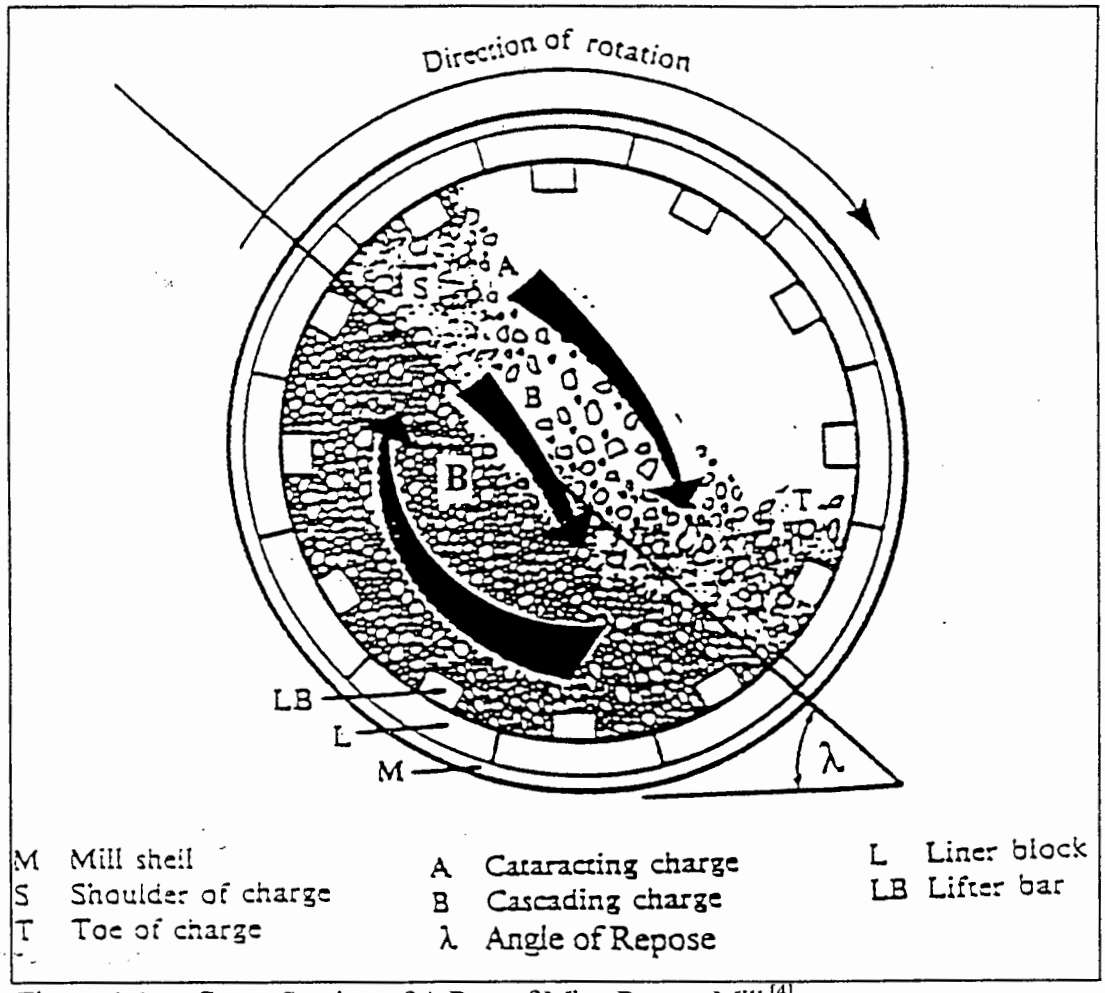

Figure 1.1 : Cross-Section of A Run of Mine Rotary Mill [4].

The wear rate of the liners are affected by the geometric configurations of the various types of lifters as well as the material from which the lifters are manufactured [2]. Liners which incorporate lifter bars can reduce liner wear and increase the life of the liners by 4 to 5 times. The liners are generally produced from white iron or rubber, depending on the applications and designs of the mills. White iron is highly wear resistant to

sliding loads but is also highly wear susceptible to impact loads. Rubber on the other hand has very good impact characteristic but wears rapidly due to sliding effects.

It has also been established that lifter bars of different profiles can influence the charge motion in the mill [5]. This could allow lifter bars to be designed that would optimise the charge motion in order to achieve maximum crushing effectiveness. The optimum charge motion is dependant on various parameters for various applications. Some of the variables involved would be the type and hardness of the ore, the degree of required reduction and the amount of water added to the charge. This leads to the uncertainty regarding the effects of lifter bar geometry on milling performance.

To maximise the mill throughput, a liner that produces the most favourable charge motion for rapid reduction of the ore is needed. Due to the lower grades of ore that are presently being mined the mill feed rate has been increased to maintain similar gold output. The increased feed rates lead to coarser grinds which lead to larger fractions of gold being lost to the dumps. The mills therefore have to run at an optimum efficiency to produce an optimum fineness of grind.

As a consequence of the expense and difficulties encountered in full scale investigations, it is imperative to establish a sound theoretical basis and an experimental back-up on model mills. Due to the very aggressive environment in a working mill it is difficult to obtain useful information of the motion of the rock in the mill. Model mills can be used to determine results over a large range of operating conditions. The scaling factor in experimental models is still very much unknown and results obtained from the experimental models can only be used as comparative guidelines [6].

Much work has been performed during this century on the effect of specific types of lifter bars on the performance of various mills. All this work has been experimental and no effort was made before the 1980's to determine a mathematical model to predict the effect of lifter bars on the charge motion in rotary mills. Nates[7] attempted to model a ball on the inside of a rotating cylinder while Powell[4] created a theoretical model to predict the outermost trajectories of balls in a mill with lifter bars with straight leading

edges. Von Bentheim[8] furthered this work by developing a model to predict the motion of a ball in a mill with a wave liner.

This thesis extends the work reported by Nates, von Bentheim and Powell and establishes a two dimensional theoretical model for a single ball inside a rotating mill with arbitrary shaped liners. This allows for the consideration of wear on the lifter bars as well as the opportunity to determine whether rounded lifter bars have an advantage over straight faced lifter bars. The procedure followed in this thesis consists of deriving a theoretical model to predict the ball's path and experimental work in a perspex mill. The experimental work included the testing of six lifter shapes.

A series of mathematical formulae relating to the motion of the ball will be used to derive a theoretical model to predict the path of the ball in the mill. The model will predict the path of the ball on the lifter as well as the parabolic trajectory of the ball after it has left the lifter. A set of results (ball paths) is obtained for every set of the six lifters groups. By changing the operating variables (mill speed, ball size, mill diameter and coefficient of friction) for each liner group, the paths can be monitored over a range of operating conditions. Each set is fitted to the perspex mill with clear side panels. The motion of the charge in the mill is analysed from the filmed results obtained using a video camera. The objective is to correlate the theoretical predictions and the experimental observations.

In order to achieve these objectives, the thesis develops a mathematical formulation to predict the path of one particle on the inside of a rotating mill with varying shaped lifter bars. The governing equations are solved numerically and the results are presented and discussed. An investigation has been included on how the various operating conditions affect the experimental results and the mathematical model was used to gain a deeper insight into the observed effects. Recommendations have been included for further development of the theoretical analysis..

2. LITERATURE SURVEY

The papers investigated in this survey deal with the development of the mechanics of tumbling ball mills and the effect of the various parameters on the crushing efficiency and ball behaviour. Various aspects of ball milling have been included in the survey, which are divided into two general sections.

The first set of papers deal with the history of the development of the general model for ball mills. This includes the investigation of the ball motion in the mill by considering the rotational paths in the load. It also illustrates the types of motion of the various layers of balls and how this motion effects the crushing action and power consumption in the mill. An investigation is also undertaken of the flow characteristics of the en masse region i.e. charge slippage, charge surge and radial segregation of the load. These principles give a better idea of the charge motion, charge size distribution and of the effect of forces such as cohesion and hence charge pressure on the load.

The second topic covered is that of mill design and specifically lifter bar design on the lifting action, crushing effectiveness and power consumption of the mill. The lifter bars are essential in prolonging the life of the mill liners thereby saving on maintenance and replacement costs.

A short review of all the papers is presented with the most significant observations detailed where necessary at the end of each summary.

2.1 REVIEW OF GENERAL BALL MILL THEORY

2.1.1 The theory of the tube mill [9]. (H.A.White 1905)

White's work was based on the assumption that the balls in the ball mill are keyed into (trapped in) specific layers. Each layer consists of a set of balls which remain within the same layer for every rotation.

A simple experimental rig was used which consisted of various tubes of up to nine inches (229 mm) in diameter with a glass plate on each end and a water inlet and drainage hole to add water to the tube.

A "circle of reference" representing the path followed by the centres of the outermost balls was used. The balls travel up the side of the rotating tube wall until the gravitational force of the balls exceeds the centrifugal force. The balls are projected into a parabolic free flight trajectory until impacting on the lower part of the tube. Once the balls have impacted onto the tube, they again repeat this circular reference path.

White found that the curve defining the surface of departure for different layers of balls forms a semi-circle, while the curve that defines the surface of impact is found to define a Limacon or Trisectrix.

The radius and hence the tangential velocity of each layer is used to calculate the cycle times for the relative layers . In order to find the average cycle time and time in flight of the charge as a whole, the cycle time is integrated over all the layers. The average time in flight of a ball, allowing for the relative number of balls in each layer, can then be derived. By inserting an approximate average ball size relative to the mill diameter, the optimal speed for greatest average fall is found.

White also acknowledged the effect of friction and slip on the load. It was observed that higher speeds had to be used than predicted to produce a given charge motion and thus concluded that a sufficient quantity of balls must be present in order to maintain an adequate charge pressure to prevent slipping and thus allowing the keying in of the balls.

White recommended that a state of centrifuge should exist in the outermost layer in order to protect the liner against direct impact from the balls thereby causing less wear on the liner. A recommendation was also made that the load be held at 66% of the internal volume to allow for an efficient falling distance. It was also stated that the level of the water in the mill be maintained below the level of the charge at the bottom

of the mill in order to have the balls impact on dry material rather that to waste energy trying to penetrate the water.

White further stated that in order to determine the best speed at which to run a mill, the power absorbed per revolution should be maximised.

A supporting comment in the discussion of the paper was that at Glen Deep mine the mills ran most efficiently when charged with a minimum of water.

White created a base for further work in this field. The validity of different layers of balls as well as acknowledging that slip plays a role in the charge motion is established in the work.

Although all these results are obtained in an idealised system, the results are acquired by using fundamental laws of physics. A good indication of how the mill operates and what variables could be altered in order to improve the efficiency of the milling operation could be determined.

White acknowledged that the "The true use of theoretical considerations is to shape the course of practical trials". A procedure by which future research could be performed rather than finding an exact solution to the milling problems was initiated.

2.1.2 Fine crushing in ball mills [10]. (E.W.Davis 1919)

Davis analysed ball motion under the same conditions as White. Only the method of his derivations differed.

Davis investigated the parameters influencing the effect of the impact by the falling ball. The ball's velocity relative to the lining or another layer of balls was determined. This velocity was maximised for a given set of conditions. The radius of gyration of the charge was then used to determine the optimum conditions for the charge as a whole by considering the change in angle of departure with change in radius from the mill

centre. The relationship between the inner and outer radii of charge can be derived from the optimum operating conditions. The correlation between these radii and the charge volume have to be determined.

The charge cycle time was considered to be split into two periods. The first being the circular path time of the charge while rotating up the wall of the mill and the second being the period of the ball during its falling parabolic path. Both of these time intervals at the radius of gyration of the charge were calculated.

It was discovered that the ball completes 1.44 revolutions per one mill revolution. This illustrates that 56% of the balls' time is spent in the circular path, resulting in that same percentage of total charge being present in this region. The other 44 % of the balls' time is spent in the falling phase of its motion. This gives the correlation between the inner and outer radii and the charge volume.

Davis claimed that by use of his equations one can determine the charge profile, velocity of ball strike, number of ball strikes and relation between speed, diameter and volume for best theoretical efficiency.

These theories were then tested using a 76 mm diameter by 51 mm long mill containing fine sand. The experimental results illustrated a good correlation with differences being due to the interference between particles. This, Davis argued, arose because the initial velocity vectors of two adjacent particles at their departure points intersected when extrapolated a short distance. The calculations gave optimal results for impact crushing while attrition crushing predicted poorer operating conditions.
Davis did however make certain assumptions that would lead to uncertainties of the results that he obtained.

Firstly it was assumed that no slip takes place against the liner or within the body of the charge. The calculated trajectories can therefore be taken as being too generous, as the departure velocity determines these subsequent trajectories. The trajectories calculated by Davis (Figure 2.1), do not intersect, but it was later stated that the

trajectories do in fact intersect, thereby causing interference between particles and hence causing the discrepancy between the observed and calculated paths.

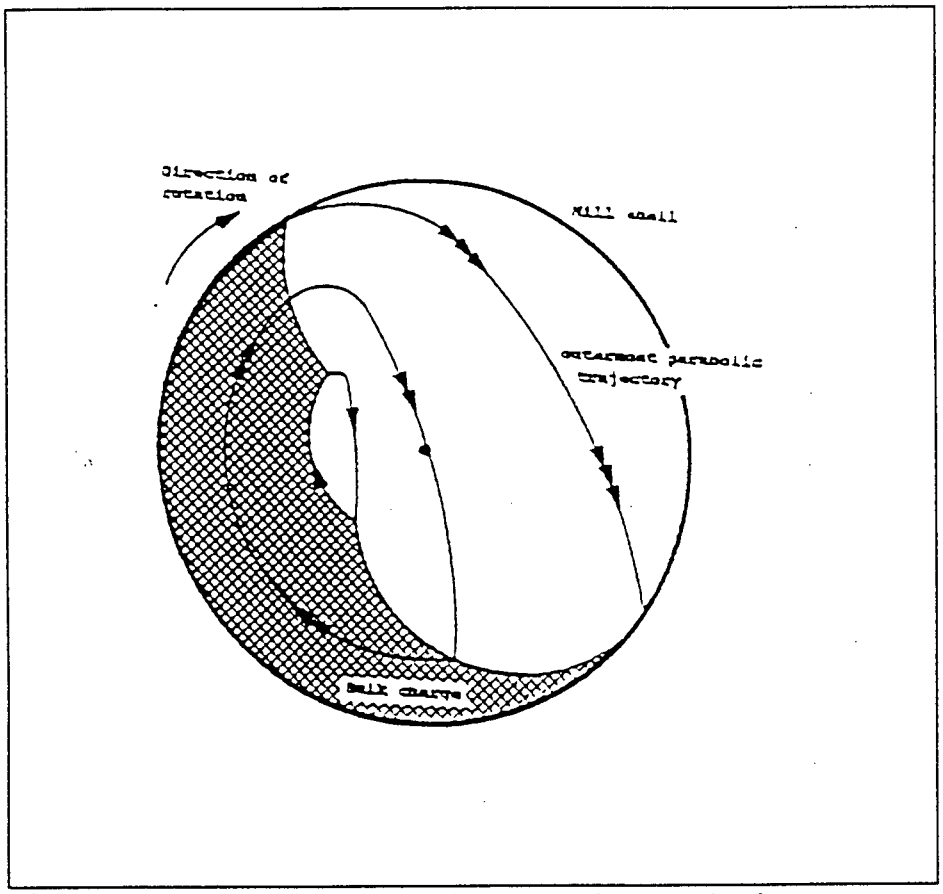

Figure 2.1: Trajectories as calculated by Davis

Secondly, in a discussion of the paper White pointed out that the inner layers of balls have a far shorter cyclic time than the outer layer. The charge calculation of the charge cycle time should therefore be summed over all the radii rather than just over the centre of gyration.

Due to the simplifications of Davis' model, the work can also be considered as a useful methodology rather than an accurate solution to milling problems.

2.1.3 Ball paths in tube mills [11]. (H.E.T.Haultain and F.C.Dyer 1922)

Haultain and Dyer undertook this work in order to confirm Davis' theories and subsequently proved that slip is in fact an important consideration in charge motion.

Two glass ended mills with diameters of 609 mm and 152.4mm (24 and 6 inches) and a length of 12.7 mm (0.5 inches) were used. The mills were loaded with brass discs, seeds or crushed marble. Each disc had four thin projections on either side to overcome friction caused by end conditions. A high-speed camera film (120 frames/second) was used to photograph the motion of the charge. The results clearly displayed that slipping did occur between the discs and lining and between the various layers of discs.

These results contradicted Davis' theoretical paths. It was also apparent from the results obtained by Haultain and Dyer that segregation of the charge occurred. The segregation was found to be dependant on the rotational speed of the mill, with the small discs migrating to the centre and the larger discs remaining at the periphery for low speeds. The opposite was found to occur at higher speeds with the larger discs migrating to the centre while the smaller discs remained on the outside. It was therefore possible to obtain a speed for which even mixing occurred, thus avoiding a central region of under-utilised large balls.

In defence of his work, Davis requested that quartz be added to the charge as well. The quartz did decrease the slip against the shell and zero slip was also observed on the main part of the circular path.

These new results still however showed inconsistencies with Davis' work and Davis claimed that this was purely due to slip near the top of the circular path. Haultain however maintained that there were significant differences between Davis' theory and observation, with slip being the important unaccounted for factor. Davis also conducted this investigation with slurry loads while the affect of slurries was unknown, this leading to more assumptions.

This study of Haultain and Dyer gave purely qualitative conclusions and were not verified using industrial conditions. These results are therefore merely a guide to the motion in an industrial mill. The work does however verify the importance of slip in the charge motion thereby illustrating the incompleteness of Davis' theory. Davis did however point to the large effect of slip just prior to departure. This fact was later verified by Vermeulen[7], who determined that it was due to the loss in charge pressure at the point of departure.

2.1.4 A laboratory investigation of ball milling [12]. (A.M.Gow, A.B.Campbell and W.H.Coghill 1930)

The experimental work was acquired from a 900 mm diameter and 150 mm long laboratory mill. First glass grids and then later glass screens were used at either ends. The observations showed that the balls' trajectories were larger than predicted by the parabolic path theory. This was attributed to the fact that the balls are in contact at departure and that interference occurs between these balls after they have left the liner. The balls remain in contact while in flight until the peak of the flight path is reached. The pushing effect of the balls in contact cause the balls in flight to continue to travel at the same speed as the peripheral speed of those balls against the mill shell.

Gow et al verified that segregation did exist as was establish by Haultain and Dyer. By also using wooden balls it was determined that segregation was purely a function of size and not mass. The smaller balls move to the outer layer at high mill speeds. This is due to their centre of mass being closer to the mill shell. Powell[5] gives a detailed reasoning for this phenomenon.

Due to the higher observed trajectory lengths, it was recommended that slower mill speeds than previously predicted as optimum should be used. A reduction of speed from 75% critical to between 50% and 65% critical was suggested.

Davis however repudiated these results by mentioning that it was possible for the angle of departure to be extended by the locking in of the 1,25 inch (31.75 mm) balls

between the 1 inch (25.4 mm) grids, as these were only spaced 6 inches (15.24 mm) apart when fixed to the mill wall. This would cause the balls to be carried much further than in industrial conditions.

The above mentioned point by Davis is the flaw of this investigation. White also alluded to the fact that if the range of ball sizes and their random packing were considered, it would be improbable that the balls could remain in contact after departure. This work cannot therefore be taken to be accurate but can be considered as a good introduction into the experimental procedure followed in milling investigations.

2.1.5 Ball mill studies [13]. (A.W.Fahrenwald , H.E.Lee 1931)

Fahrenwald and Lee undertook a ball path analysis basing it on Davis' work. The effect of ball size on mill efficiency was investigated by considering only uniform sized balls. A formula for optimising the ball size for various operating conditions was derived. It was found that for mills of varying sizes with angle of departure of the outer layer remaining constant, the formula predicts identical charge motion. From this result it was concluded that all mills should run at the same optimum percentage of critical speed.

The authors stated that "The large number of variables prevailing in this study prevent a complete statement of conditions in mathematical form". This allowed Fahrenwald and Lee to predict trends using the derived formulae, but optimum points (considering all operating variables) could only be found experimentally. The relationships between the trends and optimum points could be used to determine optimum conditions for any other mills.

By studying the power draw of a mill for variations in mill speed, ball size and load, a point of optimum efficiency was found. It was established that this point occurred at a combination of the three specified variables where the largest energy draw was observed.

In order to explain why the balls departed from the liner sooner than was predicted, a factor of slip between the charge and lining was incorporated into the model and a new formula was derived by considering this extra term. The slip factor would cause the balls to roll along the liner thereby resulting in a radial force component. This extra force component decreases the downward velocity of the ball and the resultant velocity vector constitutes a larger proportion of the radial force..

By dragging balls across a wrought-iron surface with quartz slurry of various moisture contents, it was found that the coefficient of sliding friction of the quartz decreased as the moisture content increased. From this it was determined that for a drop in coefficient of friction, a higher pressure and therefore load would be necessary to maintain the same charge motion.

In an evaluation of the paper, Powell stated that in considering the balls' rolling due to slip on the liner, the retarding effect of the surrounding charge was not considered. This retarding effect would probably prevent rolling.
This work demonstrates some useful techniques in finding optimal operating conditions by monitoring the power draw of the system. The effect of slurries and the effect of varying coefficients of friction is observed to have an effect on the charge motion. The conclusions are however not satisfactorily verified.

2.1.6 Contribution to a study of dry quasi-autogenous milling [14] (B.Marechal 1968)

Marechal considered basing his work on one of the three theories of either Davis[10], von Steiger (1929) or Joissel (1951). All the theories consider the trajectories of particles within a rotating ball mill. Davis' theory of balls inhabiting circular paths of varying radii was chosen. Marechal based this choice on the fact that Davis' theory while the most simple gave similar results to von Steiger's and Joisel's more complicated theories of conservation of volume.

Davis' theory incorporates the following three simplifications.

- Solids move perpendicular to the mill axis.
- There is no slip on the mill wall.
- Air resistance is negligible.

The calculations of the charge motion and the equilibrium surface are based upon the spiral-circular path predicted by Davis' theory but not observed in practice.

Slippage at the mill wall was assumed negligible but slippage was assumed to occur at the free surface. A curve of equilibrium of charge surface was then calculated and it was found that the mill speed and percentage of filling had little effect on the equilibrium slope (angle of repose). The coefficient of friction was found to have a large effect on the equilibrium slope. It was concluded that the equilibrium surface represents the surface below which solids rotate without slipping and above which cascading and tumbling of the load occurs.

The next step of the investigation was to determine the effect of lifter bars on the charge motion within the mill. The following set of assumptions were made.
- The lifter is of negligible height relative to the mill radius.
- The sides of the lifter are parallel to the radius vector.
- The particles follow a parabolic trajectory path after leaving the lifter bar.

It was found that the particles lying in-between the lifters were lifted slightly higher than the rest of the charge. The rest of the charge experienced only a slight increase in lift relative to that obtained with a smooth liner. The effect of the lifters decrease with an increase in mill diameter.

The lifters are assumed to act as perfect keying-in agents. This is a valid assumption for the area below the main bulk of the charge but in the area just prior to departure the charge pressure is too low to allow for effective keying-in of the charge. This causes an area to exist where the particles start to slip before departing from the liner. One of the assumptions of this work is that the particle starts to follow a parabolic free

flight path the moment it starts to slip. The actual path followed by the ball consists of the ball sliping down the face of the lifter bar until it reaches the lifter tip. At this point it will depart from the lifter bar. The path followed after departure is a parabolic trajectory.

Vermeulen [15] states that the assumption that the lifter bar sides are parallel is incorrect and that fabrication and wear changes this angle which plays a large role in influencing the charge motion.
The important findings of this work are:
- The decrease in effectiveness of the lifter bar as the mill diameter increases.
- The keying-in effect that causes an area of non slip below the main charge and slightly increases the departure angle.

2.1.7 The determination of the efficiency of the milling process[3]. (A.A.Bradley, A.L.Hinde and P.J.Lloyd 1972)

This paper investigates the relationship between energy supplied to the grinding process and the fresh surface created in grinding fine materials. The weight size distribution of slow crushing tests of single-crystal quartz and Witwatersrand reef are established and the energy consumption required to produce a given weight of - 75μm material was determined.

Approximately 70 particles, each of screen size between 6.73 and 9.53 mm were distributed on the lower plate of a hydraulic press. The crushing speed was set at 14.4 μm per second and load displacement curves were obtained directly from the instrumentation on the press. The severity of crushing was kept as low as possible to prevent the development of packed-bed conditions throughout the crush. Net crushing energies were obtained by integrating the load/displacement curve.

Various milling experiments were conducted on different sized feed material. A small centrifugal ball mill was used to grind batch samples. The ball size, ball load, mass of

feed and water content were varied until near-optimum grinding conditions were achieved as indicated by the power required to create a given weight of -74 μm material. The gross milling energies were determined and the net milling energies were estimated.

The results illustrated that the mineralogical nature of the material being crushed and the mode of crushing can influence the form of the product size distribution. It was found that there were considerable problems in making an ideal comparison between the result of ball milling and slow crushing. These problems stemmed from the experimental difficulties in being able to utilise the techniques of ball milling and slow crushing over similar size regimes.

The results showed that ball milling is a relatively efficient process when compared with all other known communition processes.

2.1.8 The modelling of transverse solids motion in rotary kilns[16]. (H.Heinen, J.K.Brimacombe and A.P.Watkinson 1983)

This paper introduces five modes of bed motion and provides a fundamental basis of these modes. The modes described are:

1. Slumping.
2. Rolling.
3. Cascading.
4. Cataracting.
5. Centrifuging.

Four models are introduced to predict bed behaviour quantitatively from measured particle characteristics and the bed/wall friction coefficients. Each of the four models apply to a boundary between each set of motions and are :

1. Slumping rolling boundary.
2. Slipping model.
3. Cascading and cataracting model.
4. Centrifuging.

All the processes within each cycle is first discussed before defining a force balance of the process from which a theoretical model is derived. This work deals specifically with the effect of liner configuration on the trajectories of the media in the mill. A brief description will be given of the cascading and cataracting model as derived in this work.

A force balance is carried out at the centroid of the bed for the cascading and cataracting model. The angle of kinetic friction is assumed to be equal to the dynamic angle of repose. This model is based on the criterion that particles project from the apex of the bed and fall beyond the midpoint of the bed surface. A parabolic flight path is assumed and the effect of interacting particles in flight are neglected.

This model predicted that the cascading/cataracting boundary is dependent on the cylinder diameter, the dynamic angle of repose of the material as well as the percentage fill and illustrated how these variables effect the motion of the charge.

2.1.9 Fluctuations in the slip of the grinding charge in rotary mills with smooth liners [15]. (L.A.Vermeulen, D.D.Howat 1986)

An investigation of the motion of rods in an experimental mill with a smooth liner was undertaken. A model mill with transparent ends was loaded to a charge level of 40 % capacity. A video camera was used to film the motion of the rods during operation. The velocities of the rods were determined by considering the successive frames of the film. The balls were found to have a large range of velocities (50-100% peripheral) with an average velocity of about 60% of the mill shell (peripheral) velocity.

Two alternating phases were determined to exist. Cataracting occurred as the charge reached its maximum angle of repose and cascading occurred as the charge started slipping back. It was therefore concluded that when cataracting takes place approximately 20% of the balls are in flight and the charge pressure decreases. This allows for slipping of the particles and hence a phase of cascading occurs. Cascading causes the charge pressure to increase so that a new phase of cataracting takes place.

An expression for slip, relating to variations of dynamic pressure is given. This expression is used to calculate rod speed which can be compared to the observed values. By making a comparison between the results obtained from the expression and the observed results obtained from the experimental work, a 5% error band was found to exist. This proves that a very good correlation exists between the calculated and observed results.

From the above observations it can be concluded that there exists a critical charge pressure at which slip and hence cascading occurs. Above this pressure, a keying-in effect takes place causing more balls to cataract onto the toe of the charge. The slip causes an increase in liner wear and simultaneously represents a large loss of energy.

This work illustrates the effective use of cinematographic techniques to analyse the motion of the particles in the ball mill. The importance of the effect of charge pressure on energy consumption and wear is also specified.

2.1.10 Physical information from the inside of a rotary mill [17]. (L.A.Vermeulen, M.J.Ohlson de Fine and F.Schakowski 1984)

Electronic circuits were developed and utilised to continuously monitor information relating to the impacts of pebbles on shell liners of an industrial pebble mill. The primary considerations of this paper is to further investigate grinding element motion on mill shells and obtain information on the impacts, amount of material in flight and power involved in projecting this material into flight.

The electronic impact sensing devices were inserted into the liner bolts of a 4.78m by 9.14 m (16 ft by 30 ft) mill at East Driefontein gold mine. The mill rotates at approximately 16 rev/min which corresponds to 82 % of its critical speed. The sensor is located in the bolt head and the piezoelectric sensor sends signals via electrical leads to a transmitting device on the outside shell of the mill. Bolts containing electrically insulated electrodes are used to detect enhanced electrical conduction of changing amplitudes when emerged in the mineral pulp.

The piezo-electric signals consisted of a series of fairly sharp peaks spaced at regular intervals. A similar set of periodic electrical conduction signals were obtained. All the signals were recorded over a period of 30 minutes.

The occurrence of the piezoelectric impact signals is found to occur at intervals of about 3.75 seconds and last for about 1 second. Five distinct impact points could be recognised on each signal. Angular positions of the five independent impact events were calculated by considering the angular speed of the mill and by determining the parabolic trajectories of falling particles. These predicted values were superimposed on the experimental results.

The following assumptions were made in the theory :

- Pebbles are spherical.
- The pebbles are keyed in due to the rotary motion of the mill.
- Interactions between pebbles at departure can be ignored.

The results (figure 2.2*a*) showed that the oversight of the interaction forces between the particles were found to give very low trajectories. The adhesive forces cause some particles to centrifuge at even 82% critical speed. This adhesion force influences the angle of departure.

By considering the cohesion effects, a new set of theoretical results was obtained. These results were found to closely match the observed results (figure 2.2 *b*).

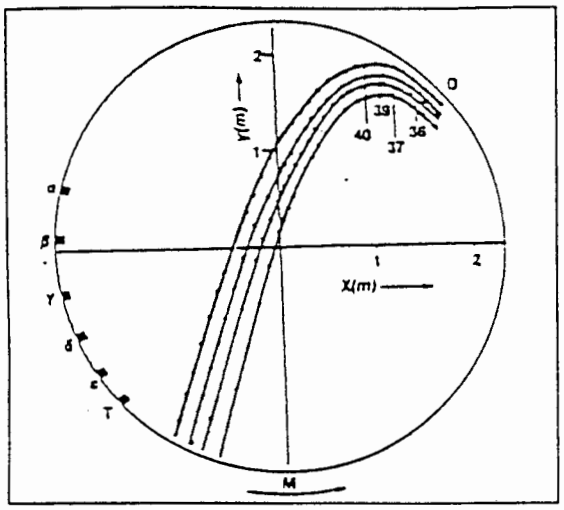

Figure 2.2*a* : Trajectories without considering the interaction of particles

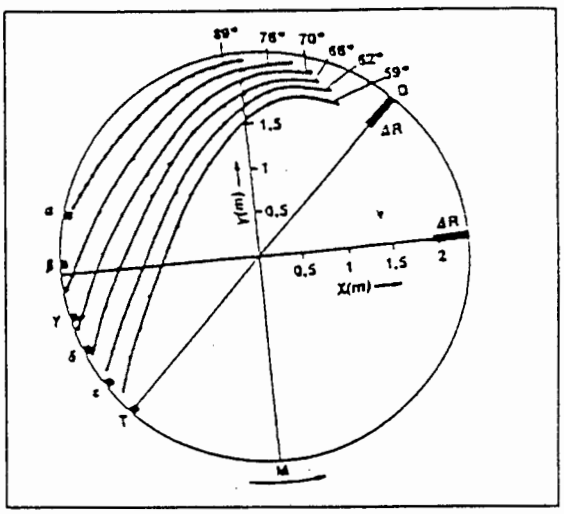

Figure 2.2*b* : Trajectories with the consideration of adhesion between particles

The work introduces a good approach in determining the internal motion of the charge in a mill using electronic sensing devices as well as considering such effects as cohesion and interaction of particles in predicting the charge motion.

2.1.11 The slip of a single particle on the inside of a rotating cylinder. Part 1. Theoretical Analysis[18]. (M.B.Nates, G.N.Nurick and B.D.Reddy 1993)

This paper presents an analysis of the slip of a particle on the inside of a rotating cylinder. This model considers the particle to slide rather than roll down the inner face of the cylinder. By assuming the ball travels only in a vertical plane and is confined to move on the cylinder's inner wall, the model is simplified, having only one degree of freedom (DOF).

In considering the orientation of forces acting on a single particle (figure 2.3), the sliding equations were derived. The friction force was noted to initially act in the direction of rotation to prevent sliding but opposes the direction of rotation as the ball starts to slide. The equation governing the particle's motion on the cylinder is a

second order, non linear homogenous differential equation. After determining the initial conditions of the problem, a Euler numerical scheme was used to solve for the position and velocity of the particle at any finite time-step on the cylinder wall.

The particle was assumed to have four possible response modes ;

- Sliding of the particle back down the rotating cylinder surface.
- Leave the cylinder surface.
- Centrifuge at high rotational speeds.
- Topple at low speeds if the particle was large enough.

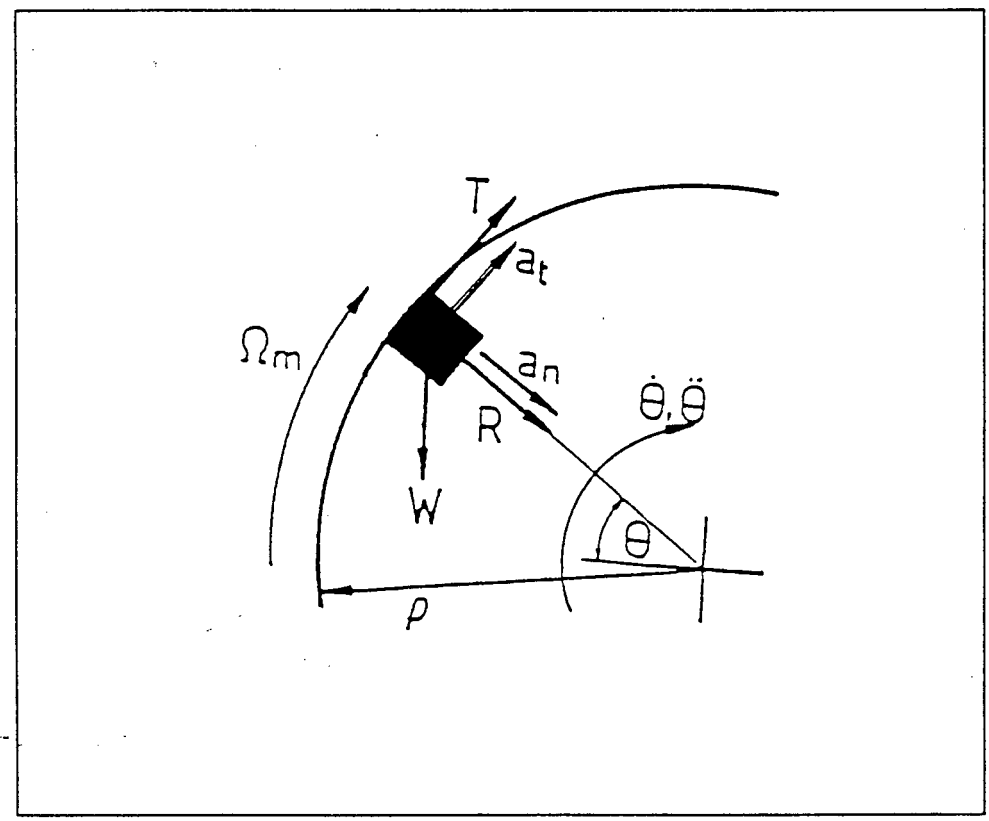

Figure 2.3 Orientation of forces acting on a particle

The model was coded in FORTRAN and the analysis was initiated by running the computer simulation with varied input values. Two parameters, coefficient of friction (μ) and rotational mill speed (Ω) were found to have significant effects on the particles motion.

Firstly the case was investigated where the particles slipped down the cylinder wall. Trends were generated for μ_{min} versus θ_{slip} (angle above the horizontal at which the ball starts to slip) at three different cylinder speeds. It was observed that as θ_{slip} tends to Davis' [10] prediction, μ tends to infinity hence there is a singularity in μ at α, where α is the angle of slip determined by Davis. It can therefore be concluded that Davis' model has an implied assumption that friction is assumed to be infinite.

In considering the centrifuged case, it was determined that as rotational speed increases so the coefficient of friction required for total centrifuging decreases.

The particle's parabolic trajectory after departure had occurred was also analysed. A variation in trajectories with a change in rotational speed and a constant friction coefficient was first investigated. Thereafter the rotational speed was kept constant and the friction values were varied to obtain a second set of results. The results showed that as μ is increased the particle slips for a shorter time before leaving the surface. This leads to the particle leaving the cylinder wall with a higher tangential velocity. The resultant increased velocity increases the particle's flight path across the cylinder. A similar phenomenon was found to occur when the rotational speed of the mill is increased.

The model considers the particle to centrifuge by two possible methods. Total centrifuging where the particle always has the same rotational speed as the mill and slip centrifuging where the particle slips but the frictional force and cylinder speed is large enough to hold the particle on the cylinder.

This work concludes that Davis' work is inadequate due to the assumption of infinite friction and that centrifuging may exist in two possible methods rather than by just one as is predicted by all past formulations.

2.1.12 The slip of a single particle on the inside of a rotating cylinder. Part 2. Experimental Investigation [19]. (M.B. Nates, G.N.Nurick and B.D.Reddy 1993).

The effect of coefficient of friction and rotational speed on the motion of the particle in the cylinder are investigated experimentally to determine whether the theory developed by Nates et al [18]. correctly predicts the effect that these parameters have on the motion of the particle. Powell [7] showed that the effects of vibration on the test mill reduced the coefficient of static friction to almost zero. To reduce the effect of vibrations on the system a 404 mm diameter by 100 mm wide steel mill with no front was constructed The open drum allowed for the elimination of end effects as described by Davis[10]. A video camera operating at 25 frames per second and a video recorder were used to record the block's angular displacement. The video images were analysed using a VCR with a single frame advance function and by quantifying the block's motion by considering one frame at a time. A square shaped mild steel pellet was used in order to eliminate any rotation by the particle.

A variable speed 0.25 HP motor was used to drive the mill and a cloth lining was fitted to the inside of the mill to vary the friction coefficient. The static and kinetic coefficients were found to be insignificantly different with the value of $\mu = 0.44 \pm 0.04$ for cloth on metal and $\mu = 0.20 \pm 0.04$ for metal on metal.

Tests were run on the two surfaces with the tests consisting of speeds ranging from 30 %.critical up to a speed were the block became totally centrifuged. The angle of slip and angle of departure were determined by considering the video images obtained from the experiments.

The aim of the first tests was to confirm that the block's motion was in fact independent of its mass. Three blocks of varying masses were tested at identical conditions to determine if there was any variation in angular displacement. It was found that the results all fell within a 6 % uncertainty range allowing for the conclusion that a particle's motion is independent of its mass.

From the experimental results it was evident that the theory did correctly predict the angle of departure and that the angle of departure does in fact increase as the rotational speed of the mill increases.

The results relating to the slip angle of the block point to the following trends. The first is that as rotational speed (Ω_m) increases so slip angle (θ_{slip}) increases. Secondly as μ increases so θ_{slip} increases. These two trends are in agreement with the trends predicted by the model.

As defined by Nates et al.[18], two types of centrifuging may exist. The audio response of the test drum was used to distinguish between the two situations. It was not possible to determine the exact speed at which each response occurred, but a range has been reported. A good correlation was found to exist between the predicted and observed results.

The experimental investigation yields results which were in good agreement with the theoretical predictions.

2.1.13 Prediction of grinding mill power [20]. (S.Morrell 1992)

A laboratory mill 305 mm in diameter and 150 mm in length with a glass front was used. The mill was mounted on 2 rollers and a motor and variable-speed controller were coupled to the driven roller, allowing the mill to obtain a range from 55% - 85% of its critical speed. A fully autogenous charge as representative of the equilibrium charge obtained in a 1.83 m by 0.61m (6 ft by 2 ft) autogenous pilot mill was used.

The aim of the experiment was to determine how the shape of the mill charge varied as the charge volume and rotational speed varied. Photographic methods were used to capture the charge shape by adding brightly coloured tracers to the dark ore. Still photographs were taken with a very low shutter speed, hence showing the shape of the charge as well as the length of the bright lines which in turn provided information on the speed of the individual particles.

A series of tests with mill loads ranging from 15% - 60% of mill volume and mill speeds ranging from 55% - 85% of critical were carried out under dry and wet conditions with no lifter bars. Toe and shoulder positions of the charge were recorded and velocities of the particles were measured.

The velocities of particles in the various layers within the charge were expressed as a fraction of the mill shell velocity. These velocities were determined for 30%, 45% and 60% mill loads. The results were expressed as a relationship between tangential velocities against the distance from the centre of the mill.

A net power equation relating to shape of charge and fractional speeds (all speeds relative to mill speed) of various layers was derived. The effect of slip within the charge, mill filling, mill speed and charge density was considered in deriving this relationship.

A gross power equation is also derived by considering power losses due to various electrical and mechanical losses.

On doing an evaluation on the model, Morrell determined that the power draw is a function of both mill speed and mill load as suggested by laboratory investigations.

The model predicts power consumption for a wide range of industrial and semi-autogenous and fully autogenous mills.

2.2 THE FACTORS AFFECTING MILL EFFICIENCY

2.2.1 Technical design of autogenous mills [21]. (R.C.Meaders, A.R.Macpherson 1964)

Meaders and Macpherson investigated the effect of the height, the method of product discharge, length of the mill, rotational speed of the mill and the spacing of the lifter bars on the efficiency of a closed circuit model mill. After optimising each variable, the tests were repeated in order to verify the first set of results. The energy used to produce one unit of new surface area was used as the basis for comparison of the results.

As illustrated in Figure 2.4, it was found that the variation in the ratio of spacing to height of the lifter bars greatly influenced the efficiency of the mill. An optimum value of spacing to height was found to be between 4 - 4,5 (This gave the minimum energy per unit of surface area produced).

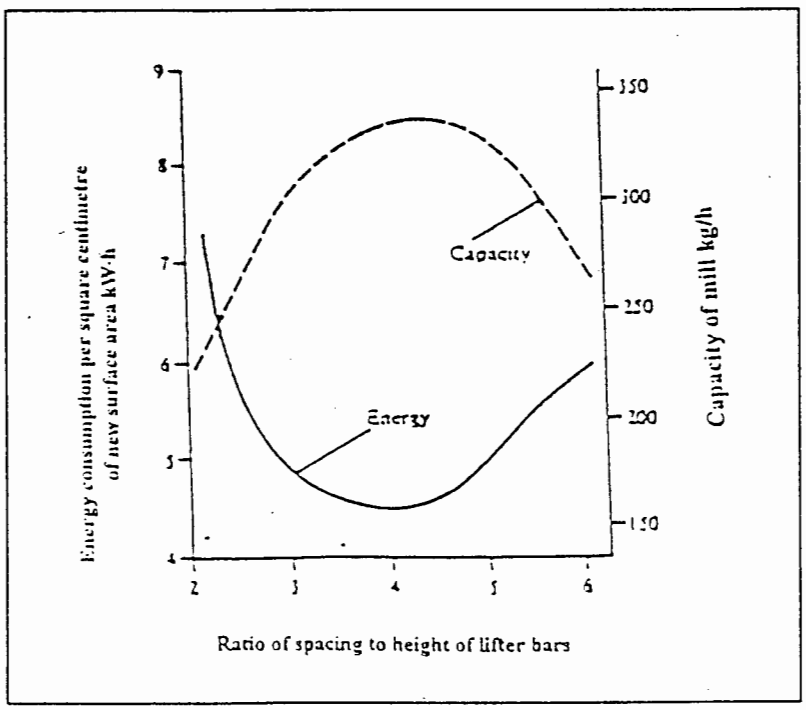

Figure 2.4 : The effect of spacing to height ratio.

It was also found that the optimum height of the lifter-bars depends on the speed of the mill. Mills with smooth lining have to be run at over 90% critical, whereas mills with higher lifter bars run optimally at a much lower percentage of critical speeds. The results conclude that the best overall condition is obtained at a speed of approximately 77% critical with a ratio of mill diameter to lifter-bar height of 17,6.

The authors deal with some essential investigations of the variables affecting mill efficiency. The results show that the mill efficiency can be optimised by finding a good correlation between mill speed, lifter spacing and lifter height.

2.2.2 Optimising ball mill liners for production and economy [22]. (D.J.Dunn 1976)

In order to obtain maximum mill efficiency, a liner which produces the desired fines in the shortest time and is most wear resistant is essential. Four mill liner profiles were tested using a 3,96 m long by x 3,65 m wide overflow ball mill.

The four tested liners were.

- Shiplap liner (Traditionally used) (figure 2.5*a*)
- Wave liner (figure 2.5*b*)
- Single wave S100 liner (figure 2.5*c*)
- Double wave S201 liner (figure 2.5*d*)

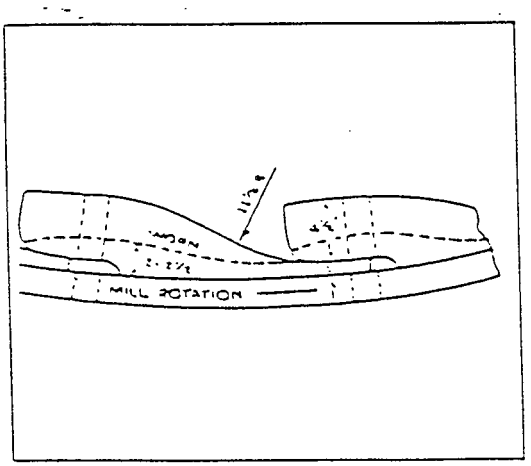

Figure 2.5*a* Shiplap liner

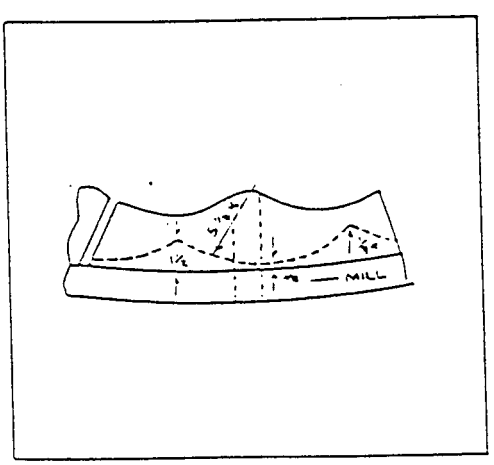

Figure 2.5*b* Wave liner

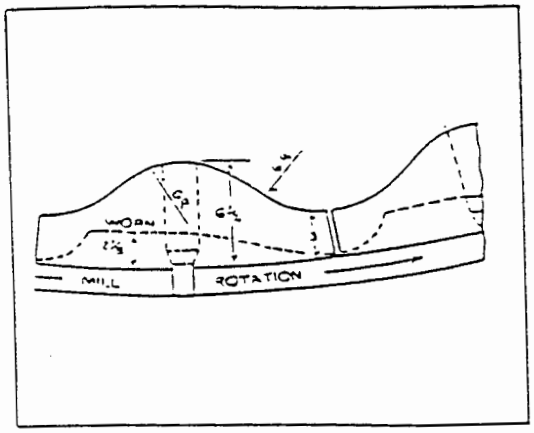

Figure 2.5*c* Single wave (S100) liner

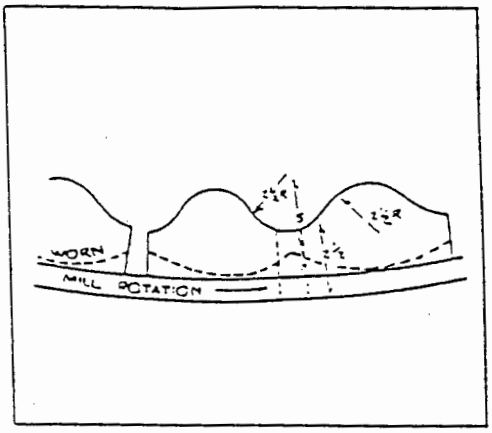

Figure 2.5*d* Double wave (S201) liner

The shiplap liner profile was found to have very low wear characteristics and changed rapidly to approximate a sinusoidal single-wave pattern. This decreased the lifting capabilities of the liner substantially. The high wear rate of this liner led to the design of the wave liner.

Initial tests on the wave liner proved that this liner had superior grinding and wear characteristics which showed an increase of 500 operating hours and a metal wear rate of 18% less than shiplap liners. It was however found that grinding capacity during periods of coarse ball mill feed (24% - 30% plus 0.3 mesh) was not satisfactory. This in turn led to the design of the single wave S100 liner.

During the first third of the life of the S100 liner better results than previous were produced with reduced grind size. After this period of optimum performance the wave tops wore down and a profile similar to the shiplap liner developed. It was however the most effective of the three liners tested.

From the results obtained testing these three liners it was evident that a higher lift liner was necessary for good grinding at low speeds. The double wave S201 liner was designed for this purpose. This liner was designed with a higher wave profile in order to develop the higher lift that was required. A marked increase in the tonnage was found to exist for reduced grind size throughout the life of the S201. The liner wear characteristics proved to be very good. A slow change in the profile occurred

eventually duplicating the single wave liner shape. The service life of the S201 was twice that of any previous designs. The increased life was attributed to the reduced sliding of the balls down the higher wave profile.

This research showed how a small change in the profiles of liners can have a large effect on operating effectiveness and wear characteristics thereby saving time in maintenance and allowing for better throughput in material.

2.2.3 The lifting action of lifter bars in rotary mills [23]. (L.A.Vermeulen 1985)

This work considers the lifting action of rectangular lifter bars of various heights on rod motion in a rod mill. A theoretical model is derived in which the lifting action of the lifter bars are quantitatively defined. The equations describe the rod's motion and position on the rectangular lifter bar as well as the path and velocity of the rod after having departed from the lifter bar.

It is evident that the rod will roll or slide down the lifter bar once the equilibrium position has been passed. The dynamics of this sliding interaction is considered in detail and all the equations describing the motion of the ball while sliding are derived and solved using numerical solution schemes. The model also solves for the rod's departure point on the liner and the parabolic path that it follows once it is thrust into free flight.

The object of the experimental work is to explore the effect of the lifter bars on the motion of the rods and compare these observed results to the results obtained using the derived theory.

An experimental mill 250 mm in length and 263 mm in diameter with see-through side panels was used and the motions of the rods were recorded with a video camera. The camera speed was 64 frames per second and the mill was run at 72% critical speed. Sixteen rows of lifter bars were fitted to the mill. Images obtained with the video camera were created into slides (one slide representing one frame) and projected onto

a large sheet of graph paper by means of a slide projector. Measurements of the angular positions of the rods at the departure points were taken. It was determined that the angles of departure were higher when groups of rods rather than a single rod was involved.

The experiments were performed using four groups of lifter bars, all of different heights. The results showed that the angle of departure of the rods are strongly affected by the lifter bar heights. A rectangular lifter bar 12.7 mm high results in a departure angle of 52° while a lifter 20 mm high results in the ball departing at 73°. This is a substantial increase in lift. The radial velocity component of the rod on the 20 mm lifter is also determined to be approximately 50% of the tangential component as the rod departs from the lifter. This however does depend on the length and the angle of the lifter bar.

An investigation was also undertaken to identify whether the rod did in fact follow a parabolic path once it departed from the lifter bar. The results of this investigation showed that this was indeed the case.

Vermeulen takes the first step in quantifying the effect of lifter bars on the charge in a rotary mill by developing a set of equations to describe the rod's motion in the mill. The work creates a base for future theoretical models and exposes an angle of research which could lead to new ideas and methods in ball milling research.

2.2.4 The design of linings for rotary mills[1] (L.A.Vermeulen and D.D.Howat 1986)

A study was made of the performance of a rod mill operating without lifter bars and with different lifter bar configurations. All the experimental work was performed in a 2.44 m by 3.66 m (8 ft long by 12 ft) wide rod mill rotating at 77% critical speed.

The performance of the mill was measured using :

- A smooth liner.
- 12 alternating lines of 75 mm lifter bars and 12 lines of liner blocks (figure 2.6 *a*)
- 24 lines of lifter bars 300 mm apart (figure 2.6 *b*).

The smooth liner showed highly unsatisfactory results. The mill could only accept low feed rates, the consumption of electrical energy (per ton) and liner material were high. The tonnage milled during the liner life was one eighth of that obtained with other liner configurations.

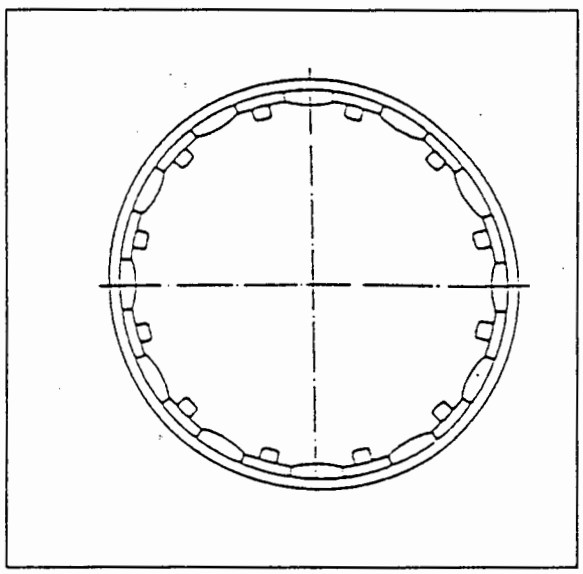

Figure 2.6*a* : 12 lifter configuration

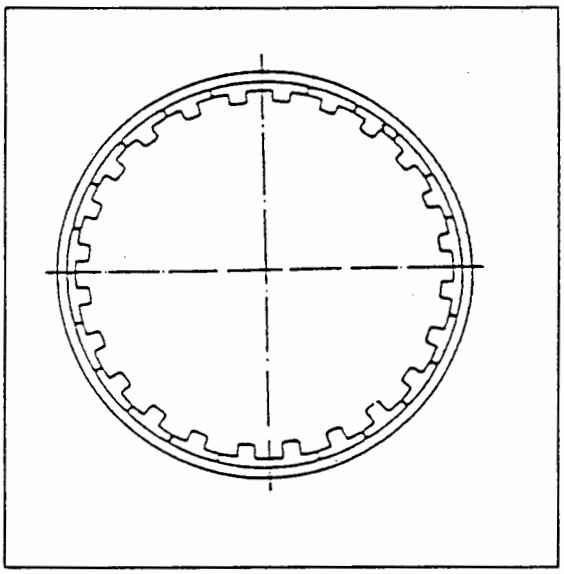

Figure 2.6*b* : 24 lifter configuration

The second configuration (figure 2.6*b*) showed an 80% improvement on the tonnage milled throughout the liner life, with a substantial drop in power consumption and 85% reduction on liner wear.

The insertion of 24 lines of lifter bars gave striking improvements over those obtained from the 12 lifter configuration. The feed rate was raised by 11.5 %, the consumption of energy was reduced by 80% and the consumption of liner metal by 43%. The liner life was extended by 50% with a substantial increase in tonnage milled before having to replace the lifters.

A series of tests were also carried out on two rod mills of equal size to determine the effect of mill speed on performance. One mill was run at 82% critical speed while the other operated at 75% critical speed. The faster mill accepted a higher feed rate of 108 t/h compared to the 67 t/h of the slower mill. However, the product from the slower mill contained 20% material smaller than 75 μm compared with 8% in the product from the faster mill. By comparing the total consumption of electrical energy in relation to the tonnage of material smaller than 75 μm milled, the slower mill is more efficient.

The optimum spacing to height ratio obtained by Meaders and McPherson [21] as 4-4.5 was verified by Howat and Vermeulen, but these values are found to be dependent on the type of rock milled, the speed of the mill and the wear characteristics of the lifters in the mill.

The height to diameter ratio of lifter bars was also investigated and the observations suggest that significant savings in liner metal and hence shorter downtimes for the replacement of worn lifters might result from the use of a lining consisting of alternating lines of higher and lower lifter bars.

This work illustrates the effects of different configurations of lifter bars on the effect of the economic variables in the mill. The effect of wear rate, power consumption and tonnage milled are all factors that are found to be highly dependant on the type of liner and the configurations of these liners in the mill.

2.2.5 Effects of lifter bars on the motion of en-masse grinding media in milling[24]. (L.A.Vermeulen and D.D.Howat 1987)

A 263 mm diameter by 250 mm long mill was charged with various media to a fill of about 45% and run at 73 % critical speed and video footage was taken through the transparent window at the front of the mill. Steel rods were used as the grinding charge in the mill. The radial and angular positions of the successive frames of the film footage were determined by projecting the images onto a computer graphics tablet, operated in

conjunction with a PC. Slight errors were introduced due to inexact location of the centre of the rods as well as photographic distortion.

The effect of two sets of lifter bars on the charge motion was investigated with the relative heights being $1.3a$ and $4.3a$ where a is the radius of a rod. The first value being close to conventional lifters while the second value is much higher than conventional lifters. Sixteen lines of bars were used giving the space to height ratios of 8.2 and 2.6 respectively which differs substantially from the 4.5 recommended by Meaders and MacPherson [21] as the optimum value for this ratio.

The rods were considered to move in co-axial layers and abrasive interactions were associated with relative motion between layers of rods.
The lifter bars were found to decrease slip on the mill wall hence exhibiting a keying in effect where the balls essentially travelled at the same speed as the mill speed. It was found that the relative slippage between layers increases for layers closer to the centre of the mill. The keying in action was found to be independent of the lifter bar height for lifter bars of up to two rod diameters in height. However, the amount of particles projected into flight is very dependant on lifter height.

The dynamic pressures and the magnitude of the abrasive forces between the particles were found to be larger in the inner layers of the charge when the mill was fitted with lifter bars. The kinetic energies experienced on the toe of the charge was also found to be larger for the mill with lifter bars.

This paper introduces cinematographical techniques to investigate the effect that various lifter bar heights and spacing to height ratios have on the shape and motion of the charge. The results develop trends for abrasion and impact intensities as well as slip and dynamic pressure for various lifter bars.

2.2.6 The effect of liner design upon charge motion in a rotary mill [4]. (M.S.Powell 1988).

Powell investigates the effect of flat-faced lifter bars with varying face- angles on the charge motion. A glass ended model mill 386 mm in diameter and 300 mm in length filled with 295 mm long and 12 mm diameter mild steel bars were used in obtaining the experimental data.

The charge motion in the glass ended mill was filmed with a high-speed camera. The mill was fitted with a wide variety of lifter-bars with different face-angles and heights and was run at a range of different speeds. The filmed trajectories of the rods were tracked . The power draw of the mill was also measured under a wide range of operating conditions.

A mathematical model was derived to predict the outer trajectory of a single rod in a mill for lifter-bars of varying face angles and heights. The model considered the effect of variables such as mill speed, friction coefficients, mill size and ball size on the motion of the rod.

A good correlation between the theoretical prediction and experimental results was found over a large range of operating conditions. It was found that lifter-bar height had a large influence on the trajectory of the rod. The trajectory increases as the height increases but the lifter bar reaches a critical height at which point the trajectory is no longer affected.

An increase in the face-angle of the lifter-bars was found to have a strong influence on the height of the outer trajectory. A linear relationship was observed between the mill speed and the impact angle. The power draw was noted to decrease as the lifter height increased.

This work illustrates some important facts about lifter bar effects on the outer trajectories and expands on previous work by Vermeulen[15,23] on determining outer trajectories for only rectangular lifter bars.

2.2.7 The design of rotary-mill liners and backing materials [2]. (M.S. Powell 1991)

This paper evaluates the wear and performance characteristics of lifter bars in relation to their height, together with cost-life performance of the backing materials used for liners in rotary mills. Powell attempts to illustrate how the liner life as experienced in these mills at present should be improved. This is accomplished by considering the effect of lifter bars on the life of the liner in a ROM mill and the performance of the mill and the effectiveness of currently available materials for the backing blocks by considering relative wear rates when used with lifter bars of a suitable configuration.

The liner wear was measured at intervals of six weeks using a specially designed liner-wear-monitor. Unevenly mounted lifter bars were excluded due to difficulty of measurements. Much care was taken to install the lifter bars squarely on and flush against the backing liner in order to obtain accurate and consistent measurement.

The investigation determined the way in which lifter bars mounted on top of a grid liner would affect the wear rate of the lining in large ROM mills. The 4.8 metre diameter mill was run at 81% critical speed and was lined with 24 rows of grids. The mill was charged with 5-10% 100 mm balls and was run at 45% charge filling. Three types of liners were considered. The mill was first lined with a flat profiled grid (figure 2.7a). This liner exhibited a life of 85 days. The second grid fitted was a v-grid with a rectangular lifter bar mounted in the groove and protruding just above the grid (figure 2.7b). The life of these grids averaged 134 days. The third grid consisted of a flat 125 mm thick liner with a 100 mm lifter bar mounted on top of it (figure 2.7c).

Extensive research was undertaken on grid 3. Results illustrated that the lifter bar heights would wear down from 100 mm to 60 mm over a period averaging between 180-200 days and that the liners behind the lifter bar height would wear down from 125 mm to 30 mm over an average duration of 656 days. This showed that grid 3 had an average life five times greater than grid 2 and eight times greater than grid 1.

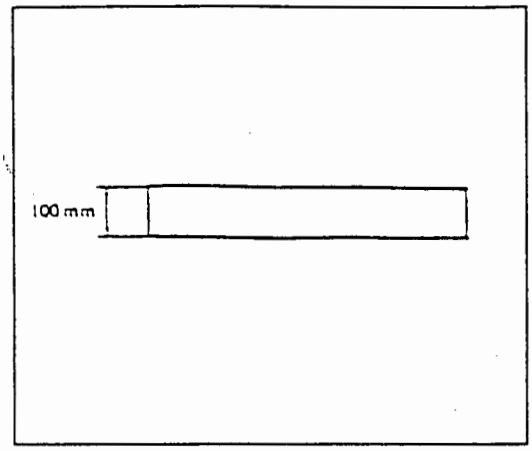

Figure 2.7a : Smooth liner (grid 1)

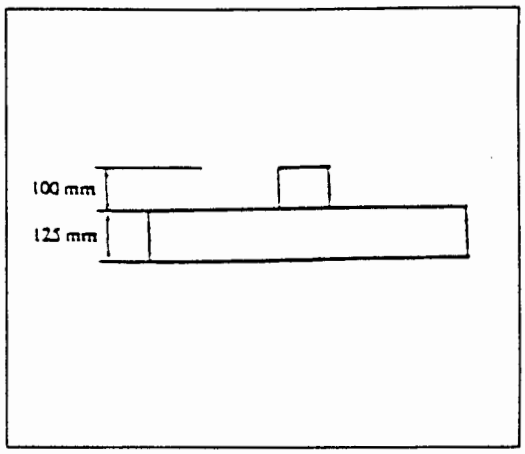

Figure 2.7b : V-grid liner (grid 2)

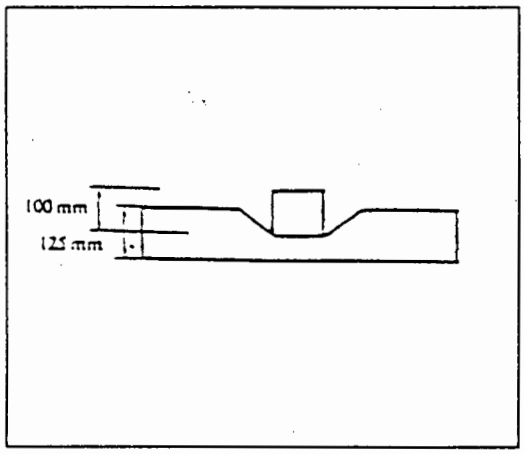

Figure 2.7c : Experimental liner (grid 3)

The short life of the lifter bars in grid 2 was due to the low protrusion of (about 30 mm above the surface) the grids. This allowed the charge to slip over the lifter bars resulting in a high rate of wear. The wear rates for different types of materials for the backing plates was also investigated.

This paper illustrates the effectiveness of lifter bars on the reduction of wear on grid liners. The height of the lifter bars are also shown to have a significant effect on the life of the liner

2.2.8 The discrete element method for the simulation of ball mills [25,26,27,28]. (B.K.Mishra and Raj K.Rajamani 1992-1994)

Mishra and Rajamani applied the discrete element method (DEM) to study the motion of ball charge in tumbling mills. The DEM is a proven numerical technique for simulating the behaviour of discrete, interacting bodies. In this analysis the motion of the charge is treated as a multi-body collision problem and all subprocesses can be quantified in this manner. Experimental work is performed to verify the numerical results.

The simulation is based on Newton's second law and requires some knowledge of the energy dissipated during the collisions. The motion of each separate ball can be computed using this formulation and hence the motion of the entire charge emerges as a result.

The only parameters which need to be specified in this simulation are the material properties of the colliding bodies. This allows full scale problems to be simulated once the material properties of the system have been accurately determined. Various configurations of lifter bars can also be considered in the analysis.

The model is implemented as a two dimensional problem and hence the ball mill is represented by a thin cylindrical section in which an assembly of discs rather than balls collide. This two dimensional DEM approximation gives adequate results for the estimation of power draw and motion analysis.

The DEM algorithm applies Newton's second law to the moving discs and a force displacement model to the discs in collision. The numerical algorithm allows every disc in the assembly to be separately identified by its radius, mass, moment of inertia and collision properties. For all the discs, a list of the discs that are in immediate contact and in near neighbourhood is maintained. The contact forces on the discs are summed to obtain the net force. From this net force the acceleration, velocity and displacement of each ball can be determined.

This Algorithm has been coded into a computer program called "2DMILL". The results of the simulation using this program give a listing of each ball's position for one full rotation of the mill.

Rajamani and Mishra identify the usage of numerical techniques in solving the ball mill problem. This technique opens a path to a much advanced ball mill analysis and theoretically could allow for the possibility to simulate a full scale mill in three dimensions.

2.2.9 The behaviour of a single particle on a corrugated liner inside a rotating cylinder[8]. (K.von Bentheim 1991)

This paper presents a model that incorporates the effect of friction and rotational speed on the behaviour of a single particle on a corrugated liner inside a rotating cylinder. The formulations developed by Nates et al[7] for the behaviour patterns of a single particle on a flat liner surface are modified and applied to the corrugated liner. The out of plane travel of the particles are ignored and hence the problem is reduced to a two dimensional problem consisting of three degrees of freedom (two translational and one rotational). It was found that the balls subjected to wear in the tube mills develop flat surfaces and become cubic in shape. This leads to the conclusion that the balls cannot readily spin when moving along the liner and it is therefore justifiable to use a block shaped particle for the analysis of a single particle on a corrugated liner in a rotating cylinder as was also reported by Nates[7].

This gives rise to two types of motion, the block may either move at the same velocity as the rotating liner or the block may slide relative to the rotating liner. For the pure sliding model, the forces acting on the block are summed tangentially and radially to the liner.

The liner of periodic shape was approximated using Fourier Analysis. Several liner shapes were approximated.

The governing equation is a second order, non linear, homogenous ordinary differential equation. This equation is of a highly non-linear nature and therefore a numerical solution scheme was used to solve for the position and displacement of the ball on the liner.

The results obtained from the model illustrated the following findings :

- The angle of departure (AOD) increases with an increased liner amplitude.
- As the coefficient of friction increases so does the AOD.
- The block will only leave the liner if the velocity of the block down the liner is large enough for the given liner configuration.
- AOD increases as the mill velocity increases.
- The trajectories are higher for larger amplitude liners and for higher coefficients of friction as well as larger rotational speeds.

Experimental work was also undertaken using an axially mounted mild steel drum fitted with various wave liners. A video camera was used to determine the motion of the ball on each of the liners. For each liner configuration the motion of the block was evaluated and the following experimental results were obtained from the video recording.

- The measurement of the coefficients of friction for each surface.
- The determination of the AOD for each surface.
- The determination of the angle of slip.
- The centrifuge speed.

The experimental findings showed good correlation with the theoretical results.

2.2.10 The influence of materials and lifter design on the rate of production of fines in a rotary mill[29]. (A.L.Hinde, S.Mahomed and M.S.Powell 1993)

Autogenous milling trials were undertaken on a variable speed batch mill with a 1.8 metre diameter by 0.5 metre length to assess the influence of various mill liner geometries on the rate of production of materials smaller than 75 μm (tons per hour) and the corresponding energy efficiencies (kWh per ton of 75 μm material produced). Four liner geometries were used in the investigation.

- 40 mm long /50 degree lifter bar.
- 70 mm long /90 degree lifter bar.
- A grid liner.
- 70 mm long /50 degree lifter bar.

The mill power was monitored by a set of torque transducers mounted on the drive shaft. The mill was run at 50% fill with ROM waste rock of +12.5 mm from a Witwatersrand gold mine. Torque readings and slurry samples were taken at regular intervals during the 90 minute duration of each run. These samples were analysed for moisture content as well as solids content finer than 75μm.

The mill power results observed as a function of time for the various liner configurations all followed a clear trend (figure 2.8). The mill power increases initially with time before passing through a maximum after which there is a steady decrease in power. The variation is thought to occur due to a change in voidage of the mill charge hence changing the torque arms generated by the slurry phase and coarse rock. The voidage tends to decrease with time as the smaller particles fill the voids between the coarser rock and the power curve levels out as this phenomenon occurs. The critical time period in the test is found to exist between 40 to 60 minutes. During this period the pulp has a solid content that conforms to normal milling practice (70 % solids).

The results show that the grid liner uses the most and the 70 mm long /90 degree lifter uses the least energy to produce the same amount of material smaller than 75 μm. The rates of breakage of the +12.5 mm ore was also recorded for each liner set and it was again found that these rates were highest for the 70 mm long /90 degree lifters (18 % higher than the grid liners). The 70 mm lifter bars also produced 16% more 75 μm material than the 50 mm lifter.

By monitoring the net energy expenditure per ton of new 75 μm material produced, it was found that a reduction in energy requirements of 33% was recorded when the face angle of the lifter was increased from 50° to 90°. The lifter bars were found to be 21% more energy efficient than conventional grid liners.

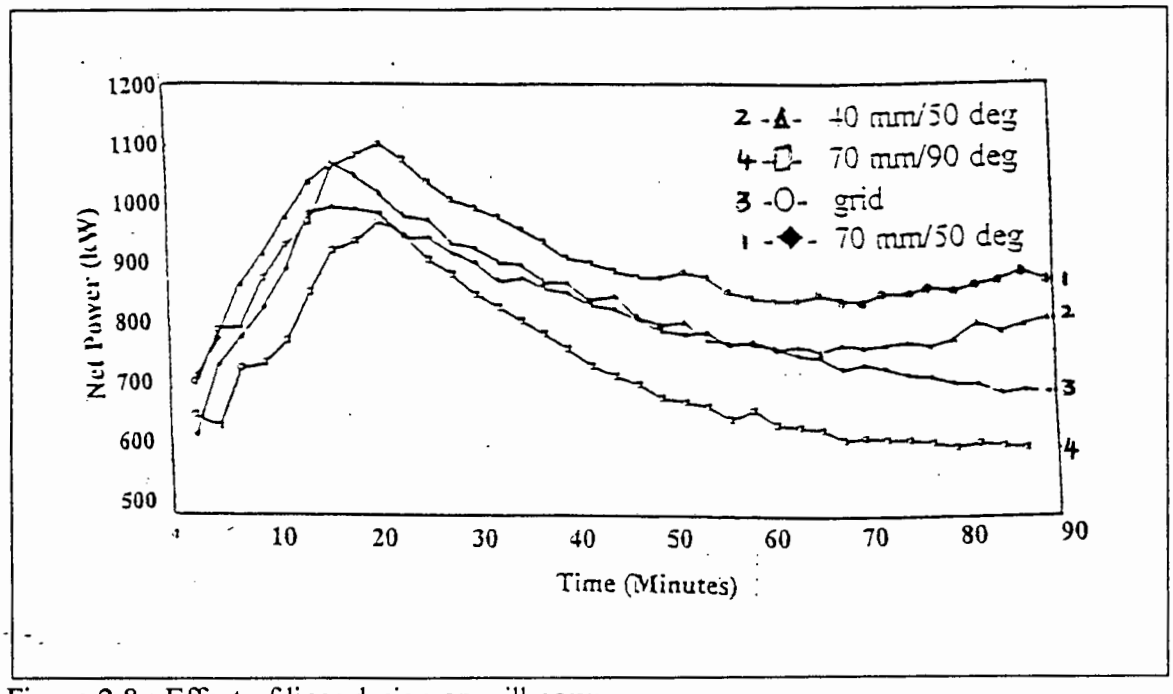

Figure 2.8 : Effect of liner design on mill power

This work illustrates the enhanced grinding rates and decreased energy expenditure with the use of lifter bars over traditional grid liners. It is evident from the results obtained in this work that operating costs of the mills could be largely reduced if the shapes of the lifter bars were optimised.

2.2.11 A study of charge motion in rotary mills with particular reference to the grinding action [6]. (M.S.Powell 1993)

Powell undertook a study to develop a fundamental understanding of the grinding charge in a mill and to correlate this with metallurgical performance of different mill liners. The motion of the balls deep within the mill charge was analysed. X-ray filming and gamma camera filming was used to track a radioactive ball in the mill. The ball was tracked over many revolutions and over a range of mill speeds and liner configurations.

The results illustrated that the trajectories of the balls are very smooth throughout the charge and that the balls do not rotate about their own axes. The actual centre of mass of the charge was determined and it was found to provide the correct form of the torque curve when the torque-arm method was used.

The amount of the slip was determined to be independent of the liner configuration once the charge is keyed into the rotary motion of the mill. The angle of repose of the charge was found to be totally dependent on the centre of rotation of the mill and the face angle was found to effect both the maximum impact energy as well as the amount of work undertaken by the charge. Radial segregation was noted to occur according to the mass and size of the balls. There existed a speed for which no segregation occurred but where equal mixing was evident. The liner design was noted to have an affect on the segregation.

Milling trials were undertaken on a 1.8 m diameter batch mill. The investigation determined the influence of liner design on the rate of production of fines in the mill running in autogenous mode. The torque of the mill was monitored with strain gauges attached to the drive shaft. The results of the milling experiments were compared with the motion of the grinding media.

Powell determined that a change in liner configuration cause variations of up to 40 % in the rate of production of fines in the mill. The height and spacing of the lifters were found to be linked and the mill diameter was also observed to affect the optimal

spacing-to-height ratio. The power draw of the mill was determined to be a function of the mass of grinding media as opposed to the total mass of the charge.

Powell concluded that it is possible to minimise the energy consumption while maximising the milling rate. In order to do so, the lifter must have a sufficiently high profile to key-in the outer layer of grinding media while optimising the impact point of the charge on the mill.

3. THEORY

This chapter presents the derivation of the theoretical model which models the prediction of the outer trajectories of a single ball in a rotating mill with lifter bars of arbitrary parabolic shapes.

The theory has been developed specifically for lifter bars which have had their profiles constrained to have any parabolic shape of the form :

$$y = Ax^2 + C$$

Where A and C are constants and can be changed to obtain a desired shape of lifter.

The system has been modelled in such a way that A must always be negative. In this thesis the A values are referred to in terms of the modulus values. Larger values of A are thus further away from zero but are negative and smaller values of A are the negative values closer to zero.

The system is modelled by considering only one ball on one parabolic lifter bar which is fixed to the inside of a rotating cylinder (Figure 3.1).

The theoretical model considers all six phases of the ball's motion. A separate set of equations is derived for each phase. The six phases relate to the type of motion the ball undergoes in one full cycle (from the neutral position (Figure 3.2) to the point of impact on the mill liner) and are :

- The Equilibrium phase.
- Rolling.
- Transition from rolling to sliding.
- Sliding.
- Departure.
- Parabolic trajectory.

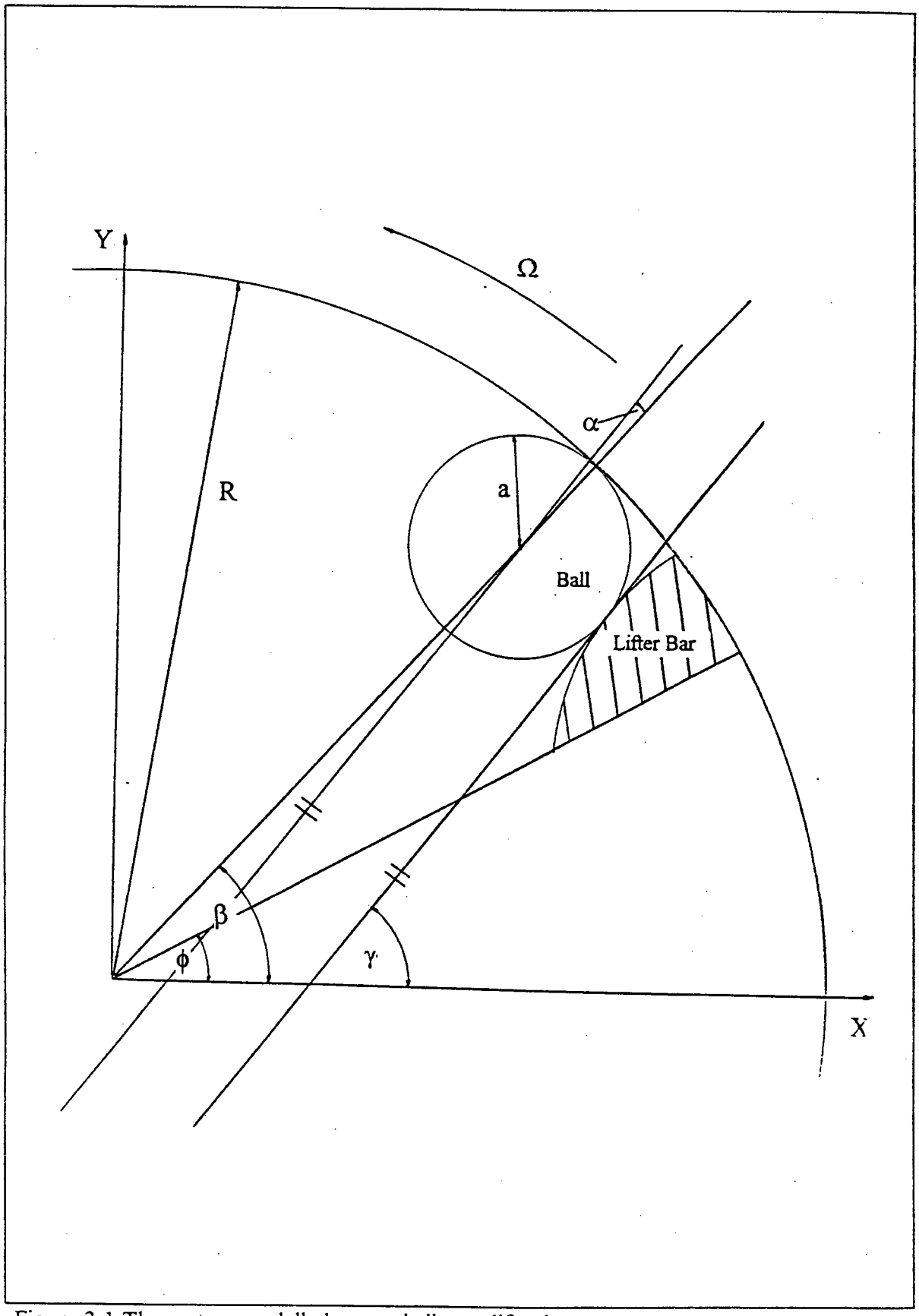

Figure 3.1 The system modelled as one ball on a lifter bar

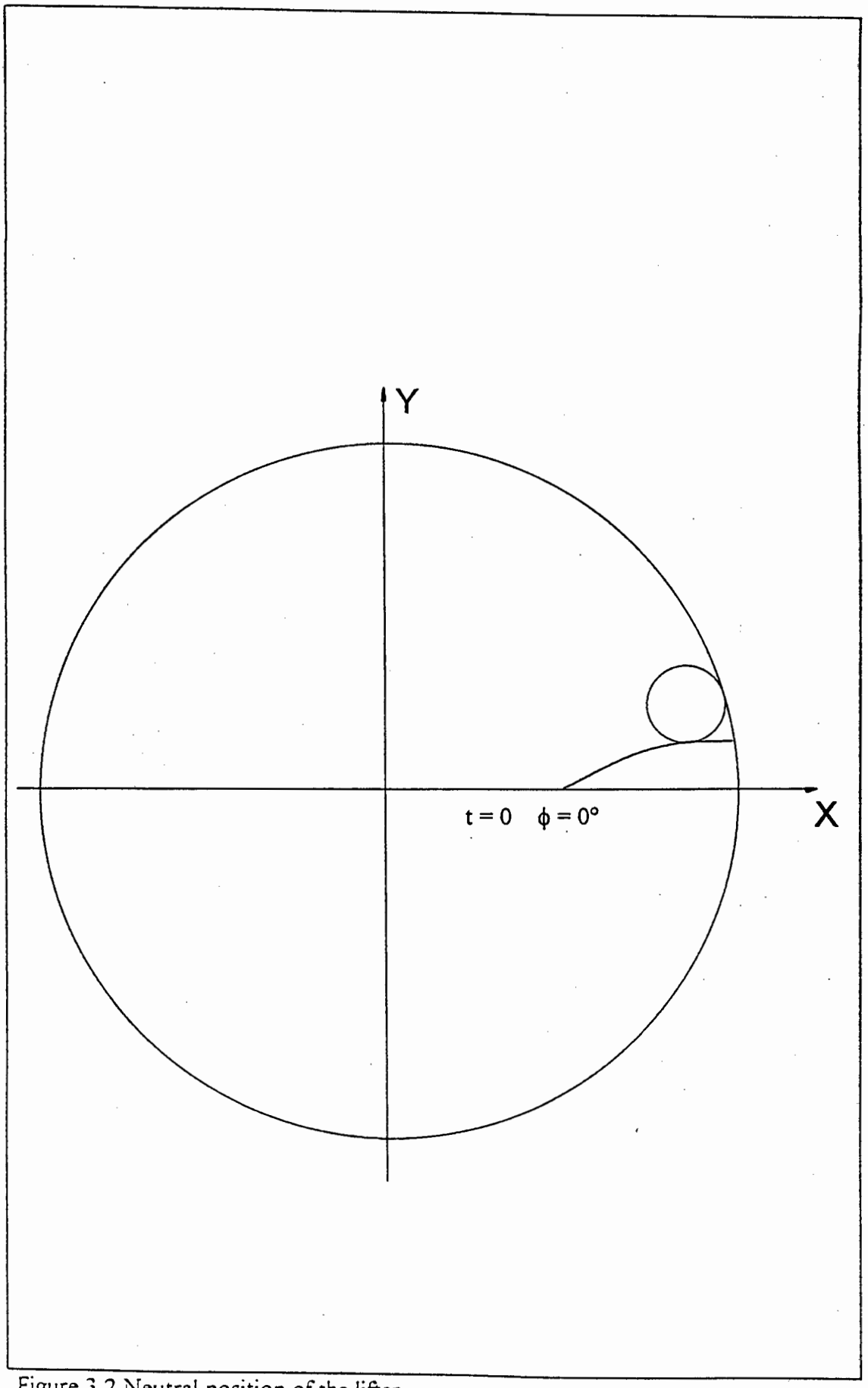

Figure 3.2 Neutral position of the lifter

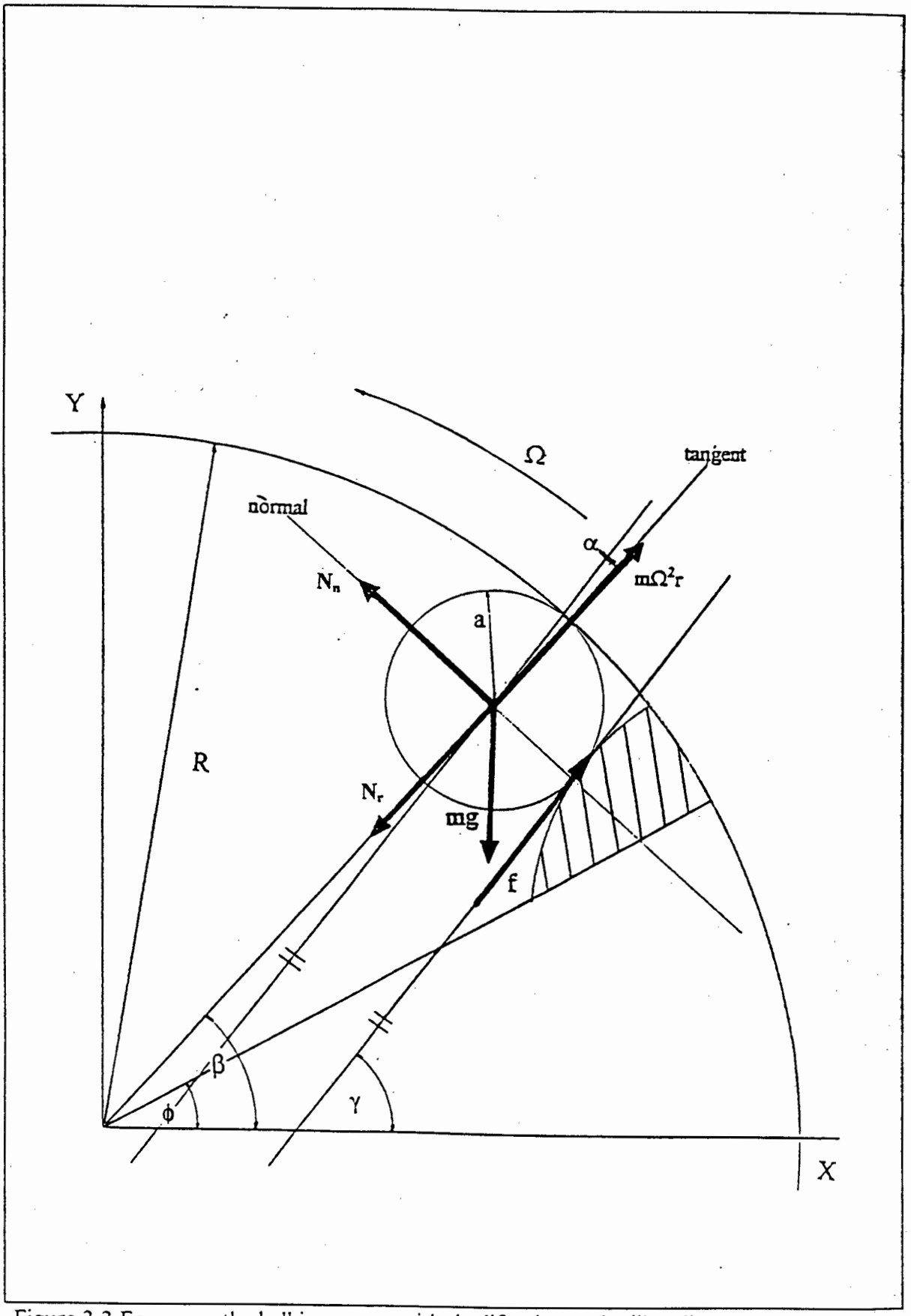

Figure 3.3 Forces on the ball in contact with the lifter bar and mill wall

All the forces acting on the stationary ball are illustrated in figure 3.3 and these forces are :

mg - The gravitational force (Acting vertically downward)

$m\Omega^2 r$ - The centrifugal force (Acting radially outwards)

N_n - Normal force on the lifter face.

N_r - Radial force at the mill wall.

f - Friction force between the ball and the lifter.

The three equations governing the ball's motion are :

The sum of forces tangential to the lifter face.

$[\ \Sigma\ \mathbf{F_{tangent}} = \mathbf{ma_t}\ ]$

$$mg\ \sin\gamma_t - f - m\Omega^2 r_t \cos\alpha_t + N_r = ma_{tangential} \qquad \textbf{(Equation 1)}$$

The sum of forces perpendicular to lifter face.

$[\ \Sigma\ \mathbf{F_{normal}} = \mathbf{ma_n}\ ]$

$$N_n - mg\ \cos\gamma_t - m\Omega^2 r_t \sin\alpha_t = ma_{normal} \qquad \textbf{(Equation 2)}$$

The sum of the moments about the centre of the ball (derivation in App II).

$[\ \Sigma\ \mathbf{M_{ball\ centre}} = \mathbf{I_{\ ball\ centre}}\varphi\ ]$

$$f = (2/5)ma_{tangential} \qquad \textbf{(Equation 3)}$$

Where the subscript "t" refers to time dependent variables.

Two sets of co-ordinates are used in defining the system (figure 3.4).

- A local co-ordinate system which has an origin at the radius of the mill. This system rotates as the mill rotates.
- A global co-ordinate system which has its origin at the centre of the mill. This system is stationary.

In order to simplify the equations, all the variables have been defined in terms of only x_b (local contact co-ordinate) and time. A set of geometric transformations are derived in order to define the variables in this manner. The derivation of these transformations are listed in Appendix III.

All the calculations are performed in local co-ordinates and the solutions are subsequently transformed back into the global co-ordinate system.

The equations derived in the theory apply to all the possible operating conditions.

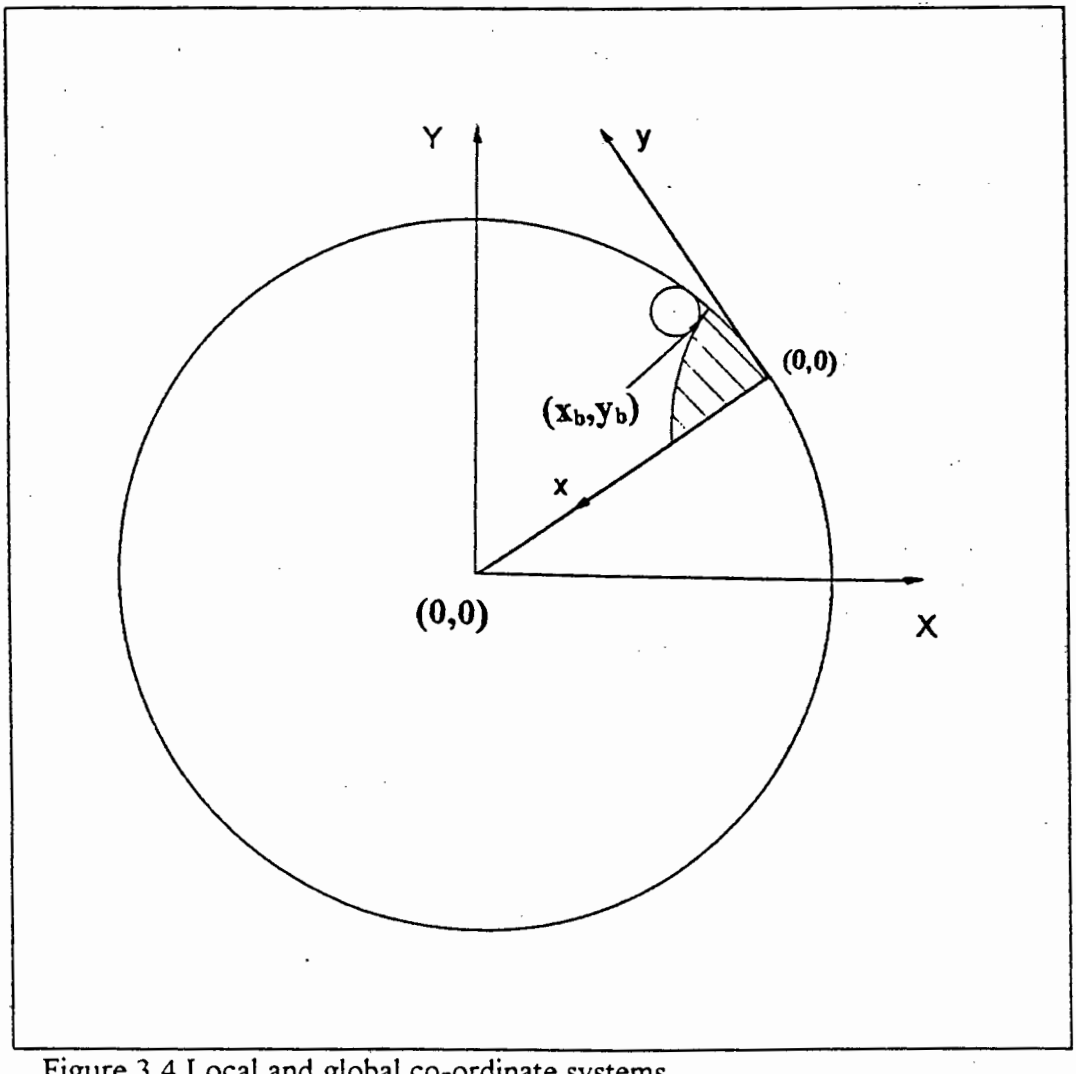

Figure 3.4 Local and global co-ordinate systems

3.1 INITIAL CONTACT CONDITIONS

The first step of the analysis is to determine the contact co-ordinates of the ball (x_{bo},y_{bo}) on the lifter while it is still in contact with the mill wall. This co-ordinate point is used as the initial condition in the numerical solution schemes.

The contact point is determined with the ball stationary in the neutral position where $\phi = 0$ and $t = 0$.

were :

ϕ = The angle of the base of the lifter above the horizontal.
t = The time of rotation from the horizontal position.

The local to global X and Y transformation equations in Appendix III are firstly simplified by substituting 0 for ϕ and t and then by using the resultant transformations to define an equation which is solved by using an appropriate iteration scheme.

From figure 3.5 :

$$r = \sqrt{X_c^2 + Y_c^2}$$

and :

(X_c , Y_c) is the global co-ordinate of the centre of the ball.

In order to determine the contact point the following must be satisfied.

$$\sqrt{X_c^2 + Y_c^2} = (R - a) \qquad \textbf{(Equation 4)}$$

The transformations are :

$X_c = R - x_c$

$Y_c = y_c$

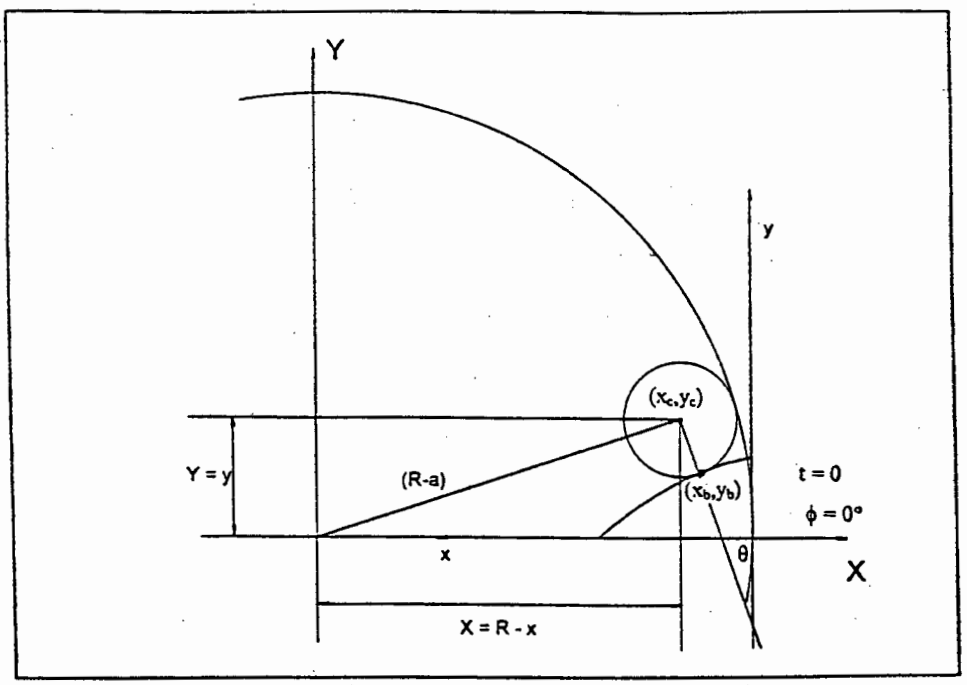

Figure 3.5 Transformation from local to global co-ordinates at the neutral position

To relate this to contact points (x_b, y_b) :

$x_c = x_b + a\sin(\theta)$

$y_c = y_b + a\cos(\theta)$

Substituting the transformations into equation 4, equation 5 is obtained and must be satisfied to determine the contact point.

$$\sqrt{\left(R - \left(x_b + a\sin(\theta)\right)\right)^2 + \left(y_b + a\cos(\theta)\right)^2} = (R - a) \qquad \textbf{(Equation 5)}$$

The equation is satisfied by applying an iterative difference method solution scheme. This method is described in detail in Appendix IV.

3.2 EQUILIBRIUM

The ball is initially at rest on the floor of the mill and as the mill rotates the ball rotates with the mill. This movement is facilitated by the presence of the lifter bar and the "keying in" effect. This is effectively the friction property between the ball and the lifter bar. This property inhibits movement of the ball down the lifter face.

As the mill rotates, an angle of equilibrium is reached where the sum of forces acting along the tangent of the lifter bar at the point of contact becomes zero. At this point the mass component along the tangent overcomes the equivalent centrifugal component and the normal force at the mill wall (N_{re}) becomes zero.

The ball is stationary until this equilibrium angle is reached and therefore the tangential and normal acceleration terms acting on the ball on the lifter are zero until the equilibrium angle is exceeded. The distance from the centre of the mill to the ball remains fixed until the ball starts to roll down the lifter bar. The distance from the centre of the mill to the centre of the ball at equilibrium is :

$r_{te} = (R - a)$.

The equilibrium angle is not dependant on whether the ball will initially exhibit a rolling or sliding motion down the lifter face. Vermeulen[23] and Powell[7] illustrated that the equilibrium angle is only dependant on the static coefficient of friction (μ_s).

The equilibrium equation is derived as follows :

Substituting $N_{re} = 0$, $a_{tangential} = 0$ and $r_{te} = (R - a)$ in equation 1, gives

$mg \sin\gamma_{te} - f - m\Omega^2(R-a)\cos\alpha_0 = 0$ **(Equation 6)**

The friction term is :

$f = \mu N_n$ **(Equation 7)**

Setting $a_{normal} = 0$, $r_{te} = (R - a)$ and rearranging equation 2 yields :

$N_{ne} = mg\cos\gamma_{te} + m\Omega^2(R-a)\sin\alpha_0$ **(Equation 8)**

where N_{ne} = Normal force component at the equilibrium point.

Combining equation 8 and equation 7 with equation 6 the following equilibrium relationship is obtained.

$g\sin\gamma_{te} - \mu(g\cos\gamma_{te} + \Omega^2(R-a)\sin\alpha_0) - \Omega^2(R-a)\cos\alpha_0 = 0$ **(Equation 9)**

where :

$\alpha_0 = \gamma_0 - \beta_0$

as derived in Appendix V.

Equation 9 cannot be solved explicitly and a Newton Raphson scheme is used to determine the equilibrium angle (Appendix VI). This scheme gives rise to the following equilibrium equation.

$$\gamma_{te_{i+1}} = \gamma_{te_i} - \left[\frac{\Omega^2(R-a)\left[\cos(\alpha_0) + \mu\sin(\alpha_0)\right] + \mu g\cos(\gamma_{te_i}) - g\sin(\gamma_{te_i})}{-g\left[\mu\sin(\gamma_{te_i}) + \cos(\gamma_{te_i})\right]}\right]$$

(Equation 10)

Where from the definition of the equilibrium variables :

$\alpha_{te} = \alpha_0$

$\beta_{te} = \gamma_{te} - \alpha_{te}$

The time taken for the ball to reach equilibrium is given by (Derivation from Appendix III equation A - 6) :

$$time_{te} = \frac{\gamma_{te} - \arctan(-2Ax_b)}{\Omega} \qquad \textbf{(Equation 11)}$$

The mill rotation angle is :

$\phi_{te} = \Omega \cdot time_{te}$

3.3 ROLLING

Assuming the ball starts to roll before it slides the following derivation determines the equation governing the ball's rolling motion down the lifter face.

The ball is no longer in contact with the mill wall and N_r is therefore equal to zero.

Combining equation 1 and 3.

$mg \sin\gamma_t - (2/5)ma_{tangential} - m\Omega^2 r_t \cos\alpha_t = ma_{tangential}$ **(Equation 12)**

and simplifying equation 12 :

$g \sin\gamma_t - (7/5)a_{tangential} - \Omega^2 r_t \cos\alpha_t = 0$ **(Equation 13)**

Let $a_{tangential} = \ddot{S}$

therefore :

$$\ddot{S} = \frac{5\left(g\sin(\gamma_t) - \Omega^2 r_t \cos(\alpha)\right)}{7} \qquad \textbf{(Equation 14)}$$

From Appendix VII

$$\ddot{S} = \frac{\ddot{x}}{\cos\left(\gamma_t - \Omega t\right)} \qquad \textbf{(Equation 15)}$$

and :

$$\dot{S} = \frac{\dot{x}}{\cos\left(\gamma_t - \Omega t\right)} \qquad \textbf{(Equation 16)}$$

Equating equations 14 and equation 15 and rearranging :

$$\ddot{x} = \frac{5\left(g\sin(\gamma_t) - \Omega^2 r_t \cos\left(\alpha_t\right)\right) \times (\cos(\gamma_t - \Omega t))}{7} \qquad \textbf{(Equation 17)}$$

Equation 17 is first transformed into a system of two first order linear differential equations.

Let the transformation be :

$$\dot{x} = v \qquad \textbf{(Equation 18)}$$

so :

$$\ddot{x} = \dot{v}$$

Substituting this transformation into equation 17 yields :

$$\dot{v} = \frac{5\left(g\sin(\gamma_t) - \Omega^2 r_t \cos\left(\alpha_t\right)\right) \times (\cos(\gamma_t - \Omega t))}{7} \qquad \textbf{(Equation 19)}$$

Equation 18 and 19 make up the system of first order equations which are solved by a fourth order Runga Kutta scheme (Appendix VIII - 2). The results obtained from the Runga Kutta equations give the x velocity ($\dot{x}$) and the x position of the ball on the lifter bar during the rolling phase of motion.

The initial conditions required to solve the first step of the scheme are x_{bo} and $time_{te}$. The value of x_{bo} is obtained from the solution of equation 5 and the value of time ($time_{te}$) is determined from equation 11.

3.4 MAXIMUM ANGLE FOR PURE ROLLING

It is evident from equation 3 that friction during rolling is directly proportional to tangential acceleration. As the ball accelerates the friction increases. This process continues until the acceleration becomes large enough to overcome the limiting friction $\mu_s N$. Beyond this point the acceleration is too high for rolling to occur and the ball will start to slide down the lifter face.

From equation 7 limiting friction is defined as :

$$f = \mu_s N_n$$

Rewriting equation 2 yields :

$$N_n = mg\cos\gamma_t + m\Omega^2 r_t \sin\alpha_t + ma_{normal} \qquad \textbf{(Equation 20)}$$

where :

$$a_{normal} = \frac{\dot{S}^2}{\rho} \qquad \textbf{(Equation 21)}$$

From Appendix III

$$\rho = \frac{[1+4A^2x^2]^{\frac{3}{2}}}{2|A|}$$

Substituting equation 3 and equation 20 into equation 7 yields :

$$\ddot{S} = \frac{5\mu}{2}[g\cos(\gamma_t) + \Omega^2 r_t \sin(\alpha_t) + \frac{\dot{S}^2}{\rho}] \qquad \textbf{(Equation 22)}$$

Substituting equation 14 into equation 22, yields :

$$\frac{\left(g\sin(\gamma_t) - \Omega^2 r_t \cos(\alpha_t)\right)}{7} = \frac{\mu}{2}\left[g\cos(\gamma_t) + \Omega^2 r_t \sin(\alpha_t) + \frac{\dot{S}^2}{\rho}\right] \qquad \textbf{(Equation 23)}$$

which must be satisfied before sliding can occur.

3.5 SLIDING

At the transition point where the ball reaches an acceleration large enough to overcome static friction the ball will exhibit a mixture of sliding and rolling. It was determined by Vermeulen[23] that this motion can be modelled as pure sliding.

The expression governing the ball's sliding motion is determined by rewriting equation 1 to facilitate the limiting friction i.e. (substituting equation 7 into equation 1 and letting $N_r = 0$ due to the ball having left the mill wall).

$$mg \sin\gamma_t - \mu_k N_n - m\Omega^2 r_t \cos\alpha_t = ma_{tangential} \qquad \textbf{(Equation 24)}$$

Noting that :

$$a_{tangential} = \ddot{S}$$

and

$$a_{normal} = \frac{\dot{S}^2}{\rho}$$

and substituting equation 20 into equation 24 gives the governing equation defining the ball's sliding motion down the face of the lifter bar as follows :

$$\ddot{S} = g\sin(\gamma_t) - \Omega^2 r_t \cos(\alpha_t) - \mu_k\left(g\cos\gamma_t + \Omega^2 r_t \sin\alpha_t + \frac{\dot{S}^2}{\rho}\right)$$

(Equation 25)

Substituting equations 15 and 16 into equation 25 and rearranging gives :

$$\ddot{x} = \cos(\gamma - \Omega t)\left[g\sin(\gamma_t) - \Omega^2 r_t \cos(\alpha_t) - \mu_k\left[g\cos(\gamma_t) + \Omega^2 r_t \sin(\alpha_t) + \frac{\dot{x}^2}{\rho\left(\cos(\gamma_t - \Omega t)\right)^2}\right]\right]$$

(Equation 26)

Equation 26 must first be resolved into a system of two first order linear differential equations before it can be solved.

Let the transformation equation for this system be :

$$\dot{x} = v \qquad \textbf{(Equation 27)}$$

from this :

$$\ddot{x} = \dot{v}$$

Substituting these transformation into equation 26 :

$$\dot{v} = \cos(\gamma - \Omega t)\left[g\sin(\gamma_t) - \Omega^2 r_t \cos(\alpha_t) - \mu_k\left[g\cos(\gamma_t) + \Omega^2 r_t \sin(\alpha_t) + \frac{v^2}{\rho\left(\cos(\gamma_t - \Omega t)\right)^2} \right] \right]$$

(Equation 28)

Equation 27 and equation 28 are solved in the same manner as the rolling equations by using a fourth order Runga Kutta scheme (Appendix VIII - 3).

3.6 PARABOLIC TRAJECTORY

As the ball slides along the lifter bar, a point is reached where the ball will depart from the lifter face and be projected into a free flight trajectory.

The ball can leave the lifter bar if one of the following two conditions are satisfied.

- The ball reaches the tip of the lifter bar and falls off the end of the lifter face.
- The normal force (N_n) on the ball becomes zero.

The method of departure relates to the speed of the mill and the shape of the lifter. The ball will fall away from the lifter before reaching the lifter tip if the contact angle (γ_t) exceeds 90°, hence causing N_n to act in the same direction as gravity (figure 3.6*a*). This

condition is also facilitated by the curve of the lifter face and is more likely to occur for lifter bars that have higher values of A (where higher A values give rise to a rounded surface).

At lower speeds and for lifter bars that are less rounded or worn, the ball will roll off the end of the lifter bar and will be projected away from the tip of the lifter (figure 3.6*b*).

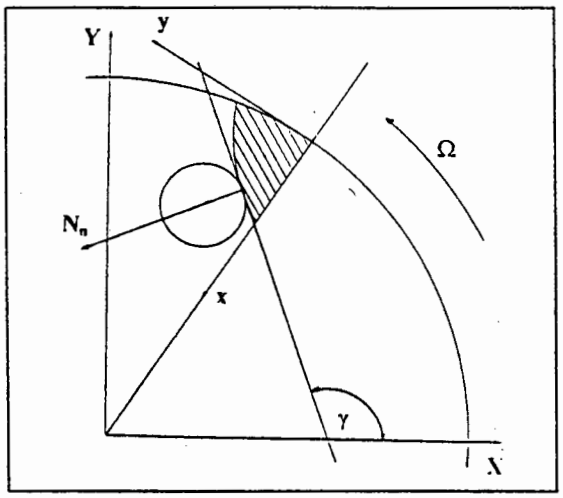

Figure 3.6*a* Departure with $N_n = 0$

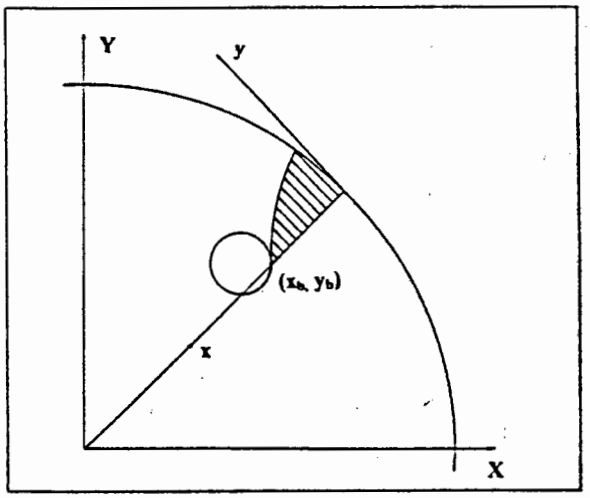

Figure 3.6*b* Departure at the limit

To determine at which point in time the ball leaves the lifter, the above mentioned conditions are monitored.

In order to determine if the ball is falling away from the lifter, equation 20 must be solved after every time step until $N_t = 0$ is satisfied. This translates to the fact that the ball has lost contact with the lifter and hence the point of departure has been determined.

Similarly, to determine whether the ball has left the tip of the lifter bar, the local y value (y_b) is monitored (where $y_b = Ax_b^2 + C$) after every time step until the limit ($y_b = 0$) of the lifter is reached. At this point the ball falls away from the lifter and is projected into a parabolic free flight trajectory.

All the departure variables (positions and angles) are calculated by the Runga Kutta solution scheme.

For determining the free flight trajectory it is convenient to change the reference frame from the local to the global co-ordinate system.

The ball may leave the lifter while $\gamma_{td} < 90$ degrees or if $\gamma_{td} > 90$ degrees. Both cases yield the same velocity equations (Appendix IX). It must also be noted that the solution to the sliding and rolling equations give the ball's velocity component in the local x direction ($\dot{x}$) and not the velocity of the ball down the face of the lifter ($\dot{S}$). See Appendix X to convert back to the velocity of the ball on the lifter face (V_L).

The departure velocity of the ball can be determined by considering the resultant of two velocity components, the velocity of the ball down the lifter face (V_L) and the velocity of the ball due to the rotational component of the mill (V_r) (figure 3.7).

Where :

$V_L = \dot{S}$

$V_n = \Omega r$

From Appendix IX

$V_x = - [V_n \sin(\beta_d) + V_L \cos(\gamma_d)]$ **(Equation 29)**

$V_y = [V_n \cos(\beta_d) - V_L \sin(\gamma_d)]$ **(Equation 30)**

The resultant velocity is :

$V_r = \sqrt{V_x^2 + V_y^2}$ **(Equation 31)**

Determining the angle of departure from the horizontal (β_{td}) :

$$\beta_{td} = \arctan\left(-\frac{Vy}{V_X}\right) \qquad \textbf{(Equation 32)}$$

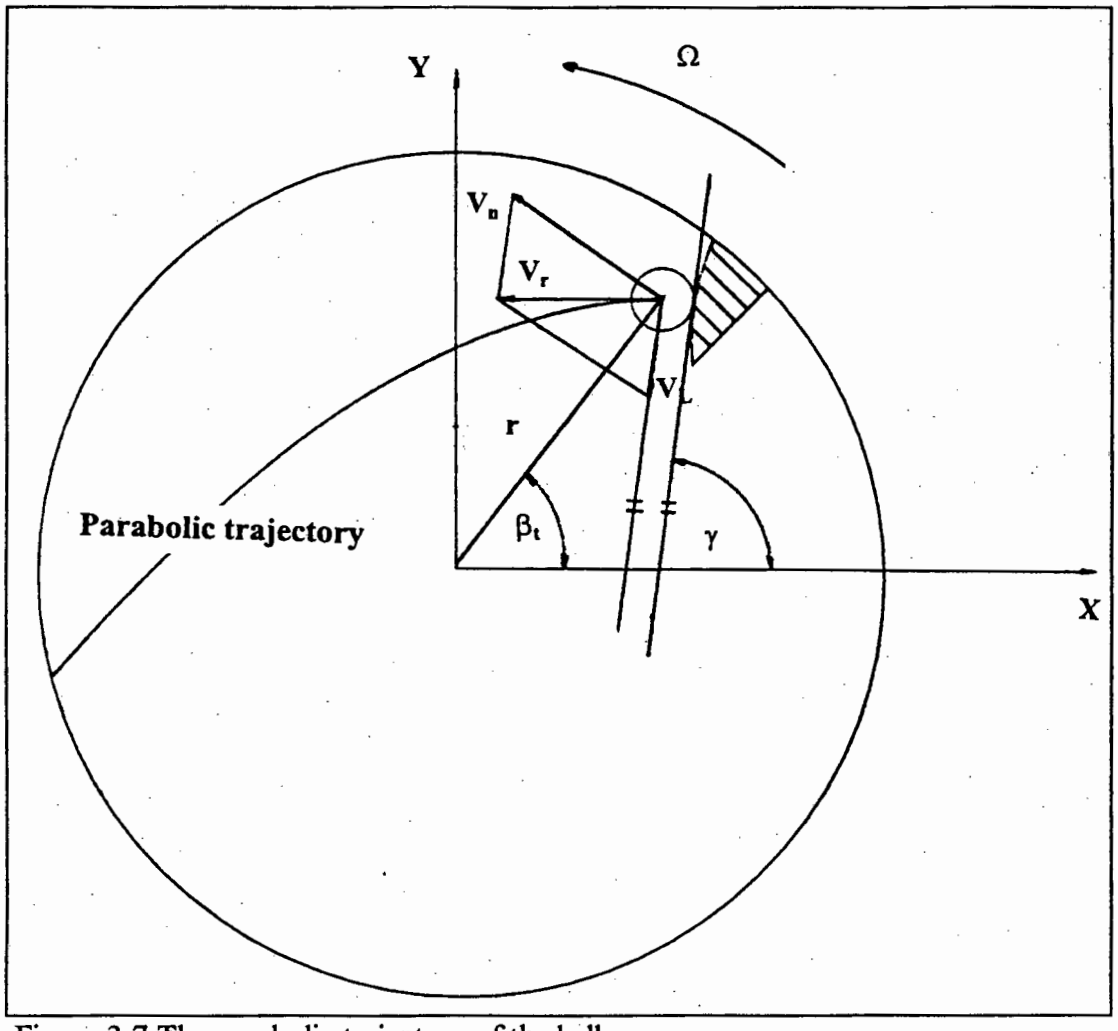

Figure 3.7 The parabolic trajectory of the ball

Once the ball is in flight the ball follows a parabolic path given by :

$$X = X_{td} + V_{xd}t_p \qquad \textbf{(Equation 33)}$$

where :

t_p = time from departure.

t_p is zero at the departure point and is stepped forward in time steps to determine the position of the ball at each time step in order to track the parabolic path.

The ball follows the parabolic flight path until the ball strikes the liner of the mill. This point is determined when the following equation is satisfied :

$$\sqrt{X^2 + Y^2} = (R - a) \qquad \textbf{(Equation 4A)}$$

The velocity of impact on the mill shell is determined by :

$$V_i = \sqrt{V_{xi}^{\ 2} + V_{yi}^{\ 2}} \qquad \textbf{(Equation 35)}$$

where :

$$V_{xi} = V_{xd} \qquad \textbf{(Equation 36)}$$

$$V_{yi} = V_{yd} - gt \qquad \textbf{(Equation 37)}$$

4. EXPERIMENTAL PROCEDURE AND RESULTS

A set of experimental tests were carried out on a model mill in order to determine the validity of the theoretical predictions. The tests were carried out to investigate visually the charge motion on the inside of the mill for varying mill speeds and lifter configurations. The power draw of the mill for the various speeds and different lifter bars was monitored in order to determine the most efficient operating condition and hence establish which is the most efficient lifter bar.

4.1 APPARATUS

- 250 mm diameter by 110 mm wide perspex mill.
- 5 mm and 6 mm diameter metal balls.
- Six sets (12 per set) of parabolic perspex lifter bars.
- Electric motor with a variable speed gearbox.
- Metal base on which the motor and mill was mounted.
- 4 rubber wheels attached to the drive shaft on which the mill runs.
- Tachometer.
- One spotlight.
- 16 strips of reflective tape.
- A10 - E video camera with a 10 mm video tape and accessories.
- Television Monitor.
- Video Recorder with a frame advance function.

A 250 mm diameter by 110 mm wide perspex mill with clear removable perspex side panels was used. Twelve lifter bars were bolted to the inside of the mill. The mill was filled with metal balls of 5 mm, 5,5 mm and 6 mm diameters. Six sets of varying shaped parabolic lifter bars machined from perspex were used in the experimental procedure (Figure 4.1). The lifter bars all had the form $y = Ax^2 + C$, with A and C having varying values to obtain lifter bars of various heights and profiles.

An A10-E Canon video camera was mounted on a tripod and used to capture the motion of the charge on a 10 mm video cassette. The camera operated at 25 frames per second and had three shutter speeds, 1/25, 1/500 and 1/1000 of a second. The exposure of the camera was set to an aperture setting on a scale between -2 and +1,5. A 1000 watt light was used to illuminate the mill during filming.

It must be noted that 25 frames per second was considered sufficient because :

- The mill only rotates at a maximum of 1.41 revolutions per second, thus allowing a frame to be captured at intervals of no more than 20 degrees.
- The charge pressure in the mill increases and decreases in a cyclic fashion. This causes the outer trajectories to change and hence a full cycle of charge pressure must be monitored in order to capture the full band of outer trajectories. This full cycle occurs over an interval of a few seconds and hence the slower image capturing technique can allow for a larger period of footage to be analysed.

The mill was run on four rubber wheels which in turn were connected to a constant speed electric motor with a continuously variable mechanical gearbox. Sixteen strips of reflective tape where attached to the back of the mill. A tachometer was used to monitor the speed of the mill and the rotating dial on the gearbox was used to increase or decrease the mill speed until the desired rotational speed was obtained.

The video camera had an onboard clock which was used to keep a record of the duration of each test and the position of the test on the tape. The test number was captured to film by holding a white board in front of the mill before each test.

A wattmeter was connected between the mains and the motor in order to measure the power draw of the motor for each test. The wattmeter considered the phase angle of the current and hence the power was read directly off the LED display.

The experimental apparatus is illustrated in figure 4.2.

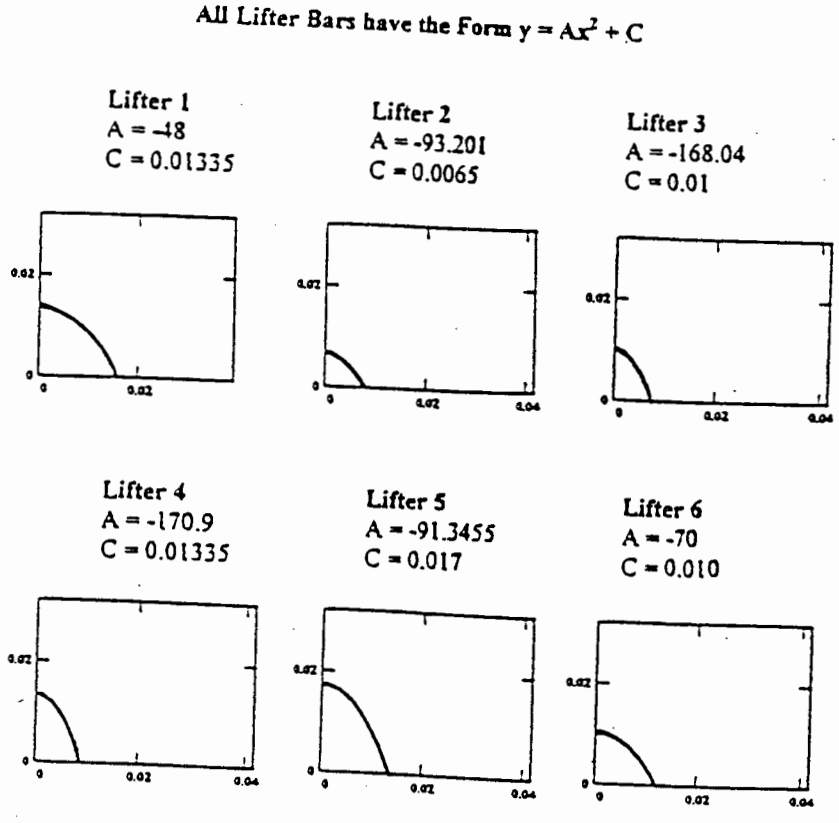

Figure 4.1 Profiles of the lifter bars used in the tests

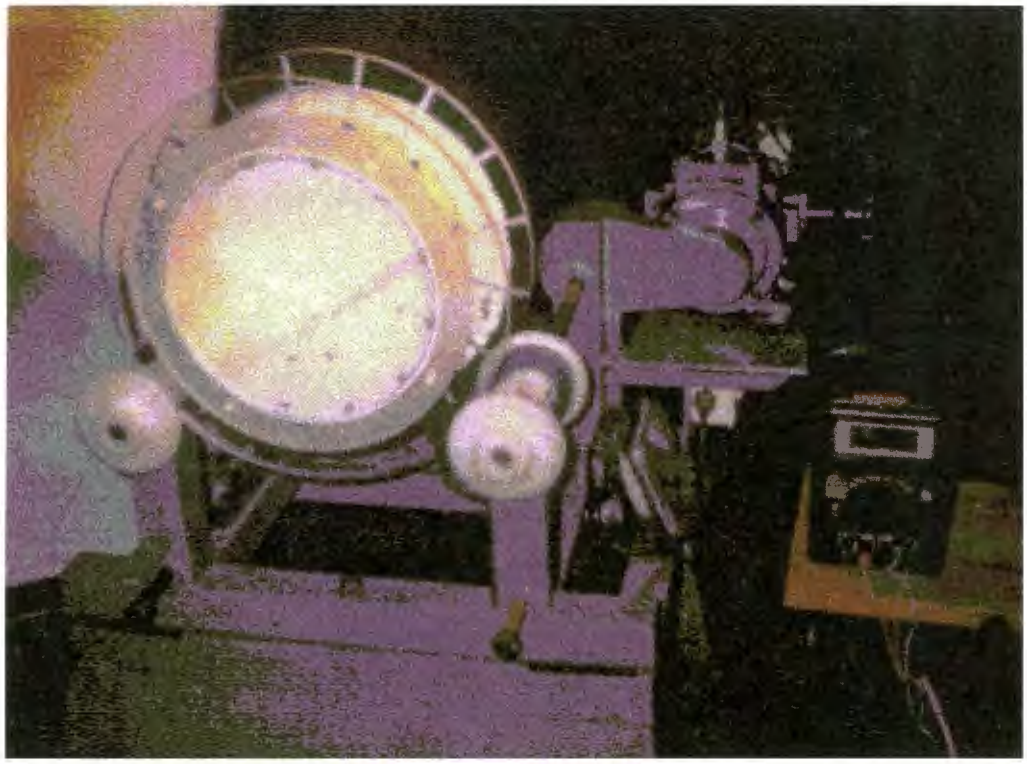

Figure 4.2 Experimental apparatus

4.2 FILMING OF THE CHARGE MOTION

The aim of filming the charge motion was to obtain data on the outermost trajectories of the media in the mill for varying mill speeds with different lifter bar configurations.

4.2.1 Filming preparations

The clear side panels of the mill were cleaned and polished in order to obtain clear images. A set of lifter bars was bolted into the mill and the mill was filled with steel balls to the required filling ratio.

The video camera was set at approximately 2 meters from the mill and the zoom function was used to fill the viewfinder in order to obtain the largest possible image. The reason for having the camera far away was to neglect the effect of depth of the particles in the mill. If the camera is too close to the mill, the side wall of the mill can be seen and this gives rise to the perception of depth and hence errors of parallax. The camera was also set up with the centre of the lens in line with the centre of the mill in order to ensure that there was no distortion of the image.

The back of the mill was covered with a sheet of white paper and the spotlight was positioned just to the left of the mill, shining slightly down to eliminate any reflection that might be picked up by the camera.

The readings from the tachometer were used to determine the speed of the mill. The tachometer readings were divided by sixteen (16 strips of reflective tape) to obtain the actual speed.

It was decided that each test would have a duration of thirty seconds and from trial runs it was determined that a shutter speed of 1/500 th. of a second and an aperture setting -1.5 would give the best quality video images.

4.2.2 Filming procedure

The tests were run with three different loading conditions.

- 10 % fill.
- 40 % fill
- With one layer of balls covering the base of the mill (Approximately 1% fill).

Six speeds ranging from 50 % critical to 100 % critical were used. Each series of tests was started at 50 % critical speed and the speed was sequentially increased by 10 % to 100 % critical.

Each set of lifter bars was tested at all three loading conditions and each loading condition was tested at all six speeds. This yielded 18 combinations of loading and speed for each lifter bar and hence a total of 108 tests.

The Critical speeds of the mill were calculated using :

$$\text{rpm} = \frac{42.3 \cdot \%\text{critical}}{\sqrt{D} \cdot 100} \qquad \textbf{(Equation 38)}$$

Where D is the internal diameter in metres.

The percentage critical mill speeds for the 250 mm diameter mill translated to the following rotational speeds :

Table 4.1 Mill Speeds

50	60	70	80	90	100	% Critical
4.42	5.31	6.21	7.09	7.97	8.86	rpm
42.3	50.76	59.22	67.68	76.14	84.6	Rad/s

4.3 ANALYSIS OF THE FILM

The main aim of the film analysis was to determine and plot the outer trajectories of the balls in the mill. These experimental results are used to make comparisons with the theoretical predicted trajectories. A visual representation of the charge motion in the mill could also be obtained from the analysis of the film footage. The effect of lifter height, lifter profile and mill speed on the shape of the charge motion was determined. The effect of volume fill on the charge motion and on the paths of the outer trajectories of balls in the mill was also investigated.

4.3.1 Analysis preparations

The film analysis was carried out by copying the film footage from the 10 mm video cassette onto a VHS video cassette and using a VHS video machine with a frame advance function to track the paths of the outer balls by looking at one frame at a time on a television monitor.

Care was taken to obtain a good transcript of the video footage when copying it into VHS format. It was also determined that the video recorder which was used had a good pause function and gave clear images when the film was stationary. The television screen had a flat surface so that no distortion was possible.

4.3.2 Analysis procedure

A transparent plastic sheet was placed over the television monitor and the outline of the mill was traced onto the sheet. A horizontal reference line that coinciding with the horizontal axis of the mill was drawn through the centre of the sheet. The film was advanced one frame at a time and the position of the outer balls were manually marked off on the sheet. The film footage was clear enough to identify and trace the paths of individual balls in the cateracting region. About 3 seconds of footage was analysed for each test. The balls were traced from the point of departure to the point of

impact on the mill shell. Due to the interactions of balls and the cyclic change in charge pressure, a wide band of trajectories was obtained for each test. (figure 4.3).

The size of the mill on the television monitor was not the same size as the original mill.. A scaling factor was therefore required to transfer all the co-ordinates back to the correct size.

The scaling function is :

$$\text{Scaling} = \frac{\text{Mill Diameter}}{\text{Projected Mill Diameter}} = \frac{0.25}{0.32} = 0.78$$

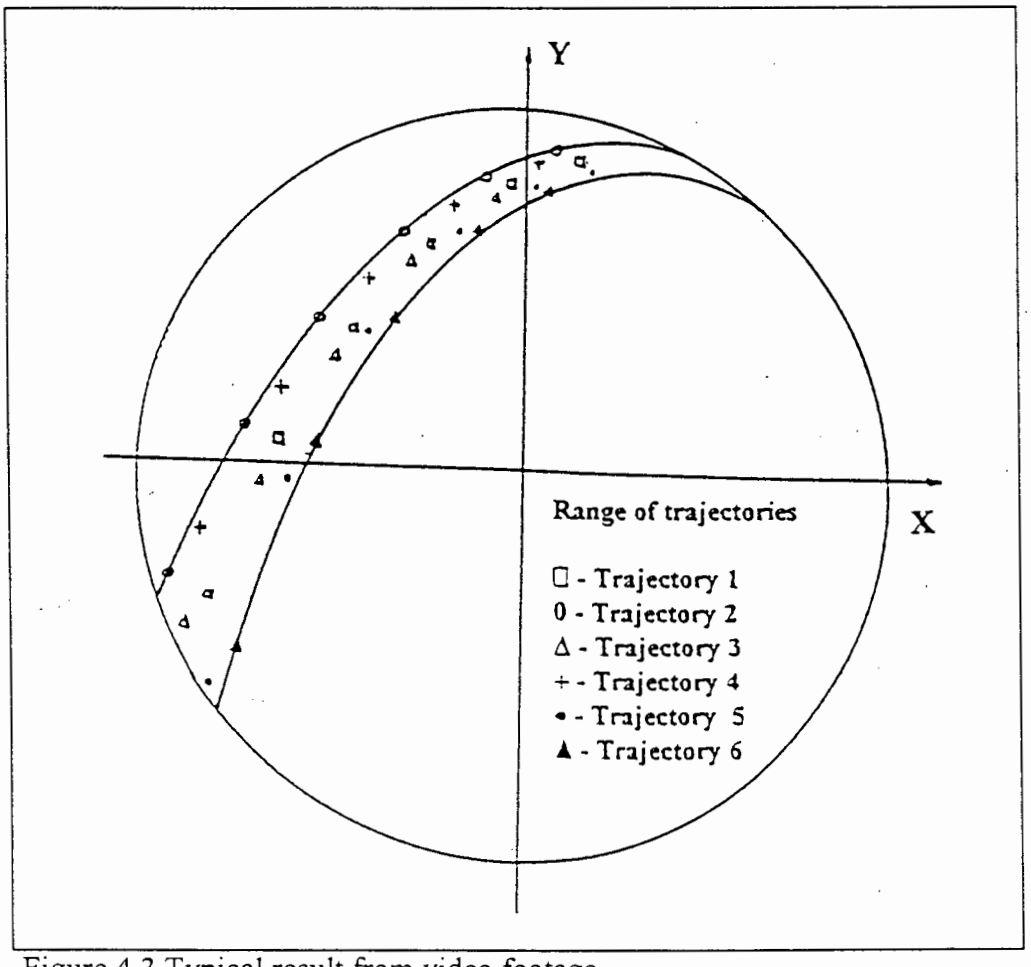

Figure 4.3 Typical result from video footage

4.3.3 Results from the video images

The results were divided into three categories, one for each percentage fill condition, thereby having 36 result sheets in each category. The 36 result sheets contained the band of plots of the outer trajectories for all 6 sets of lifter bars at all 6 speed settings.

The average trajectory of each band was used to determine discernible trends in the motion of the outer balls for the various conditions. Figure 4.4 illustrates the average trajectories for a series of solutions. All the results were analysed to determine if any trends existed between the trajectory of the media in the mill, the percentage fill of the mill, the mill speed and the lifter bar shape.

The effect on the outer trajectories by the various parameters was determined by considering three combinations.

- Determine the effect of the lifter bars on the outer trajectories by keeping the same percentage fill and the same mill speed and by only changing the lifter bars.
- Determine the effect of the mill speed on the outer trajectories by keeping the percentage fill constant and by considering only one lifter bar while varying the mill speed between 50% and 100% critical.
- Determine the effect of percentage fill of the mill on the outer trajectories by keeping the rotational speed of the mill constant and by considering only one lifter bar.

The results obtained from these experiments were used to obtain an insight into which variables are more dominant in effecting the charge motion. The results were also used to test the theoretical predictions that were obtained from the mill simulation program ("Mill simulator"). The listing of "Mill Simulator" is in Appendix XI and some simulation results can be found in Appendix XII.

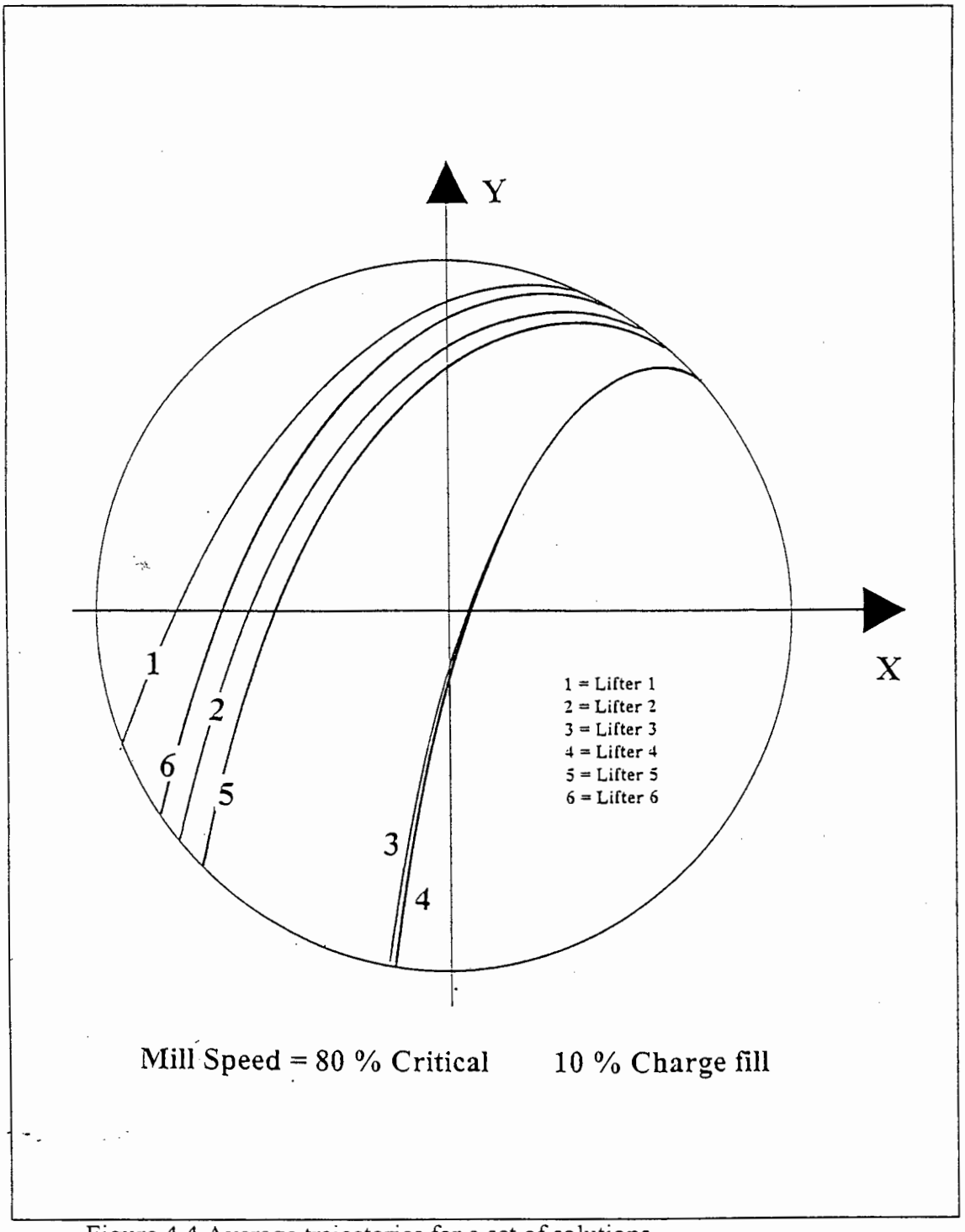

Figure 4.4 Average trajectories for a set of solutions

The results obtained from the experimental procedure are discussed in chapter 5.

4.4 POWER DRAW

The aim of this set of experiments was to plot the power draw of the mill as a function of the parabolic lifter shapes and the mill speed, for a specific volume fill.

4.4.1 Power measuring preparations

A wattmeter was connected in series with the electric motor. The wattmeter measured the direct power draw from the motor.

4.4.2 Power measuring procedure

The mill was first run at load for approximately ten minutes in order to obtain equilibrium due to heating effects in the bearings and in the gearbox fluids. The filming of the charge for a specific set of parameters, as described previously, was undertaken at this point. The power reading was noted down for each test (i.e. for each lifter bar at each speed and with each loading condition). A series of 108 power readings was obtained.

4.4.3 Results of power measurements

The accuracy of these readings were considered unacceptable due to large energy losses in the bearings and lubricating fluids. The change in power readings for the various conditions were undetectable due to these large losses.

4.5 MEASUREMENT OF COEFFICIENT OF FRICTION

An attempt was made to determine the static and kinetic coefficients of friction. Powell [4] determined that the coefficients of friction were affected by the vibration of the mill and hence could only accurately be determined for a specific speed and

percentage fill of any given system. This fact would necessitate individual coefficients of friction to be determined for all 108 tests.

It was therefore decided to conform to previous work and use the values determined by Powell [4]. A static coefficient of 0.23 (as determined for a vibrationless system) and a kinetic coefficient of 0.19 was therefore used in the theoretical calculations.

5. DISCUSSION

The experimental work will firstly be discussed and then used to support the theoretical model. Figure 5.1 illustrates the conventions used in this chapter.

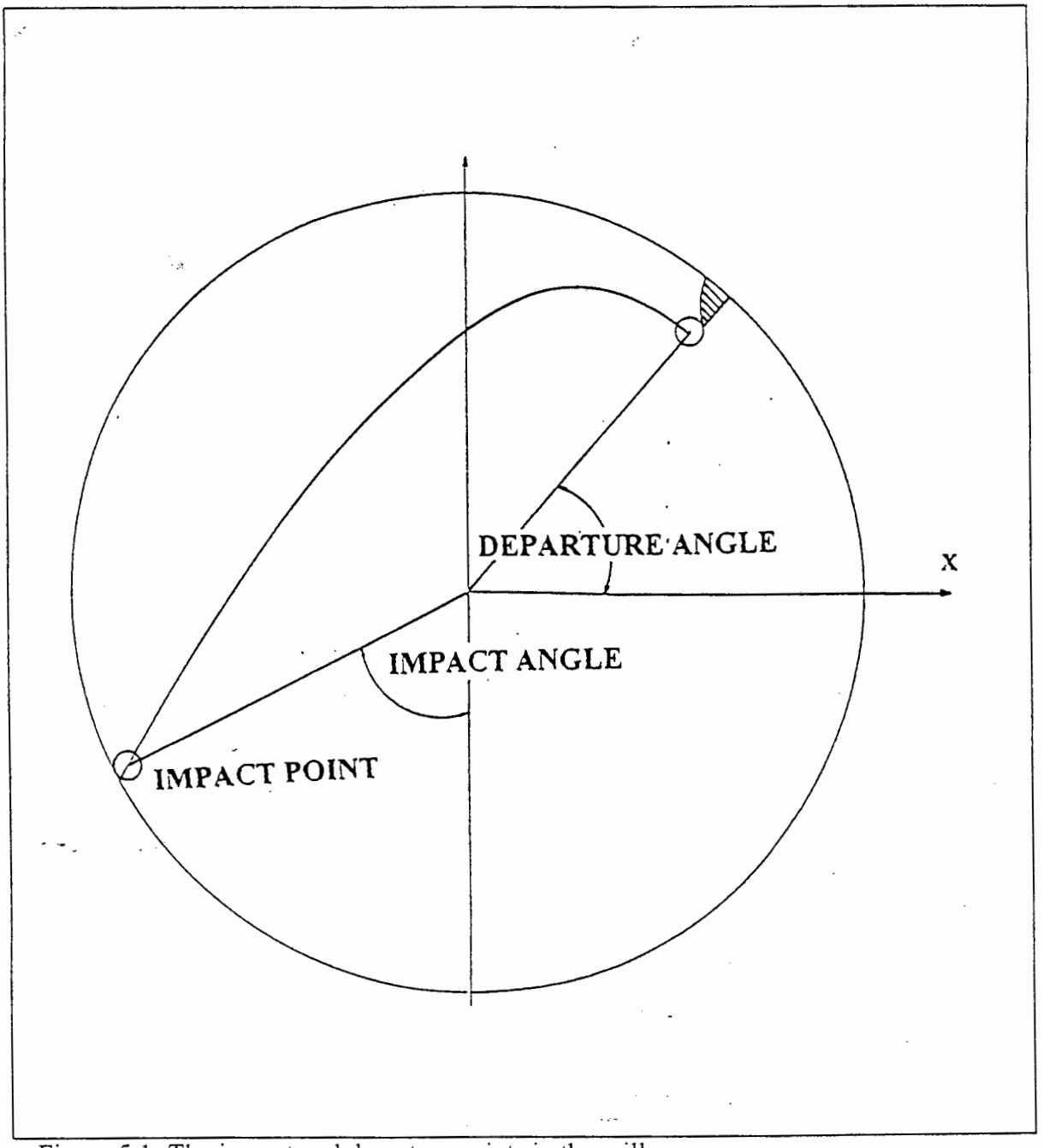

Figure 5.1: The impact and departure points in the mill

5.1 EXPERIMENTAL RESULTS

The experimental work was undertaken to obtain results by which the theoretical model could be compared as well as to analyse these results to determine the effects of lifter bar geometry, mill speed and percentage fill on the charge motion in the mill. The effect of lifter geometry, mill speed and percentage fill on the power draw of the mill was also investigated. The results illustrating the departure and impact angles for all the tests can be found in Appendix XIV.

The experimental results deal with only the outer layer of the mill charge. This is the section of the charge which is most highly effected by the liner configurations.

The results have been presented in such a way as to discus the effect of one parameter at a time on the charge motion and mill efficiency (i.e. Look at the effect lifter bars with different $|A|$ values have on a system with only one layer of balls covering the floor of the mill). In the following sections, the combined effect of these parameters on each other are investigated (i.e. The effect of % fill on the charge motion using only one specific lifter bar to determine the relationship). This will allow a full range of results to be used in the discussion illustrating the effect of all the variables on the shape of the charge motion. All the results illustrated in this chapter illustrate trends which are found to be common throughout the full range of tests.

5.1.1 Effect of various lifter bar profiles on outer trajectories

It is evident from an investigation undertaken by Vermeulen and Howat [15] that lifter bars function as slip reducers and that a mill with lifter bars show signs of reduced wear and increased liner life.

More importantly however it is necessary to determine the effect that different shaped lifter bars have on the charge motion. Powell [4,6] determined that for rectangular lifter

bars, the lifter height and face angle largely influenced the parabolic path of the outer layers of balls.

The work undertaken in this thesis considers the effect that worn lifter bars have on the outer trajectories, thereby allowing the effectiveness of worn lifter bars to be determined. The parabolic function $y = Ax^2 + C$ has been used to characterise the profiles of the worn lifter bars. The values of A and C can be changed to obtain different shapes of the worn lifters.

Figure 5.2 is a plot of the outer trajectories of media for the six parabolic lifter bars used for the case of one layer of balls covering the base of the mill.

It must be noted that the values of A are all negative in the theoretical model but are referred to as the modulus of the A values in the discussion. It can be observed that the outer trajectories are dependant on the values of A. The lifter with the lowest value of $|A|$ gives the highest trajectory and the lifter with the highest value of $|A|$ gives the lowest trajectory.

The reason for this phenomenon is that A determines the slope of the lifter face and more significantly the rate of change of the slope, where :

$$y = Ax^2 + C$$

so :

$$\dot{y} = 2Ax$$

and :

$$\ddot{y} = 2A$$

A lifter with a very steep face ($|A| = 171$) angle will cause the ball to have a lower equilibrium angle (As defined in section 3.2). The ball will start moving down the lifter bar sooner than a ball on a lifter with a flatter face angle ($|A| = 48$).

It is thus evident that a rectangular lifter bar will have a zero value of A (the slope of such a lifter is a zero). As the rectangular lifter bar wears down, the face will develop a slope and the value of $|A|$ will increase. As this value of $|A|$ increases for a specific lifter bar the impact angle decreases. The value of $|A|$ will reach a critical value at which point the impact angle will become too low and the outer envelope of milling media will not fall on the toe of the charge and will make the lifter inefficient. This is evident from the trajectories in figure 5.2. It is thus possible to identify when a lifter becomes worn down to a critical profile and needs to be replaced.

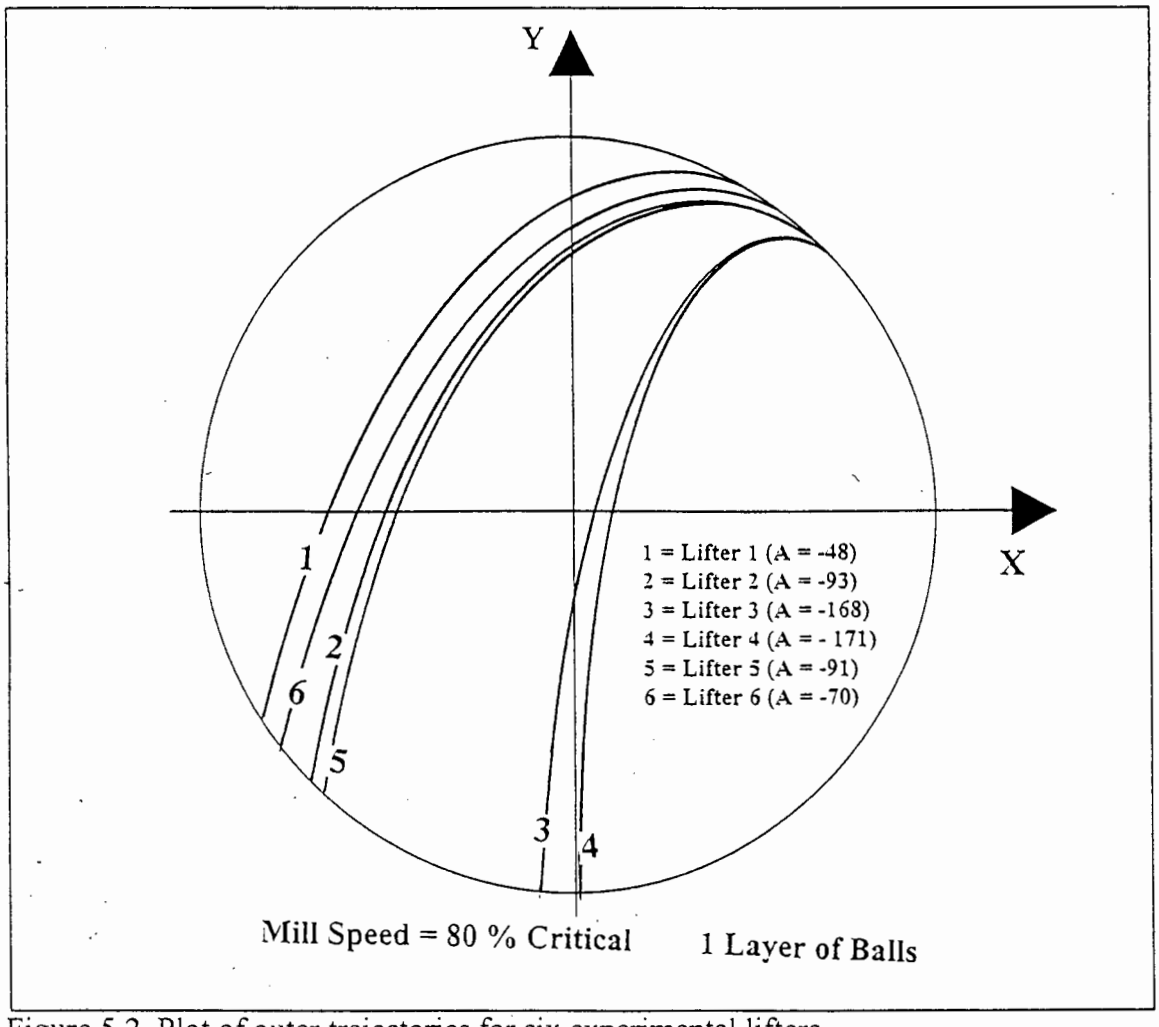

Figure 5.2 Plot of outer trajectories for six experimental lifters

5.1.2 Effect of mill speed on charge motion

Figure 5.3 illustrates the effect of mill speed on the outer trajectories of the balls in the mill.

The results illustrate that for a specific lifter bar (A = -48) the trajectories of the outer balls will be higher and the impact angle will become larger as the mill rotational speed increases. The speed can be increased until a critical speed is reached at which point the outer layer of balls will centrifuge against the mill wall.

The formula used by Powell [4,6] and adopted in this work is given by :

$$\text{Critical speed [\%]} = 100 \cdot \text{rpm}\left[\frac{\sqrt{D}}{42.3}\right] \qquad \textbf{(Equation 39)}$$

where :

D = Mill Diameter in metres.

The equation predicts the rotational speed at which a ball will centrifuge on the inside of a mill without lifters for a non-slip condition . The addition of lifters introduces an increased lifting effect. The additional lifting effect reduces the critical speed at which the balls will start to centrifuge. The balls therefore actually centrifuge at a speed lower than that predicted by equation 39.

As the value of $|A|$ tends to zero the critical speed decreases. A faster rotational speed is therefore needed to centrifuge a ball on a worn lifter than to do the same on a new rectangular lifter.

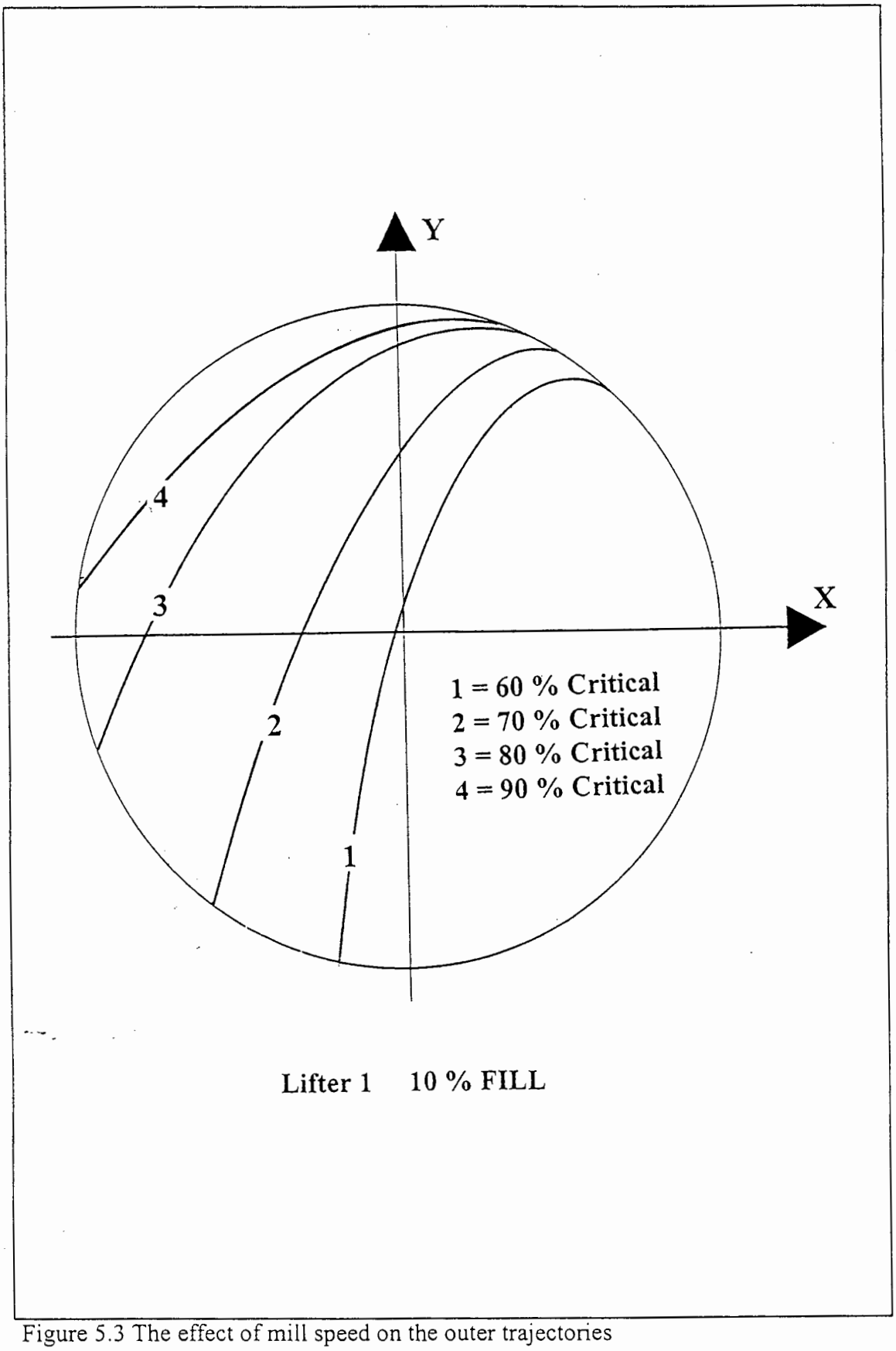

Figure 5.3 The effect of mill speed on the outer trajectories

White [9] recommended that a state of centrifuge should exist in the outermost layer in order to protect the liner against impact from the balls. The downfall of this notion is :

- A large amount of energy is required to run the mill at high speeds in order to keep the outer layer centrifuged. This does not imply that the mill will run more efficiently.
- As the lifter bars wear down, the speed required to centrifuge the outer layer of balls will increase and hence the balls will no longer centrifuge. This causes the balls to impact against the mill wall, causing damage and excessive wear to the mill liners.

In order to obtain the most efficient milling condition the mill speed should be regulated so that the balls will at all times fall on the toe of the charge. This is generally not possible as most mills run at constant speeds. It is more practical to design the liners to last longer while giving an acceptable range of impact points throughout its operating life.

5.1.3 Effect of percentage fill on charge motion

An investigation was undertaken to determine what effect the percentage fill of the mill has on charge motion. Gow et al [12] showed that centrifuging was also dependant on the percentage fill of the mill. Figure 5.4 illustrates this point. Figure 5.4 shows the results obtained from a series of experiments using the same lifter bar and the same mill speed but by varying the percentage charge fill of the mill. Similar results were obtained for all the other tests.

The outer trajectories are observed to increase as the percentage fill of the mill increases. The results compare favourably with the investigation undertaken by Vermeulen and Howat [15] where it was stated that the increase in charge pressure was the major reason for the increase in the trajectory heights and that charge pressure is proportional to percentage fill. The increase in charge pressure decreases the degree of slip between the mill and the charge and this causes the higher trajectories. The

increase in charge pressure also affects the rotational speed at which centrifuging will start to occur.

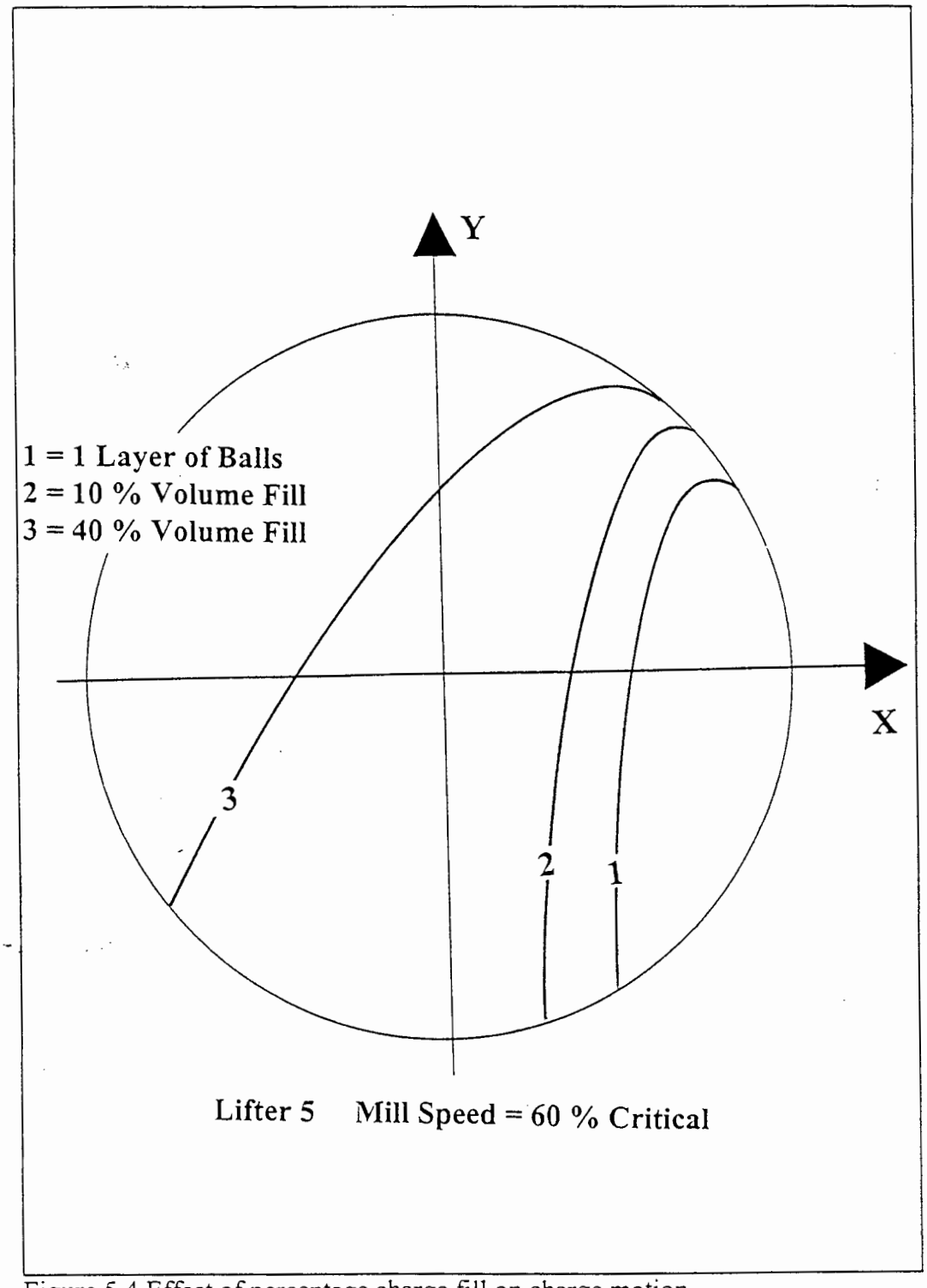

Figure 5.4 Effect of percentage charge fill on charge motion

5.1.4 Effect of lifter bar profiles, percentage fill and mill speed on power draw of the mill

Due to major problems encountered with the experimental equipment, the results obtained for the power readings were not deemed accurate. The following problems were encountered :

- The power draw of the mill was measured using a wattmeter which was connected in series with the motor. This gave fluctuations in power usage if other electrical equipment was being used in the building.
- The friction in the drive shaft bearings was very high and hence the torque on the drive shaft could not have been measured accurately. Small variations of power draw would not be detectable in this case.
- The fluid in the motor's gearbox fluctuated in viscosity as the fluid heated up.
- The dynamic modelling of the mill was inaccurate. The load-weight to mill-weight ratio of the system was approximately 0.7. This was too low. The coefficient of restitution of the balls on the perspex was too high. This caused the balls to bounce chaotically on the base of the mill.

5.2 VERIFICATION OF THE THEORETICAL MODEL

In deriving the theoretical model, the models by Powell [4] and Vermeulen[23] on determining outer trajectories for media in a grinding mill with straight faced lifter bars were considered. Some of the concepts used by Powell and Vermeulen have been modified and some of the reasoning used in determining their models have been questioned.

One of the principles under question during the derivation of the model was whether the ball first rolls and then slides or purely slides down the face of the lifter bar.

Powell's theoretical model considered the ball to initially roll and then slide down the face of the lifter bar. However, in the simulations Powell used a static coefficient of friction equal to 0 thereby neglecting the rolling part of the model. The motion of the ball on the lifter bar was assumed to be a pure sliding motion. Powell's results illustrated that the sliding model accurately predicted the observed results. The fact that Powell does not use experimentally determined friction values and that the kinetic friction coefficient used in the simulations is higher than the static friction coefficient can cause some doubts upon the exact correlation of the predicted and observed results.

Vermeulen[23] illustrated that although a ball exhibits a combination of rolling and sliding the friction is always sufficiently low for the latter to dominate. It was shown that a pure sliding model produces results which agree with the observed trajectories whereas a rolling model predicts much higher trajectories. The only doubt in this model is Vermeulen does not specify the measured coefficient of friction but uses the coefficient of friction as an adjustable variable to fit the predicted results to the observed trajectories.

The effect of the rolling/sliding as well as the pure sliding model was investigated. The simulation was set-up to consider two possible cases of the ball's motion on the lifter bar.

- The ball initially rolls and then slides down the lifter face.
- The ball only slides down the lifter face

The variables are :

- The values of A and C.
- Mill speed.
- Mill diameter.
- Ball diameter.
- Static and kinetic friction coefficient.

In comparing the theory with the experimental results, the following experimentally determined factors were used :

Diameter of Mill, D = 250 mm
Ball Diameter, a = 12 mm
Static Friction Coefficient = 0.23
Kinetic Friction coefficient = 0.19

In order to obtain experimental results by which the model could be compared, only one layer of balls was placed on the inside of the mill. This caused the effect of charge pressure to be discarded and the model (which considers the dynamic response of only one ball in the mill) could be compared with the experiments.

Figure 5.5 illustrates the comparison between the sliding model, rolling/sliding model (obtained from the "Mill Simulator") and the experimental results for one lifter profile at 80 % critical speed. Before making any conclusive statements about the validity of the comparisons between experimental and theoretical models, a few points relating to the accuracy of these results must be mentioned.

Firstly, the experimental mill is a poor equivalent of the real system with factors such as coefficient of restitution and coefficient of friction being difficult to accurately determine. Although an effort has been made to determine the experimental coefficient of friction a detailed study should be undertaken on the effect of friction in the system and how it effects the outer trajectories. This study remains outside the bounds of this thesis.

Another inaccuracy is the precision by which the departure point of the ball can be measured. Because the film speed is relatively slow (25 frames per second), the departure point appears to be higher than it actually is. This is purely caused by the fact that the ball has already left the lifter bar in the frame where the ball's position is noted as "departured". In order to accurately determine the exact point of departure a more sophisticated image processing technique should be used.

Another factor which effects the validity of the comparison is the accuracy by which the ball's path can be followed across the whole trajectory. The distance between two successive frames is large and thus the balls position can only be noted at two positions fairly far apart.

The validity of the results obtained from the experimental mill must also be questioned due to this mill not accurately representing the real system. As mentioned previously, the coefficient of restitution is excessively large giving rise to the chaotic bouncing effect of the balls as they impact on the mill wall. This in turn gives rise to an uncharacteristic vibration in the mill which may effect the friction values. Another factor which is grossly exaggerated in the model mill is the mill weight to charge weight ratio. It can thus be argued that the experimental mill is not a very good representation of the real mill and this may lead to the theoretical model predicting better "real" results than what is observed in the experimental mill. This concern may also contribute to the variation in trajectory shape and departure point of the experimental and theoretical models as illustrated in figures 5.5 and 5.6.

It is evident that the rolling model gives trajectories that are too high (as was predicted by Vermeulen) and that the sliding model more accurately correlates with the experimental results. A few inconsistencies relating to departure point and actual ball bath do exist for the sliding model, but these factors can be ascribed to the factors mentioned earlier.

The error in the hypothesis was found to be caused by the assumption that the static coefficient of friction is sufficient to cause the ball to initially roll down the lifter face. The rolling section of the model was discarded and the ball was assumed to slide from the point of equilibrium until it left the lifter. The new model was found to give better predictions of the equilibrium point, departure point as well as the actual parabolic trajectory followed by the ball. A listing of the sliding version of the "Mill Simulator" program is presented in Appendix XI.

All the results in figure XIV illustrate similar trends to figure 5.5.

Figure 5.6 illustrates the comparison of the experimental results and the sliding model. The results illustrate that the theoretical model gives a good indication of the ball path during milling. The slight deviations in departure point and trajectory shape should again be ascribed to the inaccuracies in the experimental procedure.

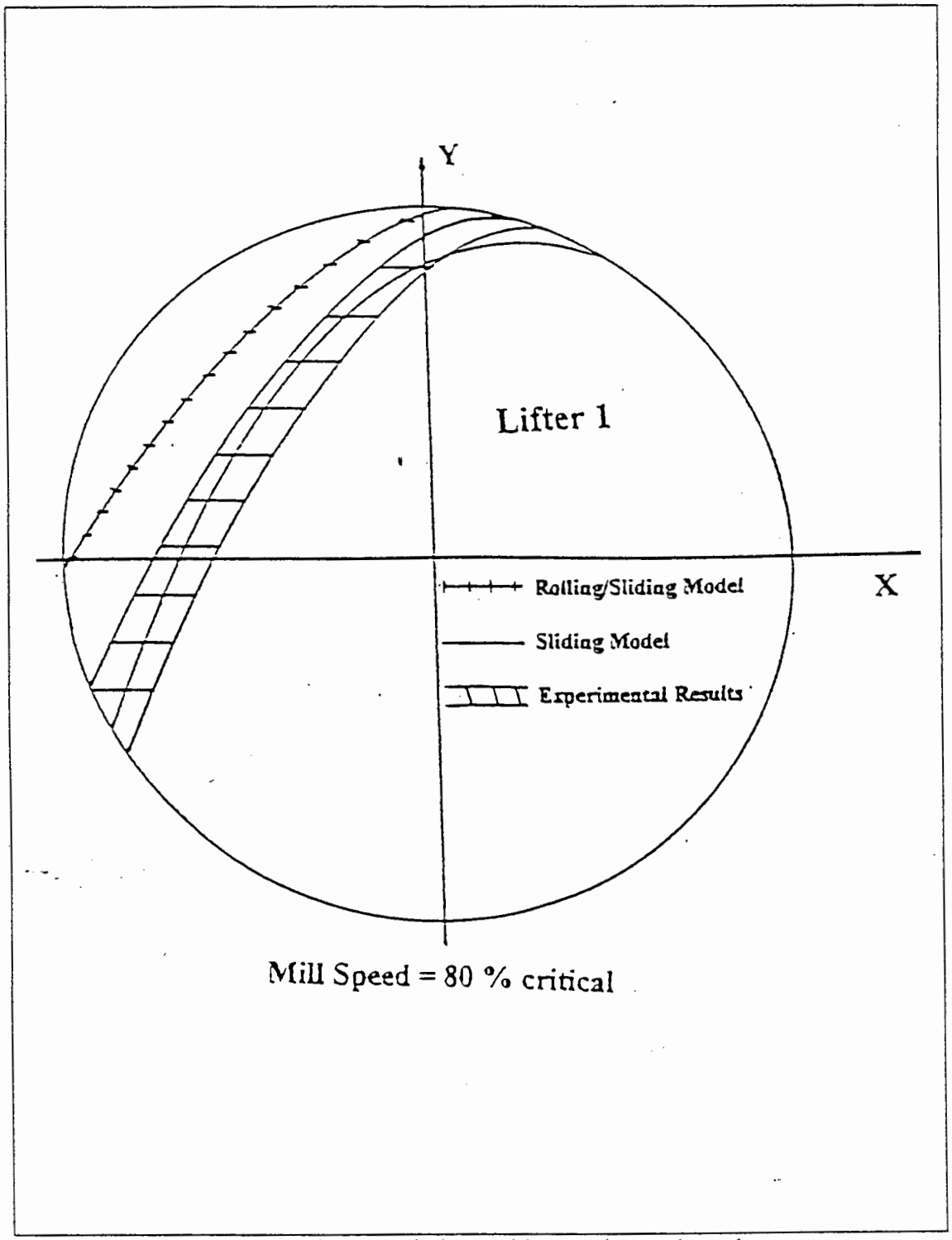

Figure 5.5 A comparison of the predictions with experimental results

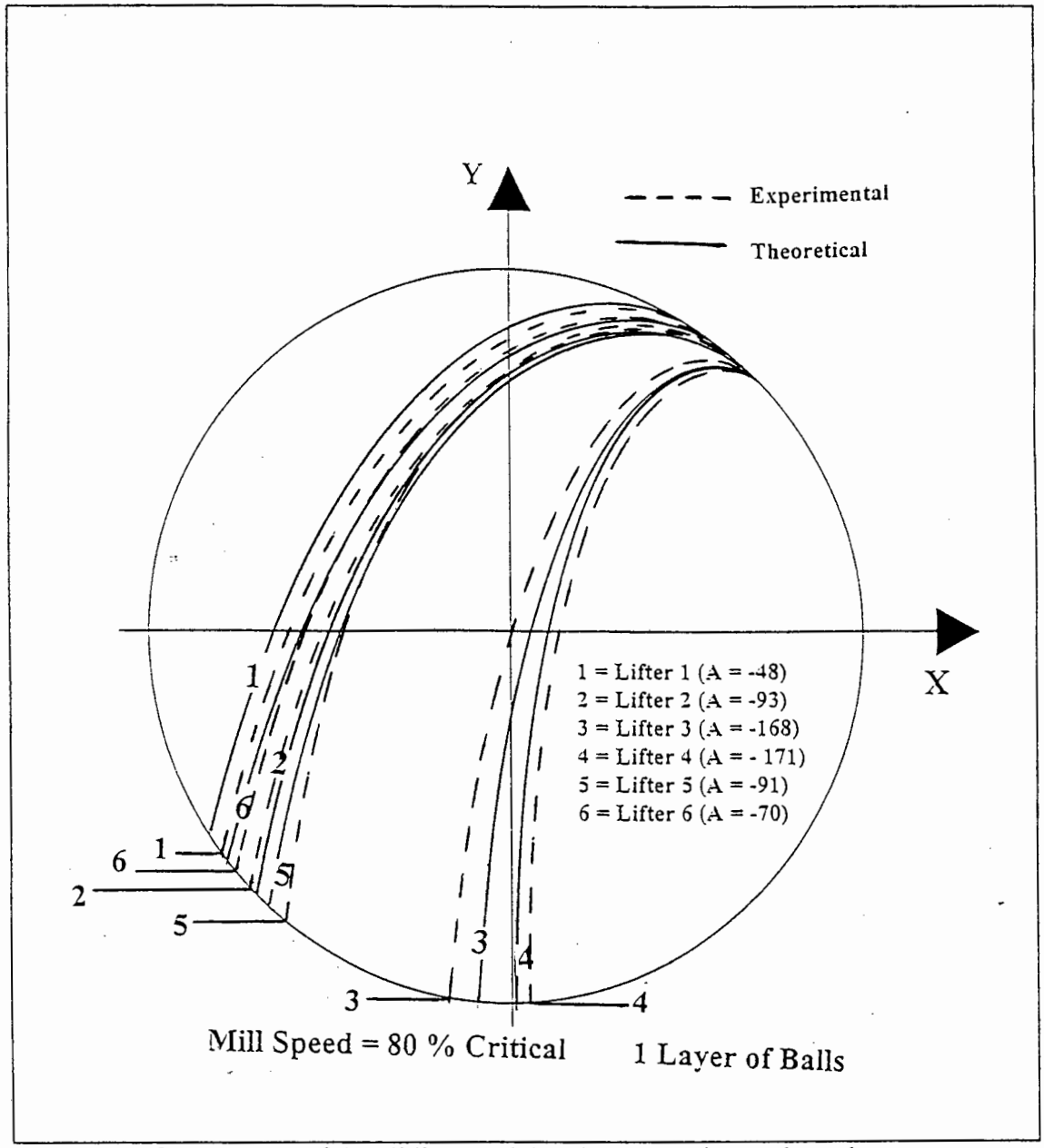

Figure 5.6 Comparison of the sliding model and the experimental results

The balls exhibit a chaotic bouncing effect at the point of impact on the mill wall due to the large coefficient of restitution between the balls and the mill wall. A number of balls do not settle on the floor of the mill before being lifted up the inside of the mill, thereby following either slightly higher or lower trajectories. This chaotic effect causes the band of trajectories viewed in the results.

5.3 RESULTS AND TRENDS OBTAINED FROM THE THEORETICAL MODEL

It has been established that there is a general correlation between departure and impact angles for the theoretical model and the experimental results. The theory can now be used to determine the effect of various parameters on the observed effects.

All the results that are presented in this section have been obtained from the "Mill Simulator" program. A set of results are illustrated in Appendix XII

5.3.1 Departure angle versus $|A|$

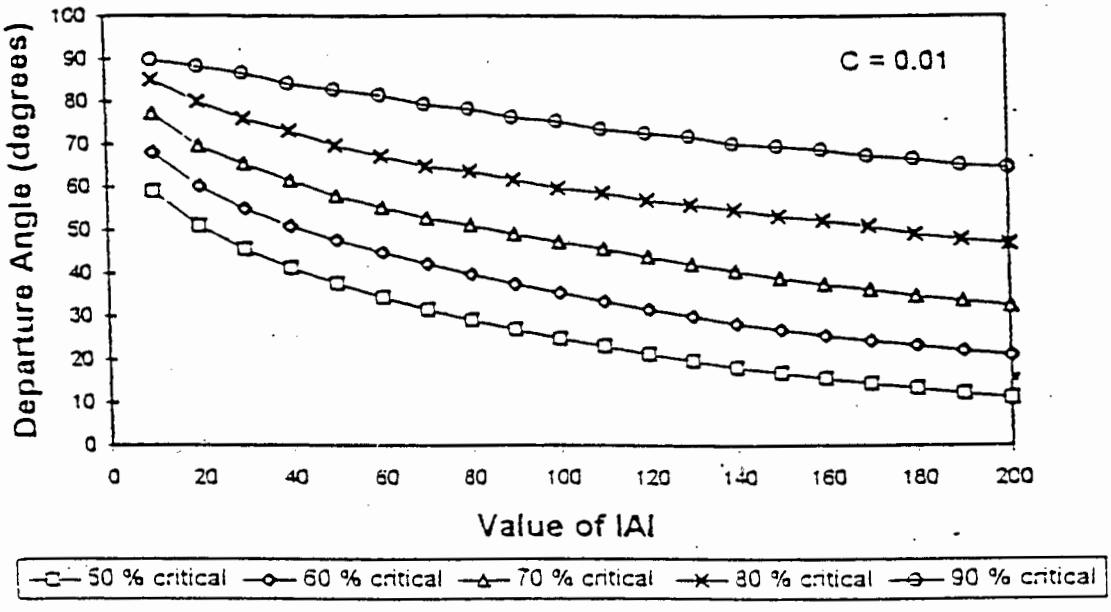

Figure 5.7 Departure angle versus $|A|$

Figure 5.7 shows that the departure angle of the ball in the mill decreases as the value of $|A|$ increases. The departure angle is not as important as the impact angle in determining the effectiveness of the lifter shape and is therefore not a critical consideration in mill design. This angle is however linked to the angle and velocity of impact. There exists a range of departure angles that will maximise the ball's falling

distance. A ball falling for a longer period of time (over a longer falling distance) will achieve a higher impact velocity. Higher impact velocities lead to higher impact energies and thus a more efficient milling condition (Providing the ball impacts on the toe of the charge).

5.3.2 Impact angle versus $|A|$

Figure 5.8 shows the comparison of the impact angles for lifters with different values of $|A|$ for a range of different mill speeds. All the other variables are constant.

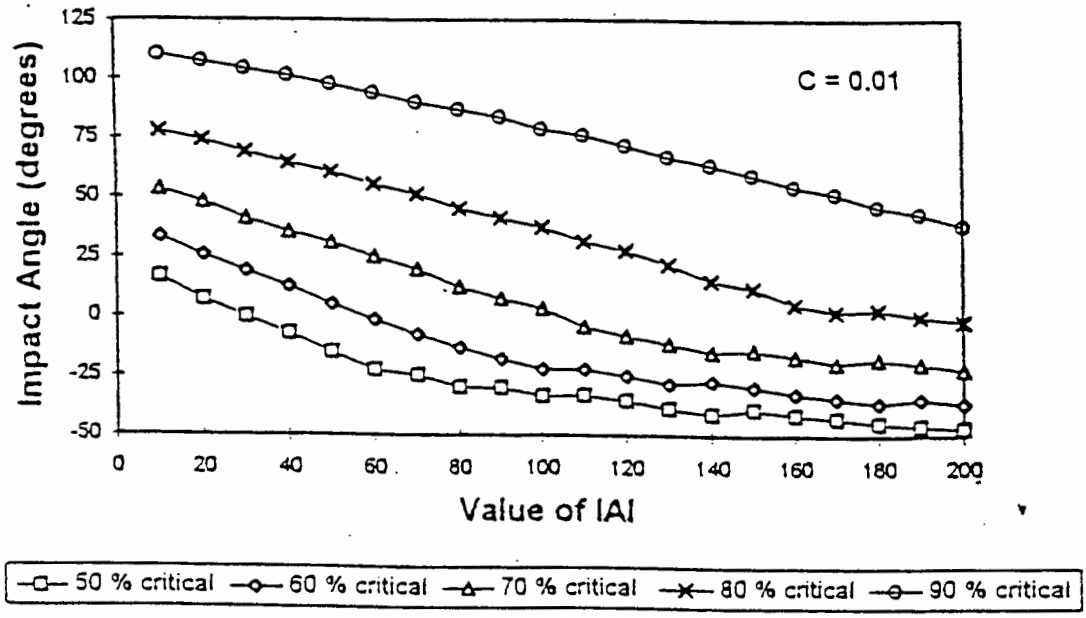

Figure 5.8 Impact angle versus $|A|$

The results show that the impact angle decreases as the value of $|A|$ increases. At the highest mill speed (90 % critical) the rate of decrease is constant. As the operating speed of the mill decreases, the slope becomes less steep for higher values of $|A|$. This occurs due to the ball falling away from the lifter bar before it reaches the lifter tip. It can be noted that the mill speed must be adjusted in order to achieve acceptable impact angles for certain lifter profiles. It is also evident that for a mill operating at a

constant speed, certain lifter bars become inefficient once they become sufficiently worn (have higher values of $|A|$).

5.3.3 Impact velocity versus $|A|$

The impact velocity may be important in determining the strain rates at which the rock is crushed. The kinetic energy at impact determines how much energy is absorbed by the crushed rock. Higher impact velocities relate to higher impact energy and possibly reduced crushing times. It could thus be important to maximise the impact velocities while keeping the impact point on the toe of the charge. A more detailed study on this phenomena should be undertaken.

Figure 5.9 illustrates some interesting points with regards to the effect the value of $|A|$ has on the impact velocity.

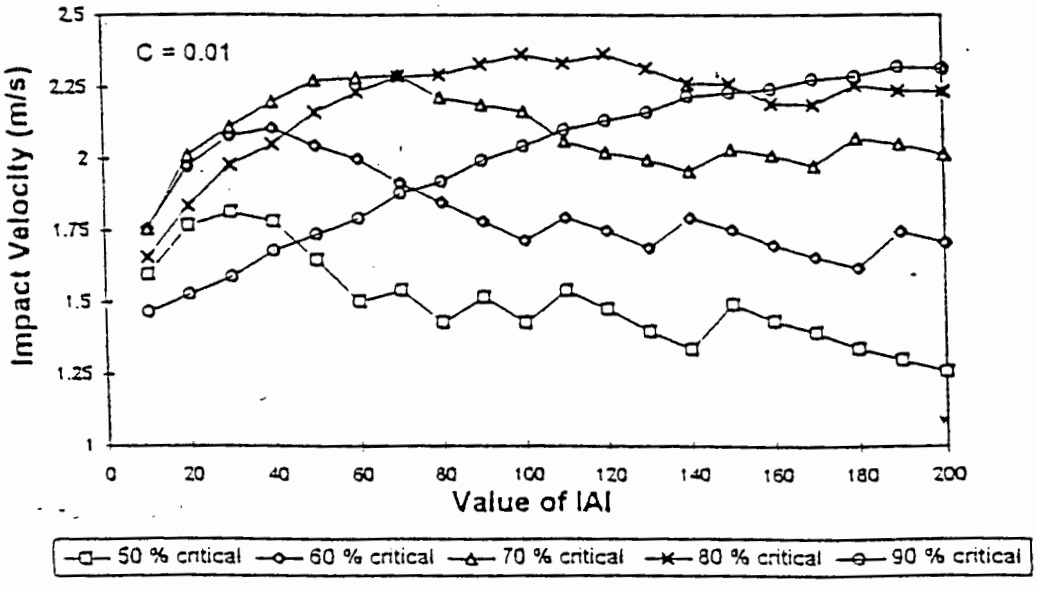

Figure 5.9 Impact velocities versus $|A|$

It is apparent that for an operating speed of 90 percent critical the lifter bar with a value between $|A| = 10$ and $|A| = 40$ imparts the lowest velocity at the point of impact. The high operating speed causes the ball to have very high impact angle which in turn does not allow for the ball to gain much kinetic energy on its short falling path. As the value of $|A|$ increases the impact velocity also increases. This is

caused by the fact that the ball attains higher kinetic energy due to the longer parabolic path which it now follows. This points to the fact that a partially worn lifter bar may perform more efficiently than a new lifter bar at high mill speeds. This assumption correlates well with the finding made by Powell[7] who also determined that a lifter with a 45 degree face angle gives better milling results than a 90 degree lifter bar.

There is a definite trend in figure 5.9. At low values of $|A|$ and low mill operating speeds, the impact velocities initially increase before reaching an optimum. This optimum value is higher for higher operating speeds and occurs at slightly larger $|A|$ values as the operating speed increases. Once the maximum impact values have been reached the trend is for the impact velocities to decrease as $|A|$ increases.

The impact velocities are the lowest for lower mill speeds (50 % and 60 % critical) at higher values of $|A|$. This is due to the slope on the lifter being substantially steep so that the ball cannot be keyed onto the lifter at low mill velocities. This causes the ball to slide off the lifter due to its own weight.

In order to determine the most effective mill speed for a specific liner for which wear characteristics are known, the impact velocity versus $|A|$ graphs can be plotted for various operating speeds (As in figure 5.9). The area can be calculated under each graph. The mill speed relating to the largest area will give a good indication of the optimum operating speed. This area relates to the speed which gives the most consistently large impact velocity for the range of wear that the lifter will experience. It must be noted that the correct impact angle of the ball must also be maintained for the mill to be operating efficiently. The range of $|A|$ values relating to acceptable impact angles can also be determined and only the area under this section of the graph can be used.

The irregularities in the graph (Specifically evident in the 50 % and 60 % critical cases) are due to the time step used in the fourth order Runga Kutta solution scheme. The time step was set to be fairly large in order to achieve acceptable results in a short

simulation time. To obtain trends rather than accurate results was the objective of this work. It is not practical to achieve accurate results by long simulations (smaller time step) for a simplified system (system with only one ball). The accuracy of the model can be refined once the effect of all the balls on the charge motion has been incorporated. As the time step is decreased, the accuracy improves considerably but the simulation time can then increase from a few seconds to many minutes or even hours (depending on the required accuracy).

5.3.4 Impact angle versus mill speed

Figure 5.10 illustrates the effect that the mill speed has on the impact angle for the six experimental lifter profiles. As in section 5.3.2, it is once again evident that lower $|A|$ values generally cause higher impact angles and visa-versa. Another consideration which must be noted in these results is the effect of the value of C.

The value of C effects the height of the lifter bars. The effect of lifter height on the charge motion will be discussed in sections 5.3.6 and 5.3.7.

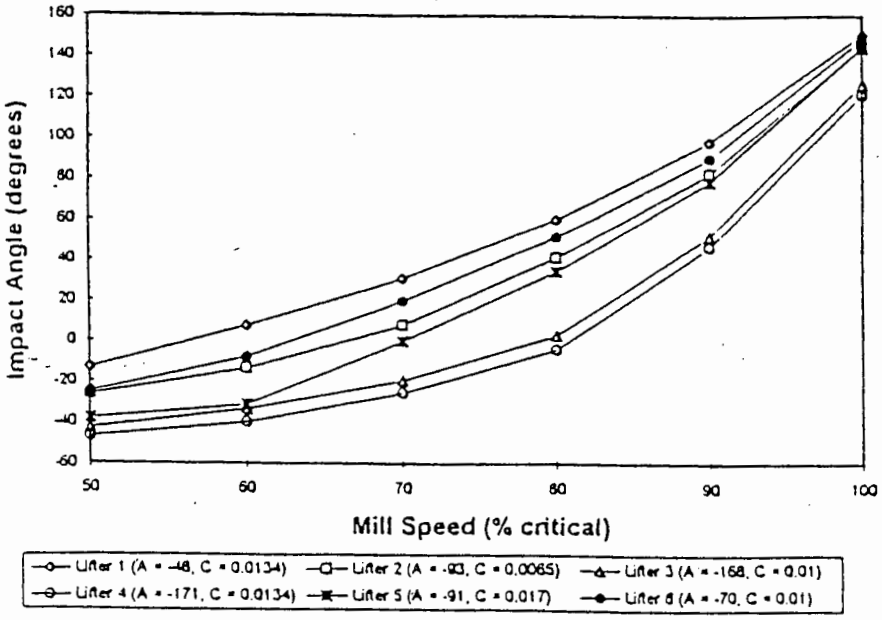

Figure 5.10 Impact angle versus mill speed

The reason for lifter 5 (A = -91) having lower impact angles than lifter 2 (A = -93) is due to the large differences in C values of these lifters. Lifter 2 is much shorter than

lifter 5 but gives rise to a higher equilibrium angle. If two lifters have identical A values but differing C values, the lifter with the lower C value will exhibit a higher trajectory. The lower C value flattens the face of the lifter bar and the equilibrium angle will be higher for this lifter. The effect of C on the shape of the outer trajectories will be further investigated and explained in section 5.3.6.

5.3.5 Impact velocity versus mill speed

In comparing figure 5.10 and figure 5.11, some interesting observations between impact velocity, impact angle and $|A|$ are noted.

From figure 5.11 it is observed that lifters with lower values of $|A|$ lead to higher impact velocities for speeds up to 70 % critical. Speeds in excess of 80 % critical cause the lifters with higher $|A|$ values to generate higher impact velocities. This is simply due to the fact that worn lifters need higher speeds to become effective whereas new lifters cause the balls to centrifuge too early at the higher speeds.

Lifter 5 undergoes some interesting trends at low mill speeds. This is caused by the lifters' high C value. This high value increases the slope on the lifter bar and the equilibrium angle is therefore largely reduced. The ball falls away from the lifter at low speeds and this gives rise to the ball not being keyed onto the lifter. Due to the above mentioned factors the ball departs from the lifter very early and does not reach an elevation which allows it to achieve higher impact velocities. At higher mill speeds the ball is keyed onto the lifter and can slide most of the way to the end of the lifter thereby achieving higher departure angles and larger impact velocities.

In order to determine which lifter will cause the highest impact energy to the load it is necessary to determine which of the six lifters gives the highest impact velocity at the desired point of impact. In figures 5.11 it is noted that lifters 1, 2 and 6 give the highest impact velocities at 70 percent critical with impact angles ranging from 0° to

35° as shown in figure 10. At 90 percent critical speeds, lifters 3 and 4 give rise to the highest impact velocities with impact angles of approximately 40° to 45°.

This again provides evidence that worn lifter bars may become more efficient than new rectangular lifters under certain operating conditions.

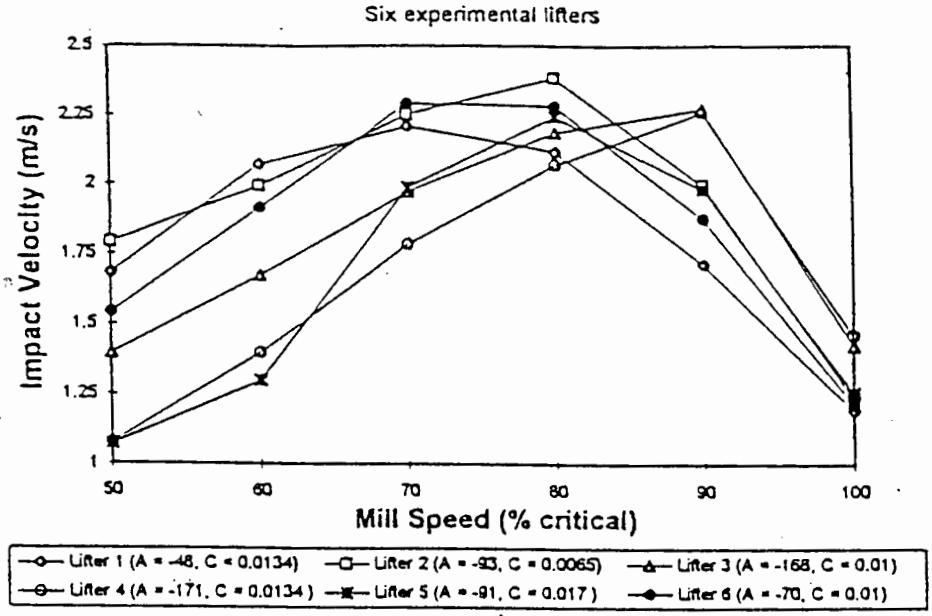

Figure 5.11 Impact velocity versus mill speed

The above predictions are only valid for a system with one ball. If the effects of charge pressure can be incorporated into the model then the theory could be used to predict charge motion for any percentage fill. The actual impact angle of the outer layer of balls could then be determined for any lifter shape and any volume fill condition.

5.3.6 Departure angle versus lifter height

Powell [4] and Vermeulen et al.[17] determined that the height of rectangular lifter bars largely effects the path of the outer trajectory. The reason for this phenomenon was generally due to the ball sliding all the way to the end of the lifter bar before falling

away from the lifter. Powell and Vermeulen also determined that there is a critical lifter height dependant on mill speed at which point an increase in the height no longer effected the outer trajectory. This critical lifter height is caused due to the ball falling away from the lifter before reaching the tip of the lifter bar.

The method by which the lifter height was varied was by keeping $|A|$ constant in the equation $y = Ax^2 + C$ and changing the value of C to obtain the desired increments in height. Appendix VIII illustrates this procedure.

Figure 5.12 illustrates how the increase in lifter height effects the departure angle for worn lifter shapes. It can be noted that for a lifter with a low value of $|A|$ (rectangular lifter with very little wear) the departure angle initially increases but then becomes relatively constant. This verifies the findings of Powell and Vermeulen.

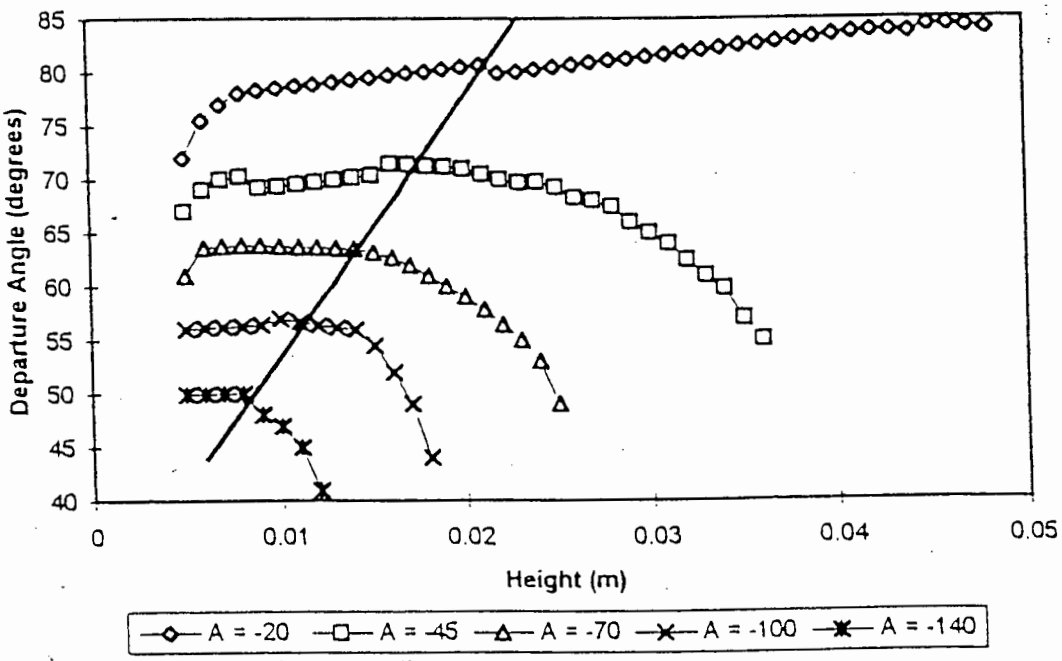

Figure 5.12 Departure angle versus lifter height

As the lifter becomes worn the effect of lifter height on the departure angle changes significantly. The departure angle initially increases and then reaches a constant before decreasing again. The reason for the departure angle decreasing is due to the way that the model has been derived. The model has the effect to increase the initial contact angle of the ball as C becomes significantly large. An increase in the contact

angle relates to a decrease in the equilibrium angle. This causes the ball to start sliding sooner. It is not possible to determine the effect of only the height on the departure angle without considering the related changing contact angle for higher values of C. Because of this, height effects are very difficult to determine using this model.

The line drawn on figure 5.12 illustrates the area below which the model can no longer accurately predict the effect of height on the departure angle. The results are meaningful for all the data above this line (i.e. small values of C where C < 0.03*Mill diameter).

5.3.7 Impact angle versus lifter height

Figure 5.13 illustrates that for a lifter with very little wear the impact angle remains constant. The results above the line accurately represent the effect that lifter height will have on the impact angle. This is due to the ball falling away from the lifter before it reaches the tip of the lifter bar. The results below the line are caused by the significant increase in the contact angle with an increase in C.

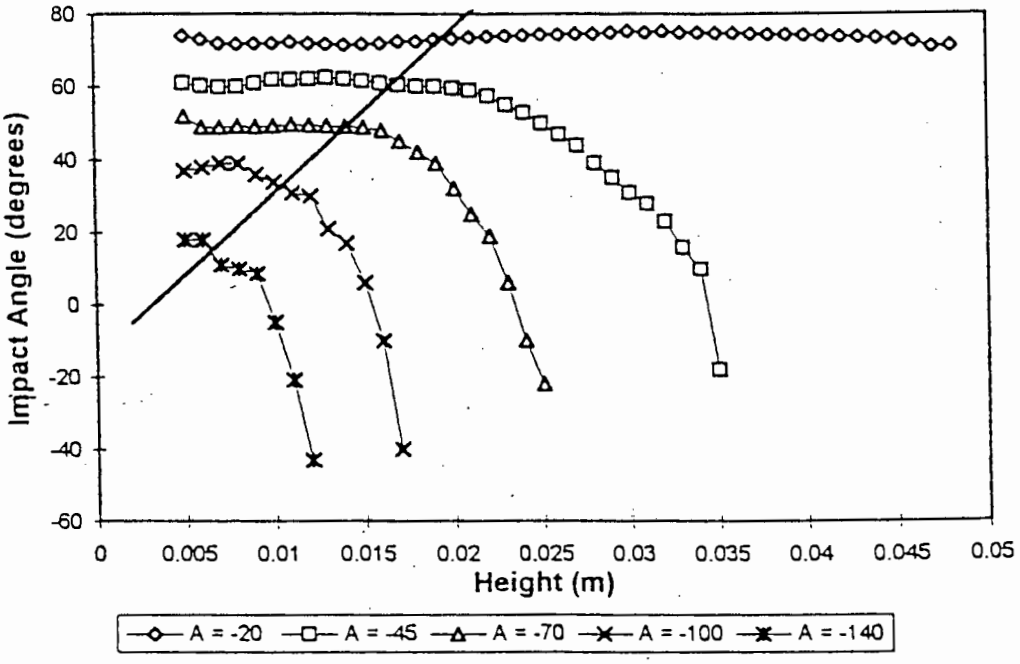

Figure 5.13 Impact angle versus lifter height

It can thus be concluded that the same principles apply for worn lifter bars as do for rectangular lifter bars. An increase in height initially effects the trajectory path but a

critical height is reached at which point the ball falls away from the lifter before reaching the tip.

5.3.8 Coefficients of friction versus departure angle

The static and kinetic coefficients are difficult to determine but it is apparent that as a mixture becomes more fluid the friction in the system will decrease. An investigation has been undertaken to determine the effect of friction on the trajectory of the outer ball.

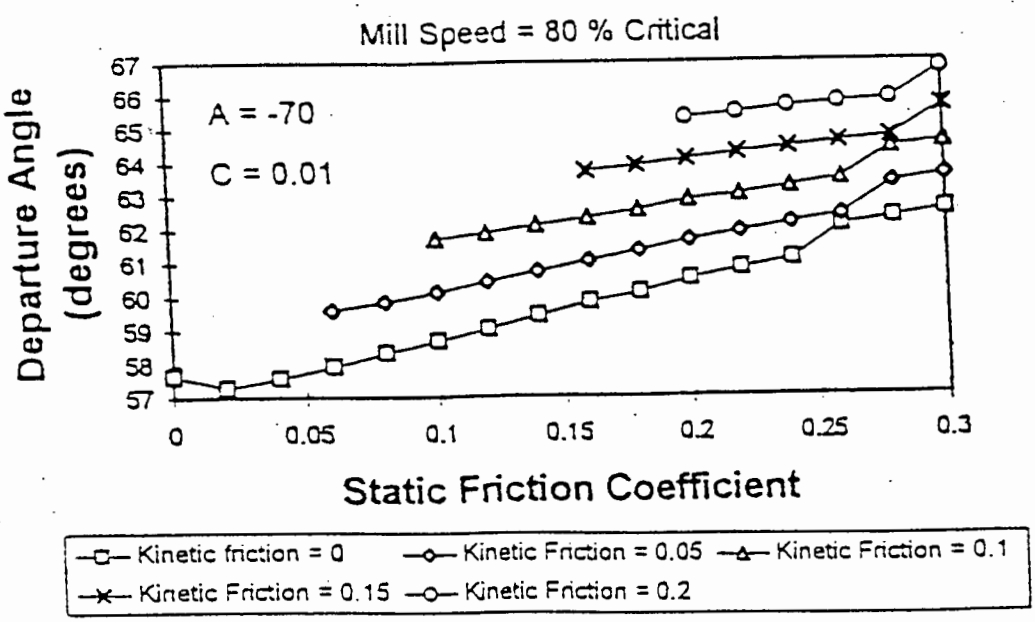

Figure 5.14 Coefficient of friction versus departure angle

Nates et al.[19] determined that the coefficient of friction for a metal on metal environment would be 0.2 ± 0.04 in a mill. Powell's[4] findings illustrated that the static coefficient of friction in the experimental mill peaks at 0.23 but decreases depending on the frequency of mill vibration. The range of friction values under investigation will be 0 - 0.3.

Figure 5.14 shows that the coefficient of friction does not have a very large effect on the departure angle. This angle only increases by 10° in the range 57° - 67° for the

range of coefficient of friction values. It must be noted that the static coefficient of friction cannot be less than the kinetic coefficient of friction and this is why there are less data points on the graph for the larger kinetic coefficient of friction cases. The results illustrate that the departure angle simply increases as the static coefficient of friction increases. This is related purely to the increased angle of equilibrium for higher static coefficient of friction values. As the kinetic coefficient of friction value increases, the ball will not accelerate as fast and will stay on the lifter for a longer period before being projected into a free flight trajectory. This gives rise to the increased departure angles for similar static coefficient of friction values but higher kinetic coefficients of friction.

From the results obtained from the "Mill Simulator" program it can be concluded for the single ball case that while a mill with lifter bars is running at a constant speed the viscosity of the fluid will not play a significant role in changing the departure angle. This is as result of neglecting the effect of the rest of the load which might increase the normal force on the ball thereby increasing the friction component in the governing equation. This would cause the coefficient of friction to have a larger effect on the charge motion than what is illustrated in the simulation results.

At a static coefficient of friction of 0.26 some interesting effects start to occur. The irregular pattern in the departure angle may refer to the fact that the friction is becoming large enough for the ball to start rolling at the equilibrium angle. The sliding model cannot predict when rolling might start to occur but will always calculate the relevant sliding values. The sliding model becomes inaccurate at this value of static friction.

5.3.9 Coefficient of friction versus Impact angle

The coefficient of friction effects the impact angle in the same way as in the case of the departure angles. The range of impact angles is much larger than the range of departure angles (26° - 53°). Figure 5.15 illustrates this.

The impact angles show an acceptable range (ball will impact on the toe of the charge) for all the conditions presented in the graph. This range varies between 25° and 50°. It must now be determined which range of friction values will give the highest impact velocities in order to determine the friction condition that leads to the best milling efficiency.

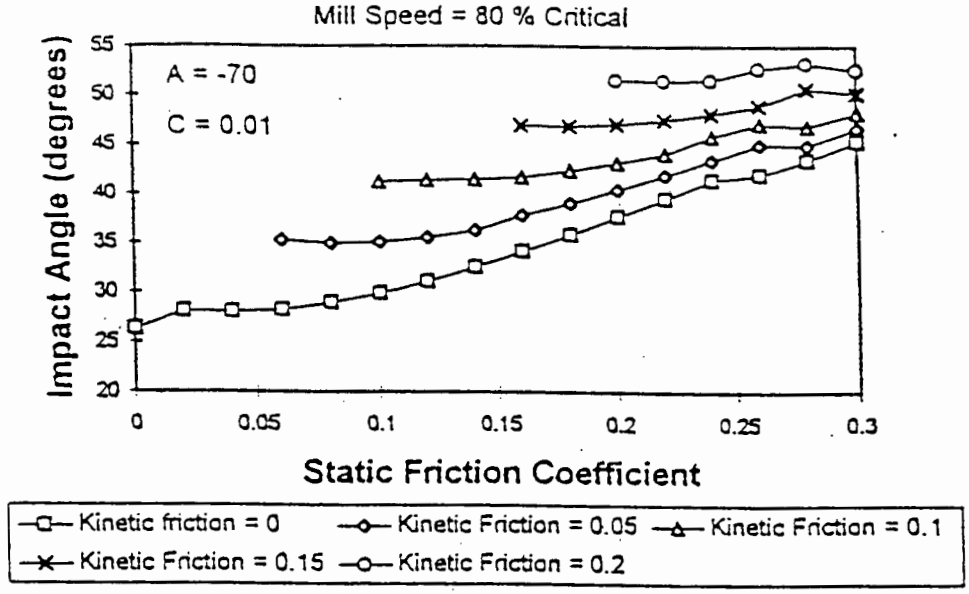

Figure 5.15 Coefficient of friction versus impact angles

5.3.10 Coefficient of friction versus impact velocity

The effect of the coefficient of friction on the impact velocities can be viewed in figure 5.16.

Comparing figure 5.9 and figure 5.16 it is clear that the effect of the coefficient of friction compared to the effect $|A|$ on the impact velocity is small. The range of impact velocities in figure 5.16 is 0.08 m/s whereas the range for a lifter bar with varying $|A|$ values operating at 80 % critical is 0.75 m/s. In dividing 0.08 by 0.75 it can be determined that the friction only has an 11 % effect on the impact velocity in this case.

Figure 5.16 does illustrate that as the static coefficient of friction is raised, the impact velocity first reaches a minimum before increasing. The decrease is caused by the slower acceleration of the ball on the lifter. This causes a reduced departure velocity which relates to lower impact velocities. The subsequent increase in the impact velocity is due to the increase in the equilibrium angle and hence the departure angle. This increase causes the ball to fall further causing higher impact energies. The increase in falling distance has a larger effect than the decreased departure velocity at the minimum point on each graph.

As described in section 5.3.9 the increase in the kinetic coefficient of friction causes the ball to remain on the lifter for longer and increases the departure angle. This causes the increase in the impact velocity.

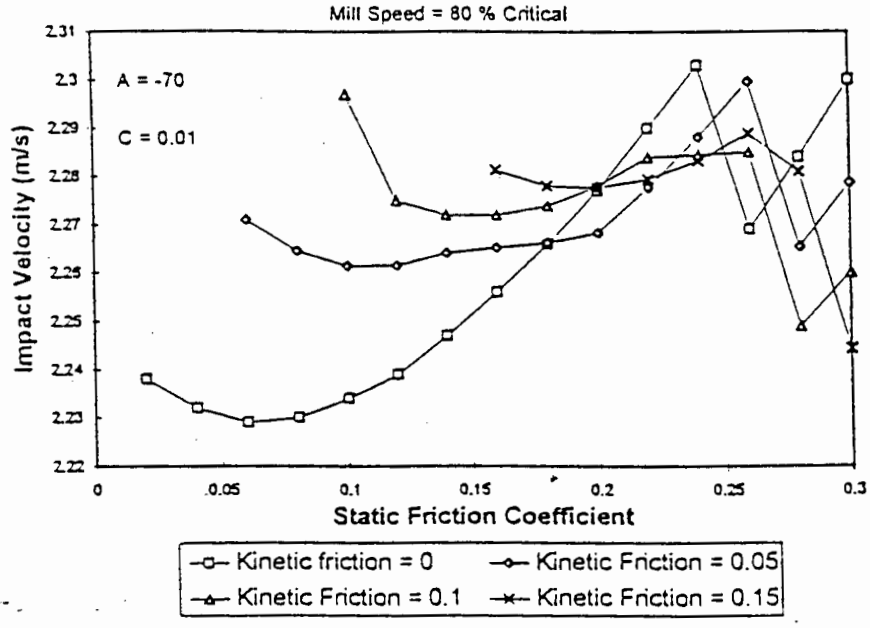

Figure 5.16 Effect of friction values on impact velocity

At coefficients of friction larger than 0.24 the impact velocities drop significantly. As illustrated in figure 5.14 and described in section 5.3.8 this drop is related to the friction becoming large enough for the ball to start rolling at the equilibrium angle.

5.3.11 Effect of ball size on the departure and impact angles

Figure 5.17 illustrates that the departure and impact angles both decrease as the ball size increases.

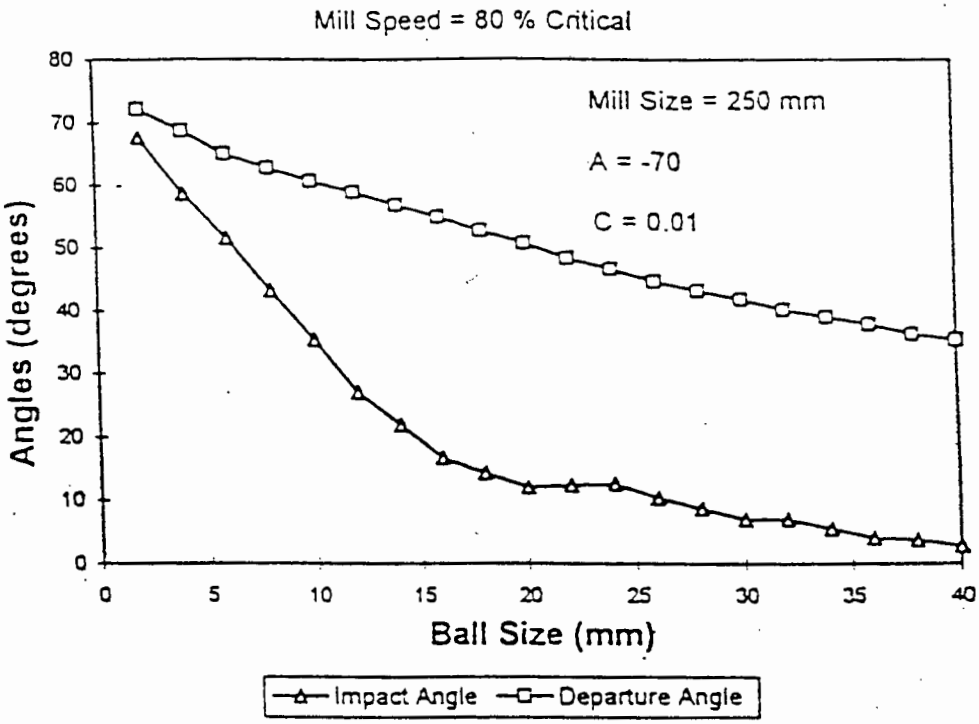

Figure 6.17. Ball size versus departure and impact angles

As the ball increases in size the centre of the ball moves further away from the mill wall and the centrifugal force decreases. This causes the ball to depart earlier from the lifter. The lower departure angles also cause the lower impact angles.

A larger ball cannot get keyed onto the lifter bar and the contact point on the lifter bar is further away from the mill wall. This results in the ball :

1. Not having to travel as far before leaving the lifter bar.
2. Touching the lifter bar at a point where the tangent is steeper. This results in a lower equilibrium angle.

It is thus evident that a smaller ball will give higher departure and impact angles.

6. CONCLUSIONS

The main findings of this work was to determine the effect of worn lifter bars on the outer trajectories of media in a ball mill. The conclusions drawn from the work are:

- Comparison of the a rolling/sliding model and a pure sliding model with the experimental results illustrates that the sliding model gives a good correlation between the observed and predicted results. The rolling model tends to over predict the trajectory heights. This finding is in agreement with Powell[4] and Vermeulen[23].

- The experimental results and the theoretical predictions confirm that the departure and impact angles decrease as the amount of wear on the lifter bar increases. However, worn lifter bars can operate more efficiently than new rectangular lifter bars under certain operating conditions. The efficiency of the lifter bars were shown to be effected by the value of A (from the parabolic lifter profile represented by $Ax^2 + C$), where A represents the amount of wear on the lifter face.

- The efficiency of the mill is partly a function of both lifter shape and mill speed. An increase in mill operating speed gives rise to larger departure and impact angles. The mill speed plays an important role in determining the efficiency of the lifter shape. At high mill operating speeds a rectangular lifter bar may give rise to impact angles that are too large (the balls do not fall on the toe of the charge), whereas a worn lifter bar may give rise to the desired impact angle on the toe of the charge.

- The mill filling ratio has a significant effect on the departure and impact angles. An increase in the charge pressure gives rise to higher departure angles and larger impact angles. As the mill filling ratio increases so does

the charge pressure. This finding correlates with the work done by Vermeulen and Howat[16].

- The impact velocity was shown to have a significant effect on the efficiency of the lifter bar. A lifter which yields the largest impact velocity at the desired point of impact will give rise to large impact energies on the toe of the charge and hence results in the most desirable milling condition. The area under the impact velocity versus |A| graph also relates to the effectiveness of the lifter throughout the operating life of that lifter bar. A larger area under the graph points to high impact energies over a large time period and hence a more economic milling condition.

- As the lifter height is increased the departure and impact angles will increase, until a critical lifter height is reached above which the impact and departure angles remain constant. Powell[4] and Vermeulen[17] also reported this finding while investigating height effects of rectangular lifter bars.

- The model illustrates that the departure angle and impact angles increases as the coefficient of friction increases. The coefficient of friction does not have a very large effect on the departure angle but causes a larger variation in impact angles. The coefficient of friction is always assumed to be small enough for the ball to slide rather than roll down the lifter face. Some inconsistencies start to occur in the sliding model when the static coefficient of friction becomes too large (ball starts rolling). The simulation results also illustrate that the effect of the change in coefficient of friction on the impact velocity is small in comparison with the effect of wear on the lifter bar.

- Further the model shows that the departure and impact angles decrease as the ball size increases. This is related purely to the centre of the ball being closer to the mill centre, causing the centrifugal force to be lower.

- Due to incorrect dynamic modelling of the experimental equipment the power readings could not be accurately monitored during the tests.

7.RECOMENDATIONS

7.1 THEORETICAL MODEL

The theoretical model in this thesis modelled a single ball on the inside of a rotating cylinder on a lifter bar with any parabolic profile of the form $y = Ax^2 + C$. The model can be extended to incorporate the following improvements.

- The lifter bar profile can be modelled as a higher order polynomial of the form

  $$y = Ax^n + C$$

  where A, C and n are variables that can be defined by the user. The existing parabolic model can very easily be modified to accommodate the new expression. This will allow for a more realistic representation of the worn lifter bar shapes.

- Another option to achieve an even better representation of the lifter profile during various stages of wear would be to construct the curve from a series of mathematical expressions, linear or polynomial. This would incorporate a curve splicing exercise on each lifter bar profile. The geometric transformations do become complicated for an expression with more than two terms. It is advisable to limit the number of terms in each part of the curve to two.

- The addition of the effect of the charge pressure into the model will give a realistic model which could be applied to industrial situations. In order to achieve this it is necessary to incorporate two extra force terms into the model. These are :

  1. The centrifugal effect of all the inner balls on the outer ball (Charge pressure effect). This can be modelled as an integral summation of the centrifugal forces of all the balls pushing on the outer ball. This force component will be:

$$F_{centrifugal} = m\Omega^2 \int_{r=r_{in}}^{r=r_{out}} r dr$$

where :

r_{out} = The distance form the mill centre to the centre of the ball in the outer layer.

r_{in} = The distance from the mill centre to the centre of the ball on the inner layer.

2. The force due to gravity components of the rest of the charge on the monitored ball need to be included in the analysis. This is the problematic term in the new formulation and thought must be given to define an accurate expression for this component.

The main problem in defining the extra terms in the new formulation will be related to determining a charge shape model that can be applied to different operating situations. This would include concepts of what the charge shape will be for different mill speeds etc. Once an acceptable charge shape model is determined then the application of the two extra force terms can be defined. Morrell[20] has defined a simplified charge shape model to determine the power consumption in mills. This model could possibly be adapted and applied to the recommended charge pressure formulation.

7.2 EXPERIMENTAL WORK

- The experimental mill should be redesigned as a scale model mill (scaled according to an industrial mill). The mill should accurately represent the dynamic system encountered in the industrial mills and must be able to determine power consumption for various operating conditions. Charge load weight to mill weight ratio must also be accurately modelled.

- As the coefficient of friction is dependant on the mill vibration, a method must be determined by which the mill vibration can continuously be recorded. A separate

study should be done on how mill vibration effects the coefficient of friction between the mill and the charge in this specific system. A calibration table can be determined for a full range of mill frequencies. This table can be used to find the coefficient of friction once the mill frequency is known. These coefficients can be used to achieve a more accurate simulation in the model.

REFERENCES

1. VERMEULEN, L.A. , HOWAT, D.D. The Design of Linings for Rotary Mills. J. S.A. Inst. Min. Metall. July 1986. pp 251-259.
2. POWELL, M.S. The Design of Rotary-Mill Liners and their Backing Materials. J. S.A. Inst. Min. Metall. Feb. 1991. pp 63-75.
3. BRADLEY, A.A., HINDE, A.L. and LLOYD, P.J. The Determination of the Efficiency of the Milling Process. J. S.A. Inst. Min. Metall. June 1972. pp. 277-281.
4. POWELL, M.S. The Effect of Liner Design upon the Charge Motion in a Rotary Mill., Masters Dissertation. University of Cape Town, Sep. 1988.
5. McIVOR, R.E. Effect of Speed and Liner Configuration on Ball Mill Performance. Mining Eng. June 1983. pp 617-622.
6. POWELL, M.S. A Study of Charge Motion in Rotary Mills, with Particular Reference to the Grinding Action. Doctoral Thesis. University of Cape Town. March 1993.
7. NATES, M.B. The Behaviour of a Single Particle on the Inside of a Rotating Cylinder. Masters Dissertation. University of Cape Town. September 1989.
8. VON BENTHEIM, K. The Behaviour of a Single Particle on a Corrugated Liner Inside a Rotating Cylinder. Masters Dissertation., University of Cape Town, April 1991.
9. WHITE, H.A. The theory of the tube mill. The Journal of the Chem., Metall. and Min. soc. of S.A. May, 1905. pp. 290-305
10. DAVIS, E.W. Fine Crushing in Ball-Mills. AIME Trans., vol. 61, 1919. pp. 250-296.
11. HAULTAIN, H.E.T., and DYER, F.C. Ball Paths in Tube Mills. CIM Trans., vol. 25, 1922. pp 276-291.
12. GOW, A.M., CAMPBELL, A.B., and COGHILL, W.H. A Laboratory Investigation of Ball Milling. AIME Trans., Milling Methods, 1930. pp. 51-81.
13. FAHRENWALD, A.W., and LEE, H.E. Ball Mill Studies. AIME Tech. Publ. no. 375. 1931.
14. MARECHAL, B., Contribution to a Study of Dry Quasi-Autogenous Milling. Third Part : Internal Mechanics of the Aerofall Mill. Mintek Translation TR-1199 (Contribution a l'etudede la fragmentation quasi-autogene en voie seche. Presented at the Faculty of Sciences, Nancy, 17 May, 1968.)
15. VERMEULEN, L.A. , HOWAT, D.D. Fluctuations in the Slip of the Grinding Charge in Rotary Mills with Smooth Liners. Int. J. Min. Proces., vol. 16, 1986. pp. 153-188.
16. HEINEN, H., BRIMACOMBE, J.K. and WATKINSON, A.P. The Modelling of Transverse Solids Motion in Rotary Kilns. Metall. Transactions B, vol. 14B, June 1983. pp 207-219.
17. VERMEULEN, L.A. , OHLSON DE FINE, M.J. AND SCHAKOWSKI, F. Physical Information from the Inside of a Rotary Mill. J. S.A. Inst. Min. Metall., vol 84, August 1984. pp 247-253.

18. NATES, M.B., NURICK, G.N. AND REDDY, B.D. The Slip of a Single Particle on the Inside of a Rotating Cylinder. Part 1. Theoretical analysis. Int. J. Min. Proces., vol. 38, 1993. pp. 67-79.
19. NATES, M.B., NURICK, G.N. AND REDDY, B.D. The Slip of a Single Particle on the Inside of a Rotating Cylinder. Part 2. Experimental Investigation. Int. J. Min. Proces., vol. 38, 1993. pp. 81-91.
20. MORRELL, S. Prediction of Grinding-Mill Power. Trans. Inst Min. Metall., vol. 101, January - April 1992. pp.C25-C32
21. MEADERS, R.C. and MacPHERSON, A.R. Technical Design of Autogenous Mills. Mining Eng., vol. 16, 1964. pp 81-83.
22. DUNN, D.J. Optimising Ball Mill Liners for Production and Economy. Mining Eng., vol. 28, 1976. pp 32-34.
23. VERMEULEN, L.A. The Lifting Action of Lifter Bars in Rotary Mills. J. S.A. Inst. Min. Metall. February 1985. pp 41-49
24. VERMEULEN, L.A. , HOWAT, D.D. Effects of Lifter Bars on the Motion of en-Masse Grinding Media in Milling. Int. J. Min. Proces., vol. 24, 1988. pp. 143-159.
25. MISHRA, B.K., and RAJAMANI, Raj K. The Discrete Element Method for the Simulation of Ball Mills. Appl. Math. Modelling, vol. 16, 1992. pp. 598-604
26. MISHRA, B.K., and RAJAMANI, Raj K. Simulation of Charge Motion in Ball Mills. Part 1: Experimental Verifications, Int. J. Min. Proces., vol, 40. 1994. pp 171-186.
27. MISHRA, B.K., and RAJAMANI, Raj K. Simulation of Charge Motion in Ball Mills. Part 2: Int. J. Min. Proces., vol. 40, 1994. pp 187-197.
28. MISHRA, B.K., and RAJAMANI, Raj K. Numerical Simulation of Charge Motion in Ball Mills - Lifter Bar Effect, Min and Mat. Proces. May. 1993. pp 86-90
29. HINDE, A.L., MOHAMED, S and POWELL, M.S. The Influence of Materials and Lifter Design on the Rate of Production of Fines in a Rotary Mill, Mintek Report.
30. MERIAM, J.L. and KRAIGE, L.G. Engineering Mechanics, vol. 2, Dynamics, Second Edition. 1987. pp 623.
31. FROBERG, C.E., Introduction to Numerical Analysis, Second Edition. Adison Wesley Publishing Company, 1970.

BIBLIOGRAPHY

1. POWELL, M.S.,NURICK,G.N. A Study of Charge Motion in Rotary Mills, Part 1 - Extension of the Theory. Minerals Eng., vol. 9 (2). 1996. pp. 259 - 268.
2. POWELL, M.S.,NURICK,G.N. A Study of Charge Motion in Rotary Mills, Part 2 - Experimental work. Minerals Eng., vol. 9 (3). 1996. pp. 343 - 350.
3. POWELL, M.S.,NURICK,G.N. A Study of Charge Motion in Rotary Mills, Part 3 - Analysis of Results. Minerals Eng., vol. 9 (4). 1996. pp. 399 - 418.
4. KUNG, L.-S.,SAMIN, L.-S. Measurement of Velocity Fields in Ball Mills. Experimental Mech., vol. 36 (3). 1996. pp. 251- 257
5. VERMEULEN, L.A. Estimation of Milling Parameters by use of a Conductivity Bolt. Mintek TM. No. 19048, Mintek, Randburg. July 1985
6. ROSE, M.E. A Treatise on the Internal Mechanics of Ball, Tube and Rod Mills. Constable, London. 1958.
7. POWELL, M.S. The Use of Lifter Bars in Rotary Mills. Mintek Report M350, Mintek, Randburg. 1987.
8. POWELL, M.S. Survey of Milling and Mill Lining Practice on the South African Gold Mines. Mintek Report M350, Mintek, Randburg. 1987.
9. JOWETT, A. An Introduction to the Assessment of Energy Requirements and Product Size in Communition. Minerals Sci. Energy, vol. 3, 1971. Pp. 33 - 43.
10. HUKKI, R.T. Grinding at Supercritical Speeds in Rod and Ball Mills. Sventsa Gruvföreningen and Jernkontoret. Prógress in Mineral Dressing, Trans. Tenth Int. Miner. Process. Congr., Stockholm 1957. Almqvist and Wiksell, Stockholm, pp. 85 - 109.

APPENDIX I

Diagrams of Mill Geometry and Forces Acting on the Ball

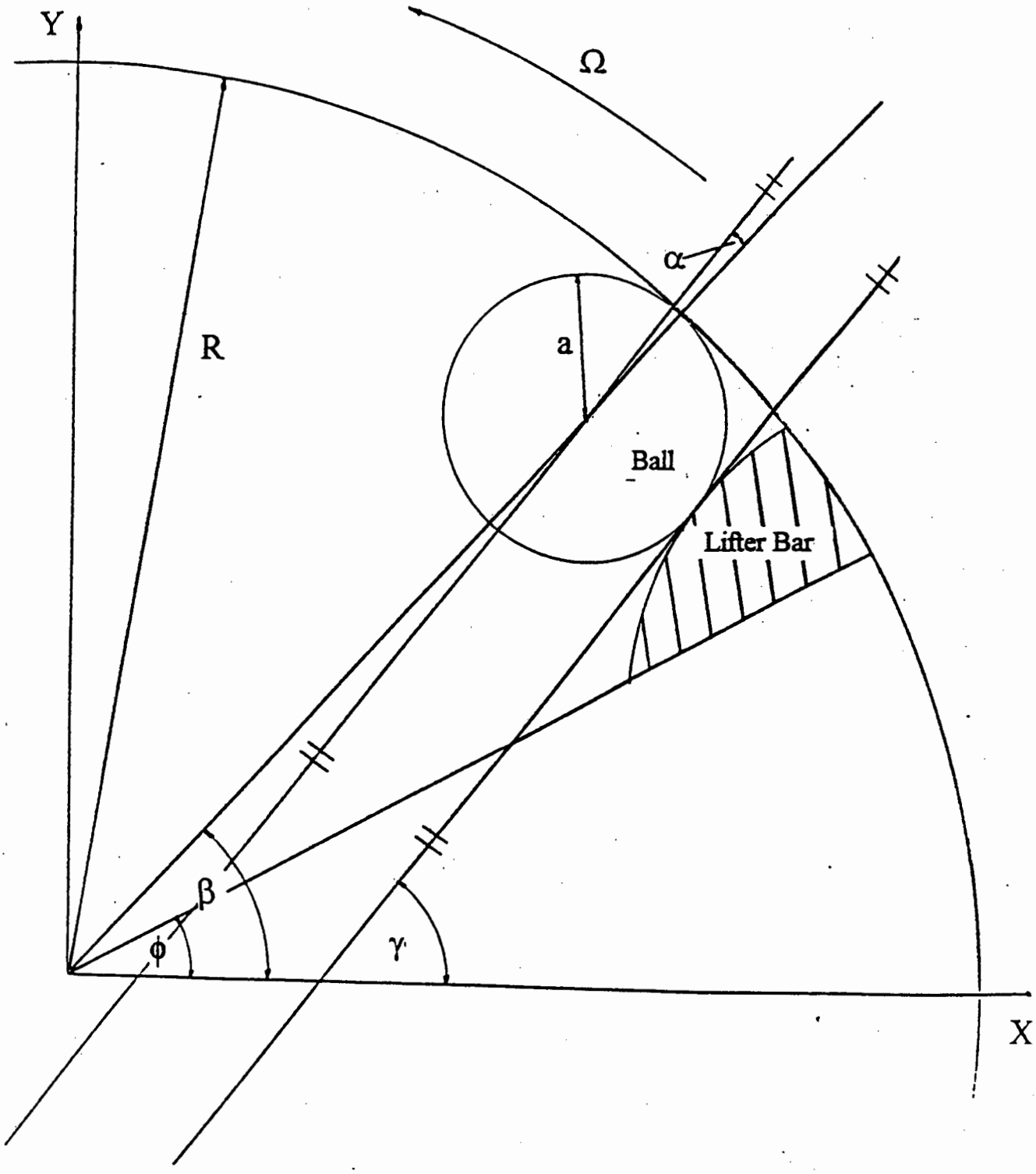

Figure I - 1. The system is modelled as one ball on a lifter bar

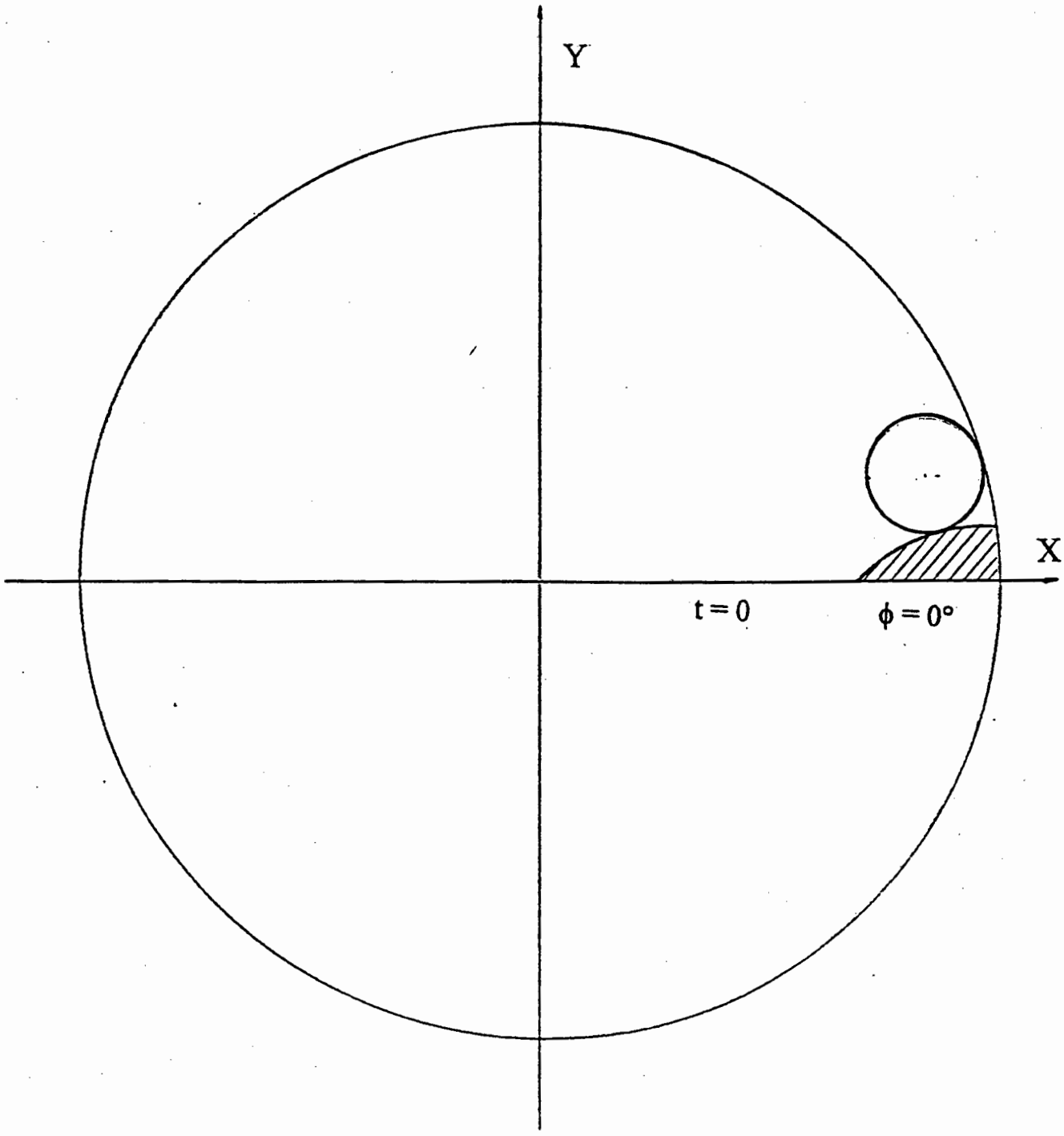

Figure I - 2 Neutral position of the lifter

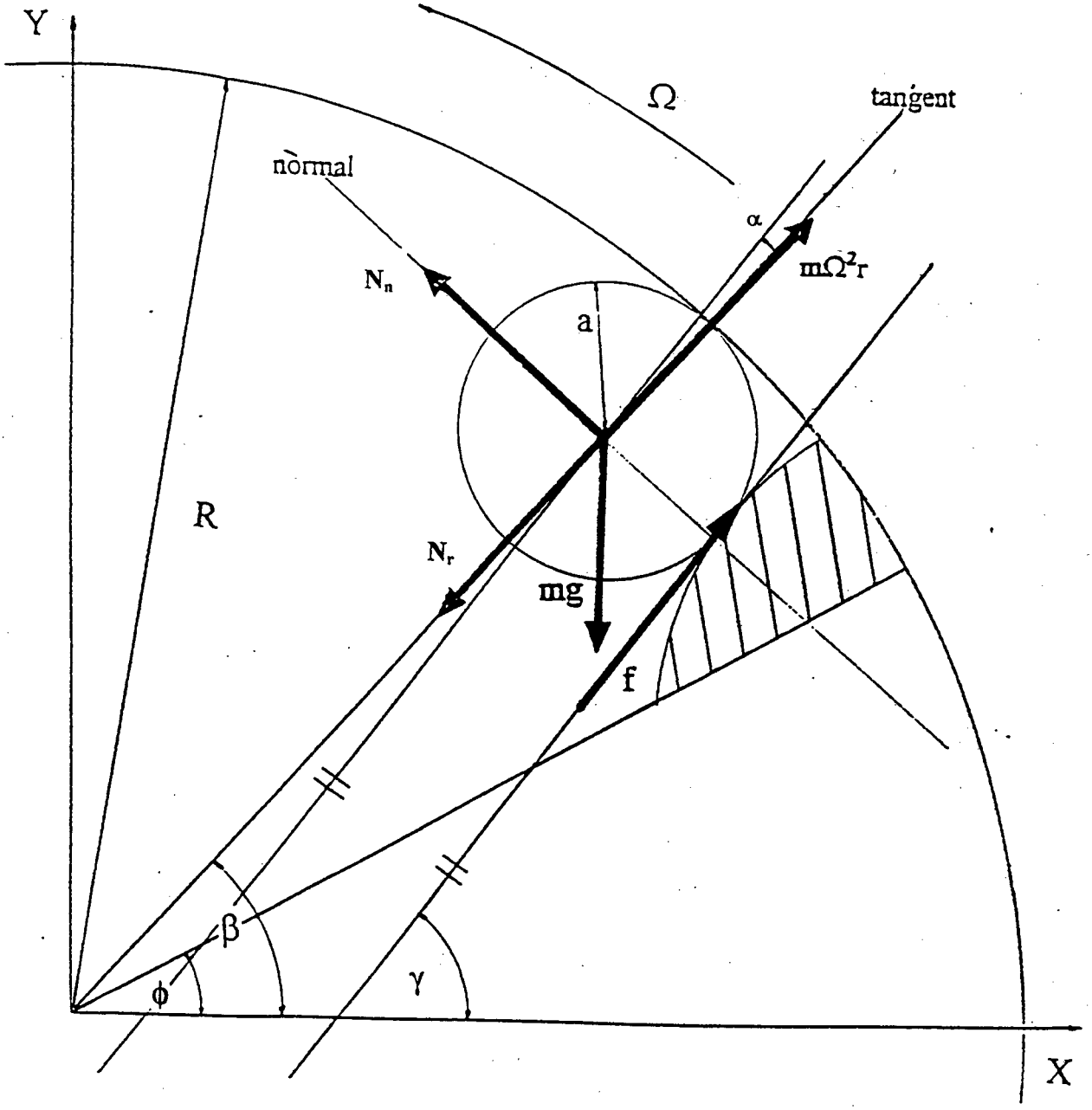

mg - The gravitational force (Acting vertically downward)

$m\Omega^2 r$ - The centrifugal force (Acting radially outwards)

N_n - Normal force on the lifter face.

N_r - Radial force at the mill wall.

f - Friction force between the ball and the lifter.

Figure I - 3 Forces acting on the ball in contact with the lifter bar and mill wall

APPENDIX II

Derivation of Equation 3

(Sum of Moments about the Centre of the Ball)

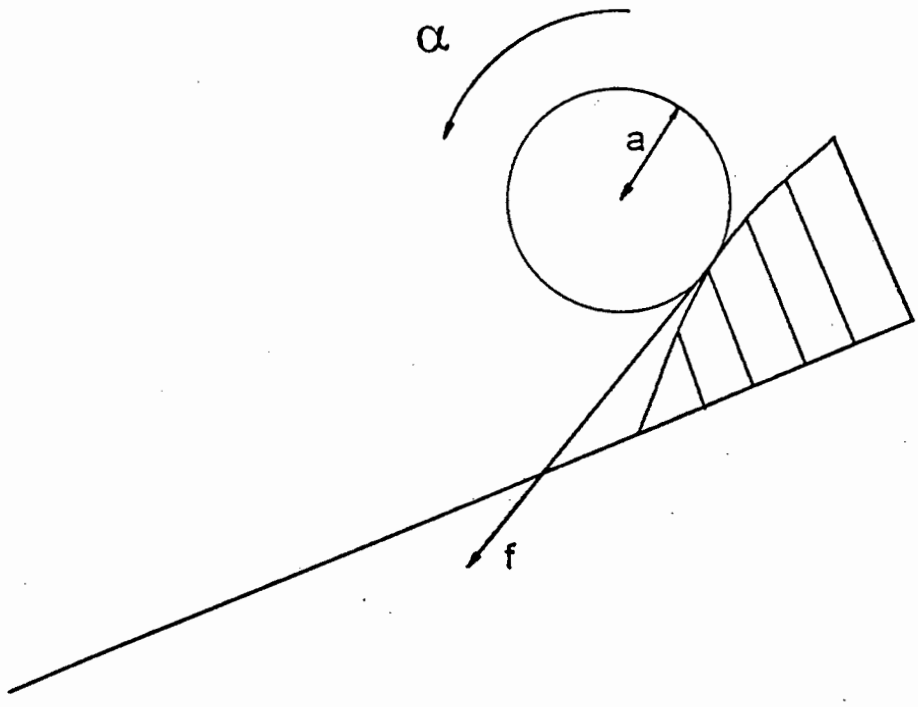

Figure II - 1 Ball rolling down the lifter bar.

In order to derive equation 3 the moments are summed about the centre of the ball. The Friction force is the only force which does not act through the centre of the ball and hence this is the only force applying a moment about the ball centre. It is also essential to note that when a ball rolls down an incline, the friction force acts in the direction of motion to counter slip which might occur on the contact surfaces.

Torque about the centre of the ball :

$f \cdot a = I_o \cdot \alpha$

Where I_o = Moment of inertia about the ball's centre.

and :

$I_o = \frac{2}{5}[ma^2]$ for a Ball.

α = Angular acceleration of the ball about its centre.

$\alpha = \frac{\ddot{S}}{a}$

Where $\ddot{S}$ = Tangential acceleration of the ball on the lifter.

therefore :

$$f \cdot a = \frac{2}{5} m a^2 \frac{\ddot{S}}{a}$$

simplifying to :

$$f = \frac{2}{5} m \ddot{S}$$

APPENDIX III

Geometric Transformations

(Local to Global)

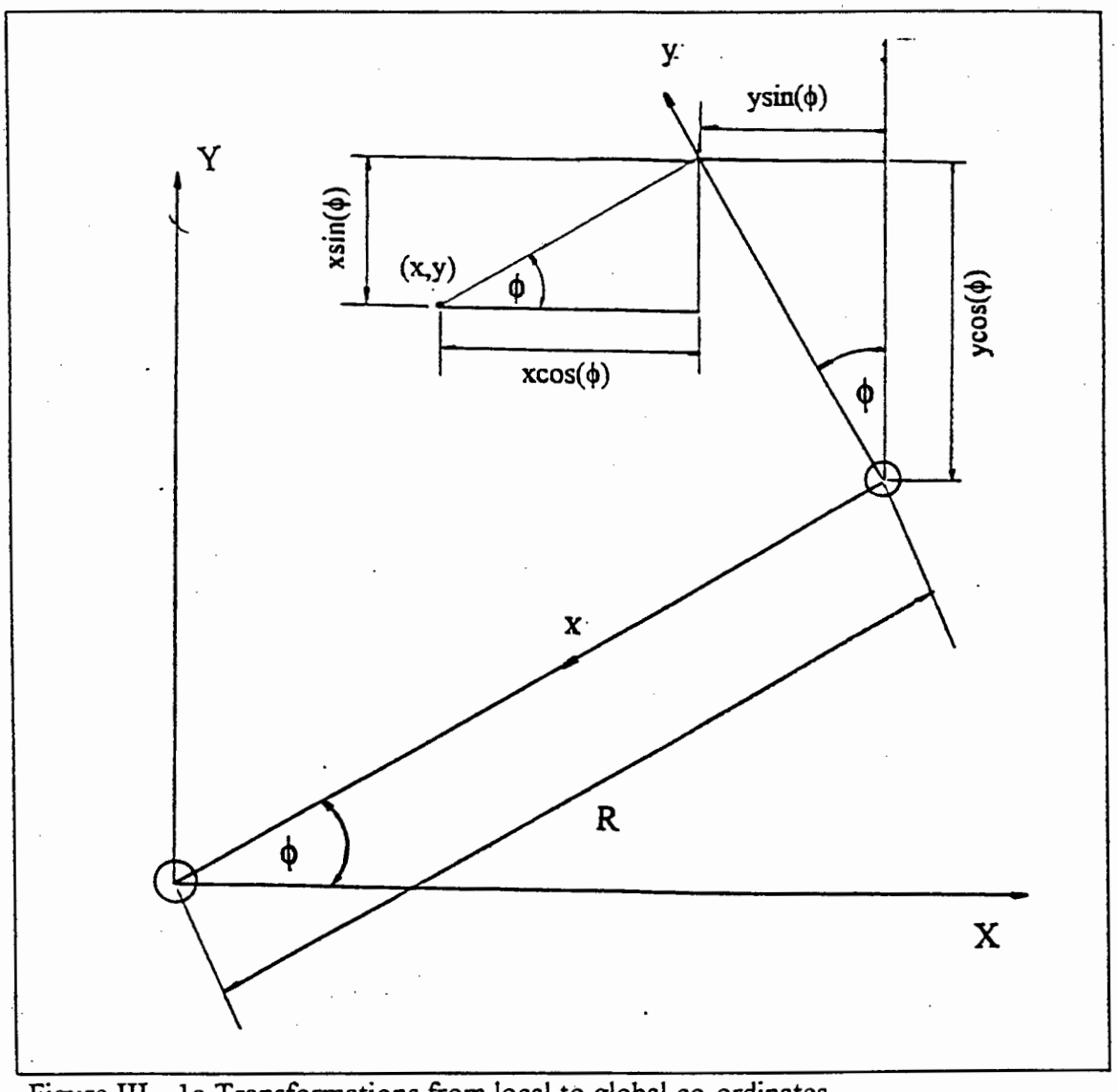

Figure III - 1a Transformations from local to global co-ordinates

The transformation from local x and y co-ordinates to global X and Y co-ordinates in the first quadrant only are :

$$X = R\cos(\phi) - [\, y\sin(\phi) + x\cos(\phi)] \qquad \text{(A-1)}$$

$$Y = R\sin(\phi) + [\, y\cos(\phi) - x\sin(\phi)] \qquad \text{(A-2)}$$

In order to determine all the variables in terms of x_b (figure III - 1b) and time we have to consider the following geometric transformations.

$y_b = Ax_b^2 + C$ (From the definition of our parabolic lifter bar)

$x_c = x_b + a\sin(\theta)$

$y_c = y_b + a\cos(\theta)$ (from figure III - 1b)

$\phi = \Omega t$ Where t = time

Therefore, substituting these transformations into equation A-1 and A-2 :

$$X_c = R\cos(\Omega t) - [(y_b + a\cos(\theta))\sin(\Omega t) + (x_b + a\sin(\theta))\cos(\Omega t)] \qquad (A - 3)$$

$$Y_c = R\sin(\Omega t) + [(y_b + a\cos(\theta))\cos(\Omega t) - (x_b + a\sin(\theta))\sin(\Omega t)] \qquad (A - 4)$$

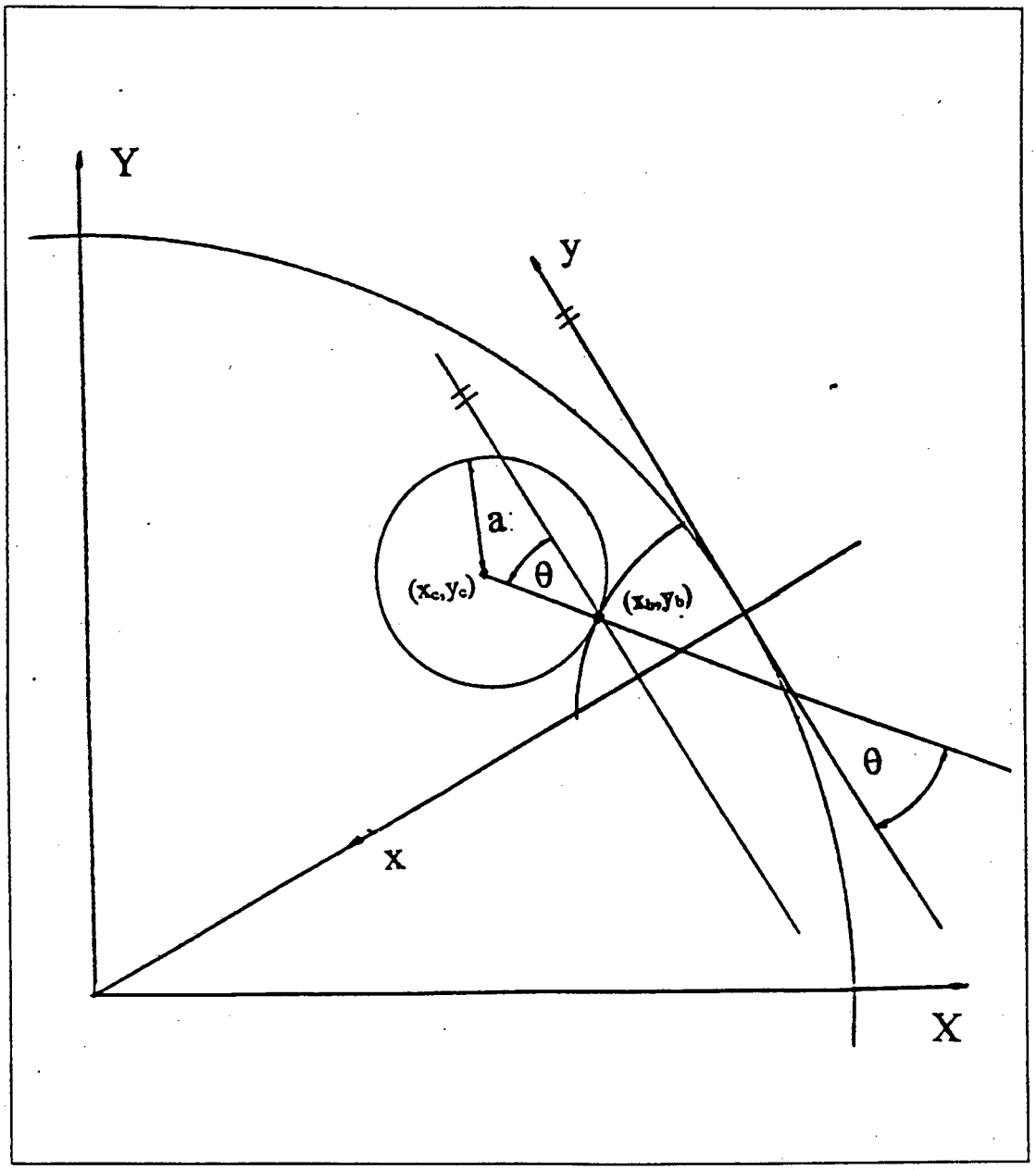

Figure III - 1b Determining the centre of the ball in terms of contact co-ordinates

The time dependant variables (subscript t) relate to those values that vary as the mill rotates.

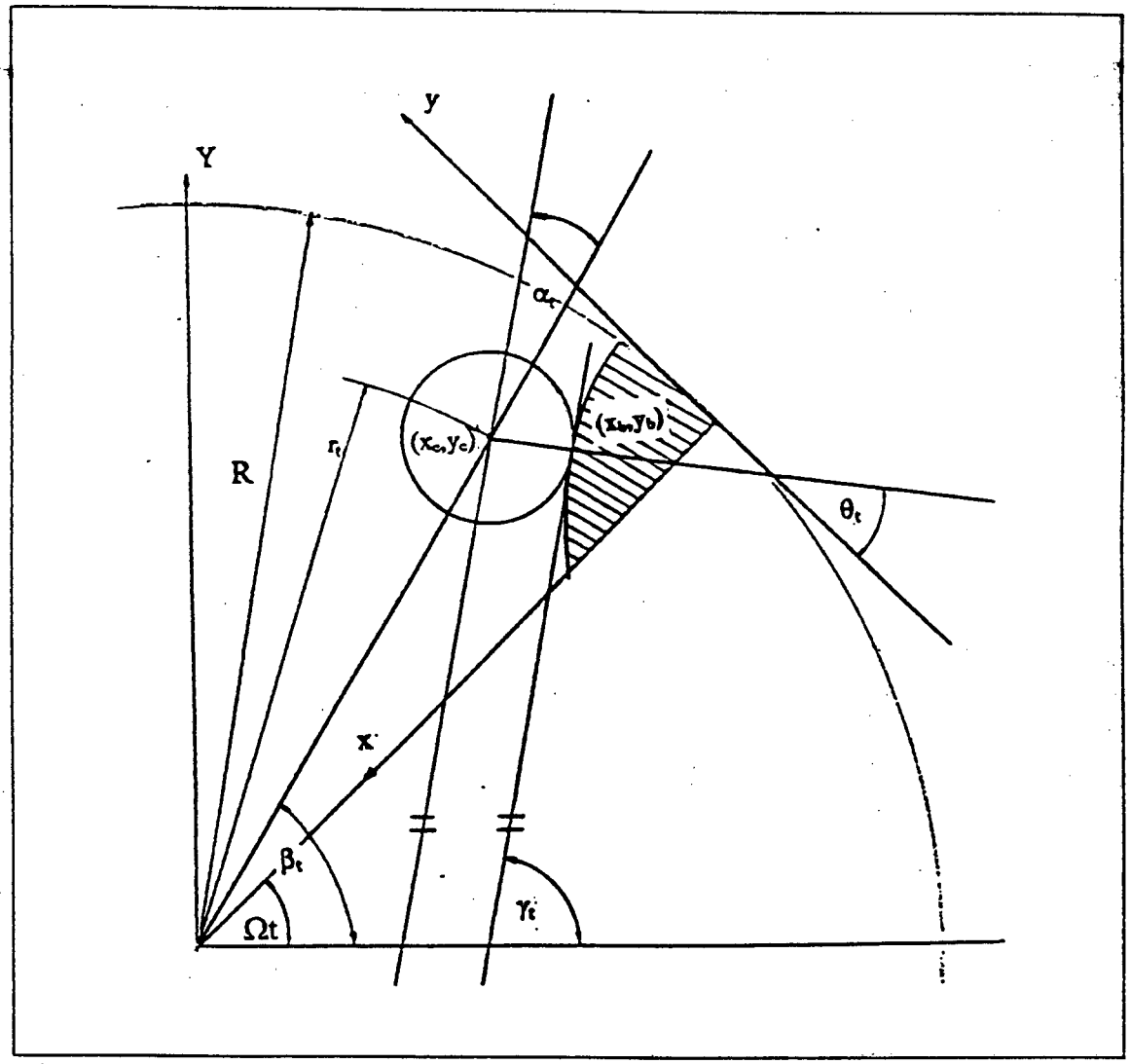

Figure III - 2 Transformations of time dependant angles into local co-ordinates

$$r_t = \sqrt{X_c^2 + Y_c^2} \qquad \text{(A - 5)}$$

Where (X_c, Y_c) is the global co-ordinate of the centre of the ball.

$$\gamma_t = \arctan(-2Ax_b + \Omega t) \qquad \text{(A - 6)}$$

$$\beta_t = \arctan\left(\frac{Y_c}{X_c}\right) \qquad \text{(A - 7)}$$

$$\alpha_t = \gamma_t - \beta_t \qquad \text{(A - 8)}$$

$$\theta_t = \frac{\Pi}{2} + \arctan\left(\frac{1}{2Ax_b}\right) \qquad \text{(A - 9)}$$

Substituting equation A-3 and A-4 into equations A-5 through A-9 and all the variables have been defined in x_b and t.

Also :

$$\rho = \left[\frac{\left[1 + \left(\frac{dy}{dx} \right)^2 \right]^{\frac{3}{2}}}{\frac{d^2y}{dx^2}} \right]$$

From [30]

Where ρ = instantaneous centre of rotation about a moving point O of the ball on the lifter (figure III - 3).

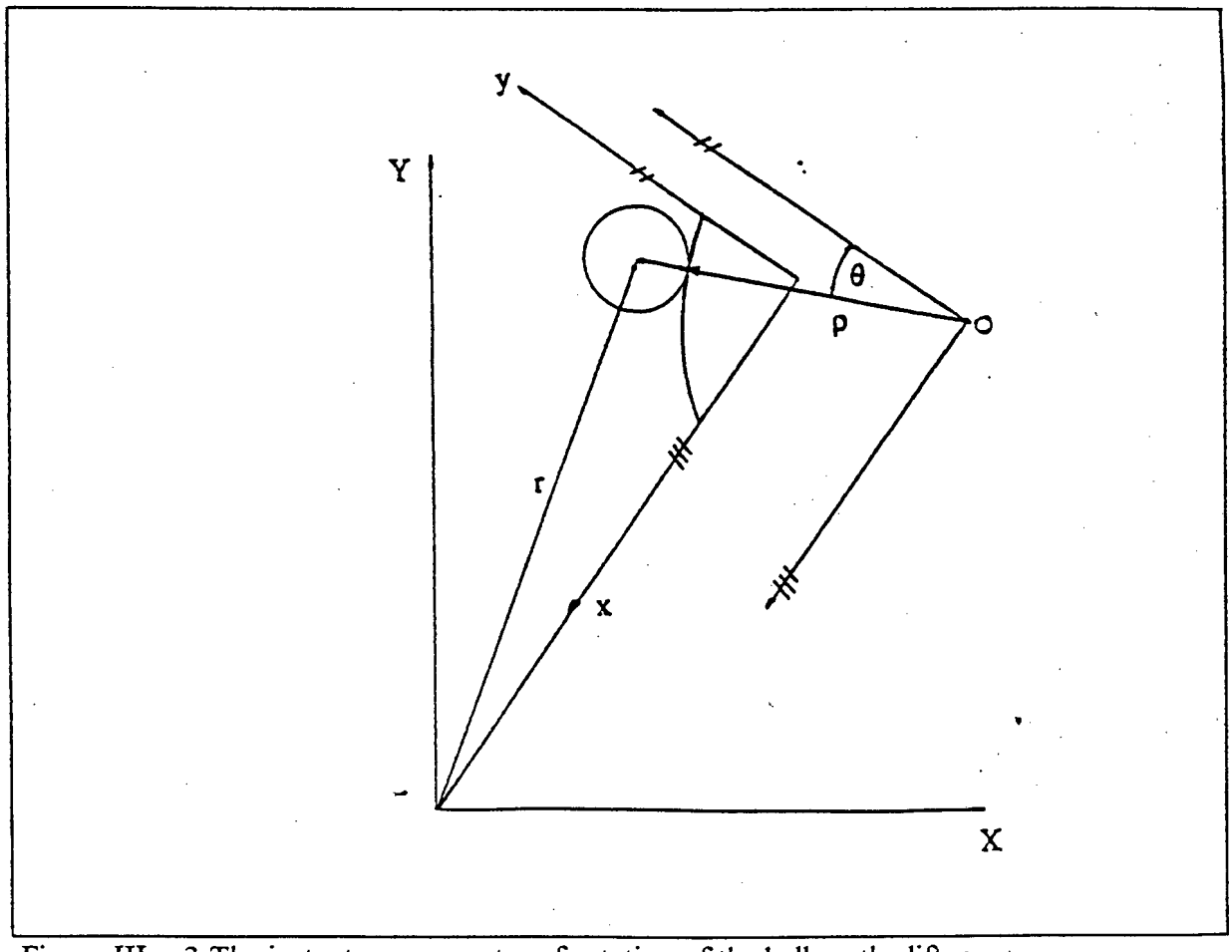

Figure III - 3 The instantaneous centre of rotation of the ball on the lifter

For a parabolic lifter of the form $y_b = Ax_b^2 + C$:

$$\rho_t = \frac{\left[1 + 4A^2 x_b^{\,2} \right]^{\frac{3}{2}}}{2|A|} \qquad \text{(A-10)}$$

Because A is negative in the definition of the model, the modulus of A must be used in this equation in order to obtain a positive answer for ρ_t.

APPENDIX IV

Iterative Difference Method to Solve for the Initial Contact Point of the Ball on the Lifter

The contact equation is :

$$\sqrt{\left(R-\left(x_b+a\sin\left(\frac{\Pi}{2}+\arctan\left(\frac{1}{2Ax_b}\right)\right)\right)\right)^2+\left(Ax_b^{\,2}+C+a\cos\left(\frac{\Pi}{2}+\arctan\left(\frac{1}{2Ax_b}\right)\right)\right)^2}=(R-a)$$

The iterative solution scheme to solve this equation is illustrated in figure IV - 1 and is structured as follows :

1. The point where the parabolic lifter cuts the local x axis (x_b , 0) is first determined.

$$x_{bcut}=\sqrt{\frac{-C}{A}}$$

2. Half of this value is used as the initial guess to substitute into the contact equation.

$$x_{b1}=\frac{x_{bcut}}{2}$$

3. Using this value of x_{b1} in the contact equation, the value of the right hand side of the equation is determined.

   a) If this solution is greater than (R - a) then a new value halfway between x_{bcut} and x_{b1} is used in the second iteration.

$$x_{b2}=\frac{x_{b2}-x_{bcut}}{2}$$

   b) If the value is less than (R - a) then a new value half way between x = 0 and x_{b1} is used for the second iteration.

$$x_{b2}=\frac{x_{b2}-x_{bcut}}{2}$$

4. This new value is again substituted into the contact equation and this process is continued until the desired solution is obtained.

Figure IV - 1 illustrates the procedure which was described in the four points above.

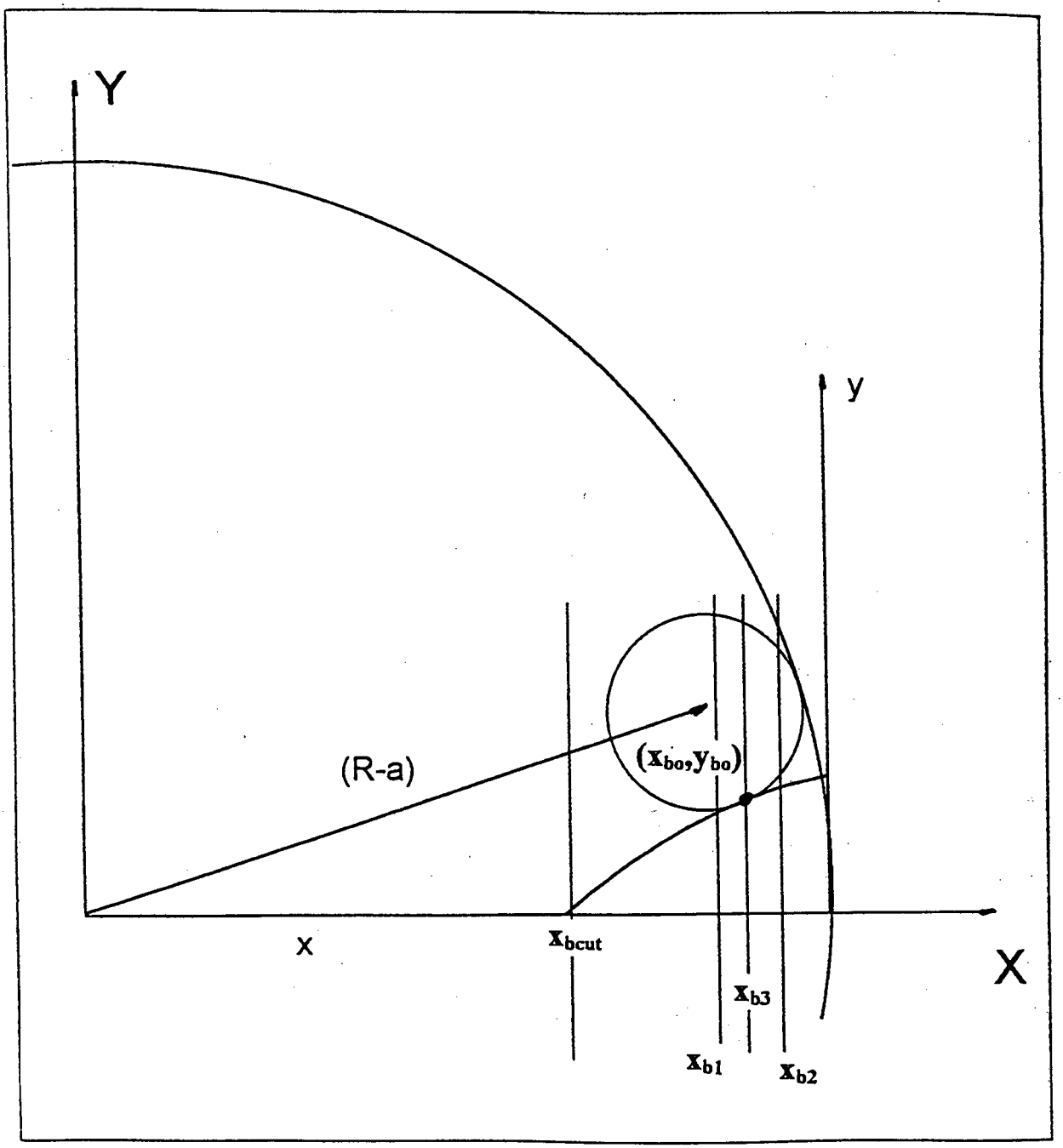

Figure IV - 1 The initial contact point of the ball on the lifter bar

An iterative scheme is used to solve :

$$\sqrt{\left(R-\left(x_b+a\sin(\theta)\right)\right)^2+\left(y_b+a\cos(\theta)\right)^2}=\left(R-a\right)$$

The geometric transformations of θ and y_b as derived in Appendix III are substituted into this relationship in order to define the equation in terms of only x_b.

APPENDIX V

Derivation of Variables at the Equilibrium Point

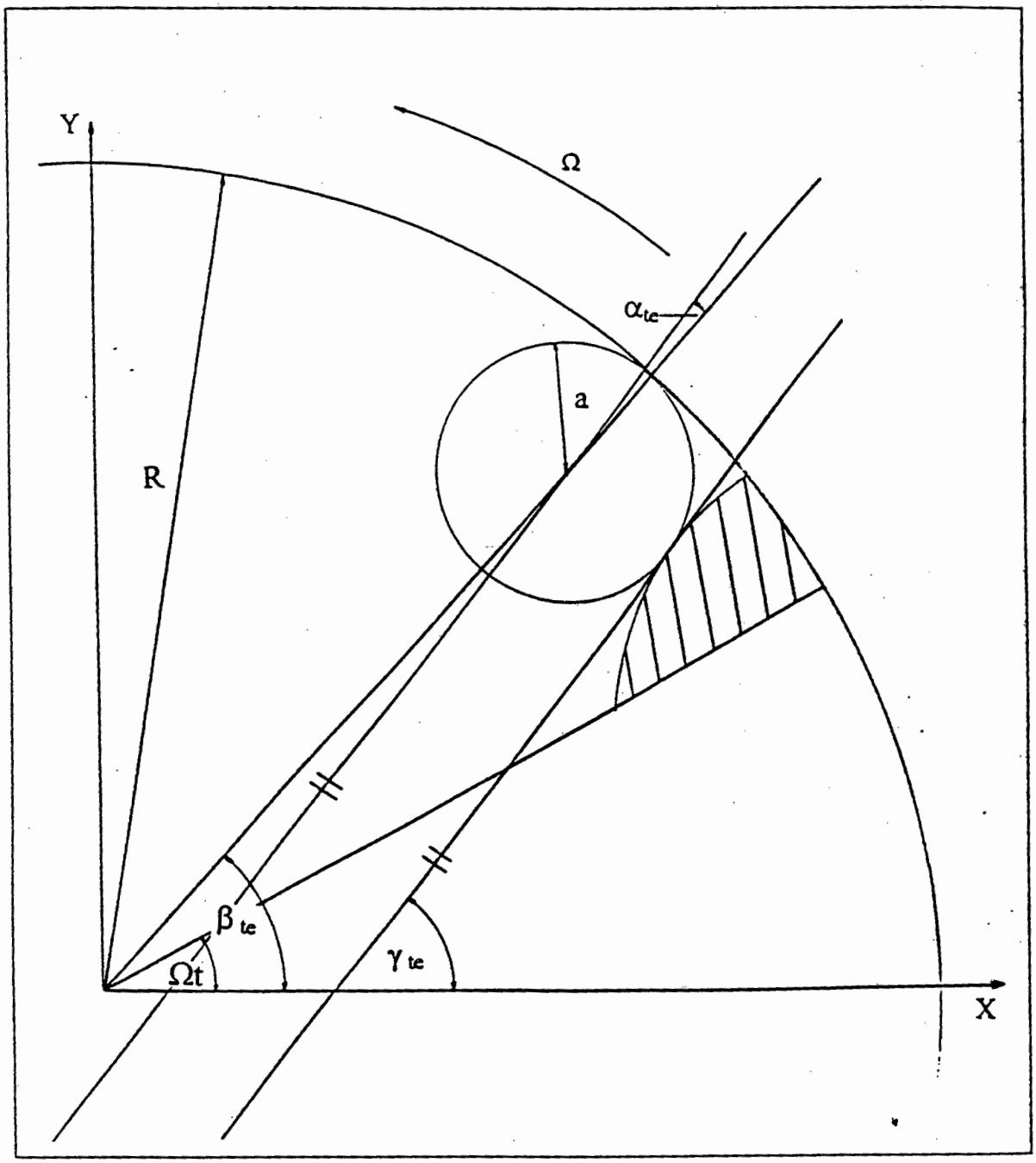

Figure V - 1 The definition of variables at the equilibrium point.

Considering that $\phi = 0$ and $t = 0$ at the neutral position, the equations in Appendix III can be simplified as follows to determine the relevant numerical values of the variables at this neutral point.

Substituting $\phi = 0$ and $t = 0$ into equations A-1 through A- 9 the following relationships are obtained :

$$X_{te} = R - x_{bo} \qquad (A - 11)$$

$$Y_{te} = y_{bo} \qquad (A - 12)$$

$$\gamma_{te} = \arctan(-2Ax_{bo}) \qquad (A - 13)$$

$$\beta_{te} = \arctan\left(\frac{Y_{co}}{X_{co}}\right) \qquad (A - 14)$$

where :

x_{bo} = Contact point on the lifter bar determined from initial conditions.

(X_{co}, Y_{co}) = Global co-ordinate of the centre of the ball at the neutral position determined by substituting (x_{bo}, y_{bo}) into equations A - 11 and A -12.

$$r_{te} = r_o = \sqrt{X_{co}^2 + Y_{co}^2} \qquad (A - 15)$$

$$\alpha_0 = \gamma_0 - \beta_0 \qquad (A - 16)$$

and :

$$\theta_0 = \frac{\Pi}{2} + \arctan\left(\frac{1}{2Ax_{bo}}\right) \qquad (A - 17)$$

APPENDIX VI

Newton Raphson Scheme to Solve for the Equilibrium Angle

The equilibrium equation is :

$$g \sin\gamma_t - \mu(g \cos\gamma_t + \Omega^2(R-a) \sin\alpha_0) - \Omega^2(R-a) \cos \alpha_0 = 0$$

This function can be written as :

$$F(\gamma_t) = g \sin\gamma_t - \mu(g \cos\gamma_t + \Omega^2(R-a) \sin\alpha_0) - \Omega^2(R-a) \cos \alpha_0.$$

The Newton Raphson Method is stated as :

$$\gamma_{t(i+1)} = \gamma_{t(i)} - \left(\frac{F(\gamma_{t(i)})}{F'(\gamma_{t(i)})} \right)$$

Now :

$$F'(\gamma_t) = g\cos(\gamma_t) + \mu\, g \sin(\gamma_t)$$

So from the definition of the Newton Raphson Method :

$$\gamma_{t(i+1)} = \gamma_{t(i)} - \left[\frac{g \sin(\gamma_t) - \mu g \cos(\gamma_t) - \mu\Omega^2(R-a)\sin(\alpha_0) - \Omega^2(R-a)\cos(\alpha_0)}{g\cos(\gamma_t) + \mu g \sin(\gamma_t)} \right]$$

The solution to this equation is the equilibrium angle γ_{te}.

APPENDIX VII

Geometric Transformations for the Velocity Terms

In order to solve equations 14 and 26 the equations have to be rewritten in terms of x and t only. All the geometric transformations relating to position (angles and distances) have been derived in Appendix III. The geometric transformations for the velocity is derived in this section. The velocity of the ball on the lifter face ($\ddot{S}$) has to be rewritten in terms of x and t. Figure VII - 1 illustrates how this transformation is derived.

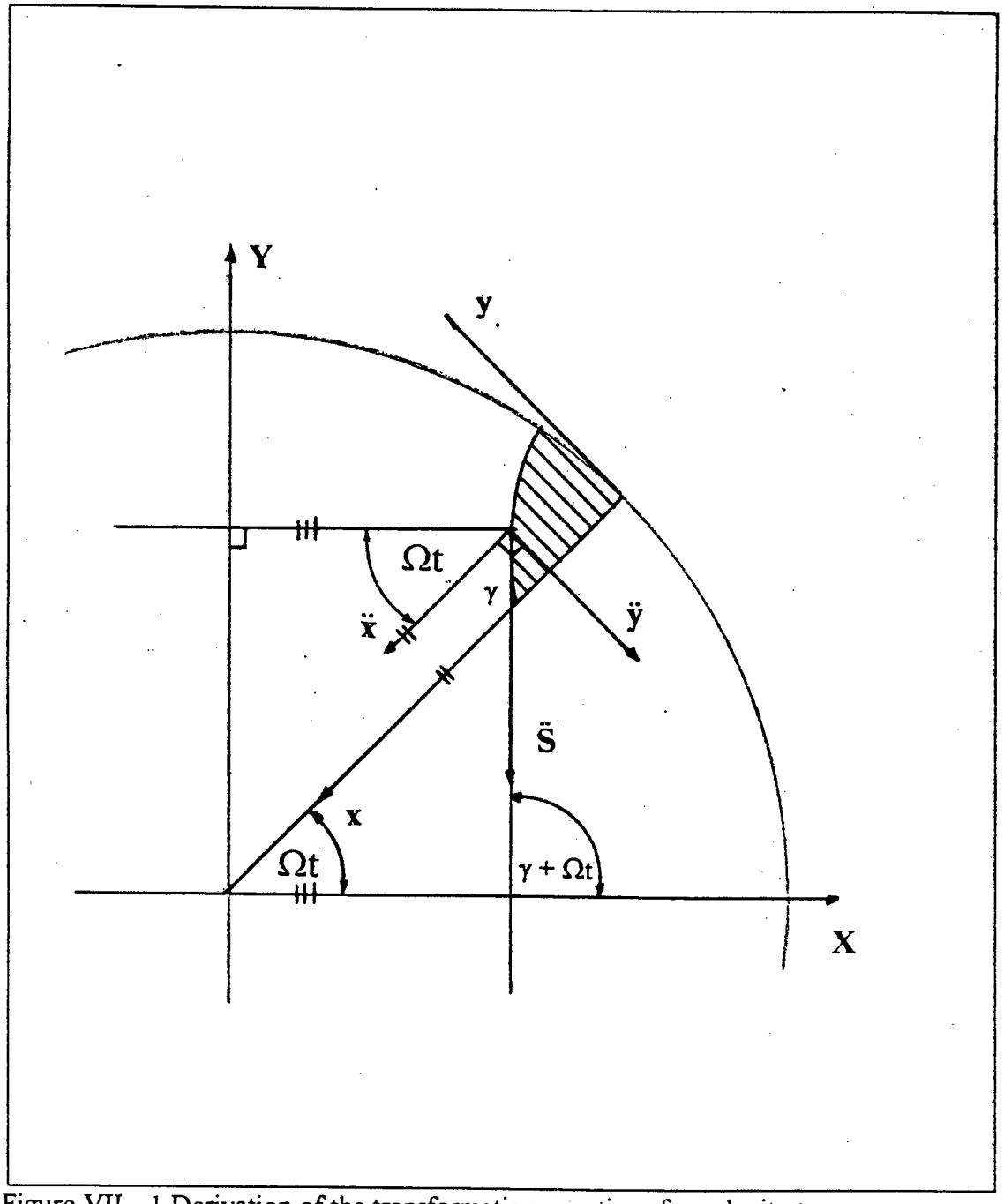

Figure VII - 1 Derivation of the transformation equations for velocity terms

From figure VII - 1 it is evident that :

$$\ddot{S} = \frac{\ddot{x}}{\cos(\gamma_t - \Omega t)} \qquad \text{(A - 18)}$$

similarly :

$$\dot{S} = \frac{\dot{x}}{\cos(\gamma_t - \Omega t)} \qquad \text{(A - 19)}$$

By substituting the transformations (A - 1) to (A - 11) as well as (A - 18) and (A - 19) into equations 14 and 26, the governing equations are rewritten in terms of only x and t. A Runga Kutta scheme is used to solve the equations in this form.

APPENDIX VIII

Fourth Order Runga Kutta Solution for Rolling and sliding

Appendix VIII - 1 Formulation of the Fourth Order Runga-Kutta Numerical Solution Scheme.

The Runga-Kutta numerical solution scheme can be used for equations of arbitrary order by means of transformation to a system of first-order.

The method is formulated as follows [29]:

For a second order equation $y'' = f(x, y, y')$, two first order equations can be obtained. Put $y' = z$ and obtain the following system of first order equations.

$$y' = z$$

$$z' = f(x, y, z)$$

This is a special case of :

$$y' = F(x, y, z)$$
$$z' = G(x, y, z)$$

which is integrated through :

$$k_1 = hF(x, y, z) \qquad l_1 = hG(x, y, z)$$

$$k_2 = hF\left(x + \frac{1}{2}h, y + \frac{1}{2}k_1, z + \frac{1}{2}l_1\right) \qquad l_2 = hG\left(x + \frac{1}{2}h, y + \frac{1}{2}k_1, z + \frac{1}{2}l_1\right)$$

$$k_3 = hF\left(x + \frac{1}{2}h, y + \frac{1}{2}k_2, z + \frac{1}{2}l_2\right) \qquad l_3 = hG\left(x + \frac{1}{2}h, y + \frac{1}{2}k_2, z + \frac{1}{2}l_2\right)$$

$$k_4 = hF(x + h, y + k_3, z + l_3) \qquad l_4 = hG(x + h, y + k_3, z + l3)$$

$$k = \frac{1}{6}(k_1 + 2k_2 + 2k_3 + k_4) \qquad l = \frac{1}{6}(l_1 + 2l_2 + 2l_3 + l_4)$$

where :

h = time step

and :

The new values are (x + k, v + l, t + h)

Appendix VIII - 2 Application of the Fourth Order Runga-Kutta Method to the Rolling Equations.

The two first order equations governing the rolling motion of the ball that are derived in chapter 3.3 are :

$$\dot{x} = v$$

$$\dot{v} = \frac{5\left(g\sin(\gamma_t) - \Omega^2 r_t \cos\left(\alpha_t\right)\right) \times (\cos(\gamma_t - \Omega t))}{7}$$

The format of the equations are thus :

$$\dot{x} = F(v)$$

$$\dot{v} = G(x,t)$$

A time constant has to be determined in order to step through the problem in small time intervals, the time constant being h.

The initial conditions have been determined and are :

$x = x_{equilibrium}$

$v = 0$

$t = t_{equilibrium}$

Setting up a procedure to step through the problem by considering the motion at finite time intervals the following is obtained :

$$k_1 = h(v)$$

In order to determine l_1 the values of γ_t , r_t and α_t must be determined for G(x,t) :

$$l_1 = h\left(\frac{5\left(g\sin(\gamma_t) - \Omega^2 r_t \cos\left(\alpha_t\right)\right) \times (\cos(\gamma_t - \Omega t))}{7} \right)$$

$$k_2 = h\left(v + \frac{1}{2} l_1 \right)$$

Similarly, values of γ_t , r_t and α_t must be determined for $G\left(x + \frac{1}{2} l_1 , t + \frac{1}{2} h \right)$ and substituted into l_2 :

$$l_2 = h\left(\frac{5\left(g\sin(\gamma_t) - \Omega^2 r_t \cos\left(\alpha_t\right)\right) \times (\cos(\gamma_t - \Omega t))}{7} \right)$$

$$k_3 = h\left(v + \frac{1}{2} l_2 \right)$$

The values of γ_t , r_t and α_t must be determined for $G\left(x + \frac{1}{2} l_2 , t + \frac{1}{2} h \right)$ and substituted into l_3 :

$$l_3 = h\left(\frac{5\left(g\sin(\gamma_t) - \Omega^2 r_t \cos\left(\alpha_t\right)\right) \times (\cos(\gamma_t - \Omega t))}{7} \right)$$

$$k_4 = h\left(v + l_3 \right)$$

The values of γ_t , r_t and α_t must be determined for $G(x + l_3, t + h)$ and substituted into l_4 :

$$l_4 = h\left(\frac{5\left(g\sin(\gamma_t) - \Omega^2 r_t \cos(\alpha_t)\right) \times (\cos(\gamma_t - \Omega t))}{7} \right)$$

now :

$$k = \frac{1}{6}(k_1 + 2k_2 + 2k_3 + k_4) \qquad l = \frac{1}{6}(l_1 + 2l_2 + 2l_3 + l_4)$$

The new values after the time step are :

$x_{i+1} = x_i + k$

$v_{i+1} = v_i + l$

$t_{i+1} = t_i + h$

The initial conditions are necessary to calculate the first step in the problem. The answers obtained from the first time step are used as the initial conditions in the second time step. This process is continued until the ball reaches the angle of limiting friction at which point the calculations for the sliding solution scheme starts.

Appendix VIII - 3 Application of the Fourth Order Runga-Kutta Method to the Sliding Equations.

The system of first order equations governing the sliding motion of the ball that have been derived insection 3.5 are :

$$\dot{x} = v$$

$$\ddot{x} = \cos(\gamma - \Omega t)\left[g\sin(\gamma_t) - \Omega^2 r_t \cos(\alpha_t) - \mu\left[g\cos(\gamma_t) + \Omega^2 r_t \sin(\alpha_t) + \frac{\dot{x}^2}{\rho\left(\cos(\gamma_t - \Omega t)\right)^2} \right] \right]$$

The format of the equations are thus :

$$\dot{x} = F(v)$$

$$\dot{v} = G(x, v, t)$$

The same time constant as determined for the rolling scheme can be used here.

The initial conditions are obtained from the last step in the rolling solution.

Applying Fourth order Runga-Kutta to the governing equations :

$$\mathbf{k_1} = \mathbf{h}(v)$$

In order to determine l_1 the values of γ_t , r_t and α_t must be determined for G(x,v,t) :

$$l_1 = h\left(\cos(\gamma - \Omega t)\left[g\sin(\gamma_t) - \Omega^2 r_t \cos(\alpha_t) - \mu\left[g\cos(\gamma_t) + \Omega^2 r_t \sin(\alpha_t) + \frac{\dot{x}^2}{\rho\left(\cos(\gamma_t - \Omega t)\right)^2} \right] \right] \right)$$

$$\mathbf{k_2 = h\left(v + \frac{1}{2} l_1 \right)}$$

Similarly, values of γ_t , r_t and α_t must be determined for $G\left(x + \frac{1}{2} l_1 , t + \frac{1}{2} h \right)$ and substituted into l_2 :

$$l_2 = h\left(\cos(\gamma - \Omega t)\left[g\sin(\gamma_t) - \Omega^2 r_t \cos(\alpha_t) - \mu\left[g\cos(\gamma_t) + \Omega^2 r_t \sin(\alpha_t) + \frac{\dot{x}^2}{\rho\left(\cos(\gamma_t - \Omega t)\right)^2} \right] \right] \right)$$

$$\mathbf{k_3 = h\left(v + \frac{1}{2} l_2 \right)}$$

The values of γ_t , r_t and α_t must be determined for $G\left(x + \frac{1}{2} l_2 , t + \frac{1}{2} h \right)$ and substituted into l_3 :

$$l_3 = h\left(\cos(\gamma - \Omega t)\left[g\sin(\gamma_t) - \Omega^2 r_t \cos(\alpha_t) - \mu\left[g\cos(\gamma_t) + \Omega^2 r_t \sin(\alpha_t) + \frac{\dot{x}^2}{\rho\left(\cos(\gamma_t - \Omega t)\right)^2} \right] \right] \right)$$

$$k_4 = h\left(v + l_3\right)$$

The values of γ_t , r_t and α_t must be determined for $G\left(x + l_3, t + h\right)$ and substituted into l_4 :

$$l_4 = h\left(\cos\left(\gamma - \Omega t\right)\left[g\sin\left(\gamma_t\right) - \Omega^2 r_t \cos\left(\alpha_t\right) - \mu\left[g\cos\left(\gamma_t\right) + \Omega^2 r_t \sin\left(\alpha_t\right) + \frac{\dot{x}^2}{\rho\left(\cos\left(\gamma_t - \Omega t\right)\right)^2} \right] \right] \right)$$

now :

$$k = \frac{1}{6}\left(k_1 + 2k_2 + 2k_3 + k_4\right) \qquad l = \frac{1}{6}\left(l_1 + 2l_2 + 2l_3 + l_4\right)$$

The new values after the time step are :

$x_{i+1} = x_i + k$

$v_{i+1} = v_i + l$

$t_{i+1} = t_i + h$

where

x = The position of the ball on the lifter (local co-ordinate).

v = Velocity of the ball tangential to the lifter surface.

t = Time taken from the neutral position.

These values are the values used in the next time step.

When the point of departure is reached the velocity down the slope (v) and time taken to reach this departure point (t) is determined from the last iteration before the loop is terminated in the sliding solution.

APPENDIX IX

Parabolic Trajectory

When the ball is projected into free flight, two velocity components are present. The first component (V_L) acts along the face of the lifter bar where the second component (V_n) is the velocity due to the rotation of the mill and acts perpendicular to the radius from the centre of the mill to the centre of the ball.

As the ball departs from the lifter, V_L acts along the tangent to the lifter face. Two situations may arise which might justify the need for two separate equations to predict the resultant ball velocity. The two situations are :

- V_L acts along the tangent when $\gamma_d < 90°$
- V_L acts along the tangent when $\gamma_d > 90°$

In order to derive the equations needed to determine the resultant velocity of the ball due to both velocity terms, both cases have to be considered.

Case 1 where $\gamma_d < 90°$

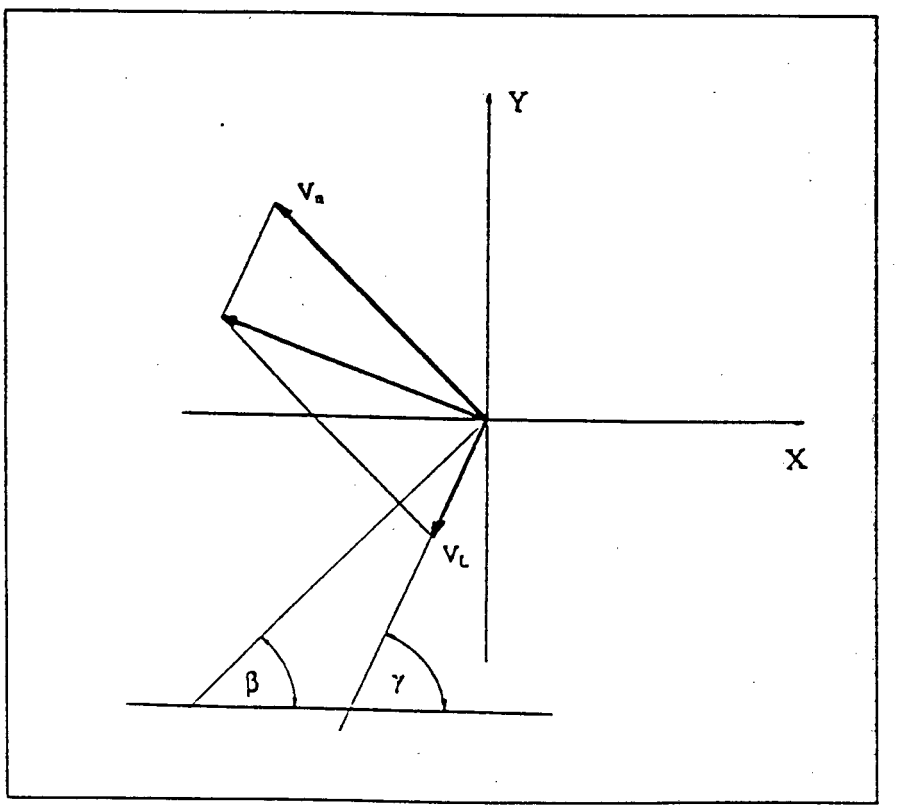

Figure IX - 1 Resultant Velocity for $\gamma_d < 90°$

The equations giving the X and Y components of velocity are thus :

$V_x = - [V_n \sin(\beta_d) + V_L \cos(\gamma_d)]$

$V_y = [V_n \cos(\beta_d) - V_L \sin(\gamma_d)]$

Case 2 where $\gamma_d > 90°$

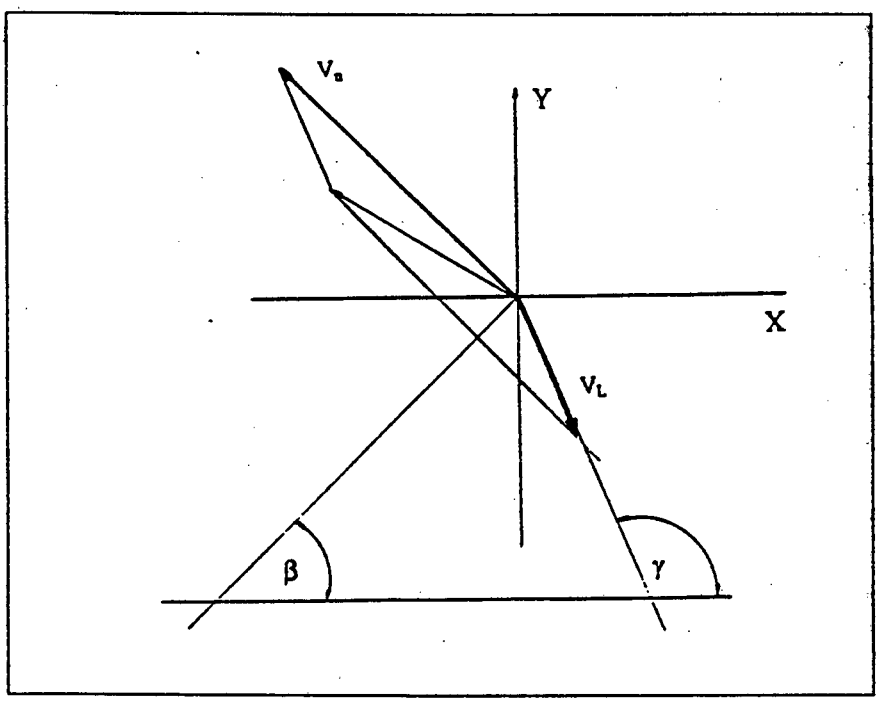

Figure IX - 2 Resultant Velocity for $\gamma_d > 90°$.

The equations giving the X and Y components of velocity are thus :

$$V_x = - [V_n \sin(\beta_d) - V_L \sin(\gamma_d - \frac{\Pi}{2})]$$

$$V_y = [V_n \cos(\beta_d) - V_L \cos(\gamma_d - \frac{\Pi}{2})]$$

Simplifying the equations we obtain :

$$V_x = - [V_n \sin(\beta_d) + V_L \cos(\gamma_d)]$$

$$V_y = [V_n \cos(\beta_d) - V_L \sin(\gamma_d)]$$

It is noted that the equations determining V_x and V_y are identical for both cases. The resultant velocity equation is therefore found to be independent of the angle γ_d in which V_L acts at the point of departure.

APPENDIX X

Transforming $\dot{x}$ Back to the Velocity Component Down the Lifter Bar ($\dot{S}$)

The solutions of the governing equations yield the velocity of the ball in the x direction ($\dot{x}$). This velocity must be transformed back into the resultant velocity of the ball down the lifter bar (V_L) in order to obtain the departure velocity of the ball.

$$V_L = \sqrt{\dot{x}^2 + \dot{y}^2}$$

where :

$$y = Ax^2 + C$$

so :

$$\dot{y} = 2Ax\dot{x}$$

therefore :

$$V_L = \sqrt{\dot{x}^2 + (2Ax\dot{x})^2}$$

APPENDIX XI

Listing of the "Mill Simulator" Program which Predicts the ball's Sliding Motion

(Written in VISUAL BASIC)

Subroutine Equilibrium

The subroutine uses a Newton Raphson numerical solution scheme to calculate the equilibrium angle which the ball will reach before it starts sliding down the lifter face.

```
Sub EQUILIBRIUM (omegaZ, MRZ, BRZ, muZ, Xoz, gammao, betao, alphao, toz,
                 gammae, betae As Double, I As Integer)

  Dim gamA, gamb, z, temp1, temp2, rot As Double

    gamA = gammao
    gamb = 0
    rot = omegaZ * 2 * 3.14159 / 60
    z = (rot) ^ 2
    I = 0
    While ((gamA > (gamb + .00001)) Or (gamA < (gamb - .00001)))
      I = I + 1
        gamb = gamA
        temp1 = (z * (MRZ - BRZ) * Cos(alphao) + muZ * 9.81 * Cos(gamA)
        + muZ * z *       Sin(alphao) * (MRZ - BRZ) - 9.81 * Sin(gamA))
        temp2 = (-(muZ * 9.81 * Sin(gamA) + 9.81 * Cos(gamA)))
        gamA = gamA - (temp1 / temp2)
      If I > 10000 Then
          MsgBox "THE BALL HAS CENTRIFUGED", 48
          Exit Sub
      End If
    Wend
      gammae = gamA
      betae = gammae - alphao
      toz = (gammae - gammao) / rot
    End Sub
```

Subroutine Initial

The subroutine calculates the initial local contact co-ordinates of the ball on the lifter bar before it has started moving away from the mill wall. Once this contact point has been determined (as described in Appendix IV) then all the initial contact angles and distances are calculated

---

```
Sub initiall (AA, CC, RR, BR, contact, theta, beta, alpha As Double)

  Dim xcut, xb1, xb2, Xl, Phi, rt, t, S, int1, Int2 As Double


    xcut = Sqr(-CC / AA)
    xb1 = xcut / 2
    xb2 = 0
    Xl = xcut
    t = 0


    theta = (3.141592654 / 2) + Atn(1 / (2 * AA * xb1))
    Phi = Atn(-2 * AA * xb1)
    S = RR - (xb1 + BR * Sin(theta))
    beta = Atn((AA * (xb1 * xb1) + CC + BR * Cos(theta)) / (S))
    alpha = Phi - beta
    int1 = (RR - (xb1 + BR * Sin(theta))) * (RR - (xb1 + BR * Sin(theta)))
    Int2 = (AA * (xb1 * xb1) + CC + BR * Cos(theta)) * (AA * (xb1 * xb1) + CC +
           BR * Cos(theta))
    rt = Sqr(int1 + Int2)

    While ((rt > ((RR - BR) + .000000001)) Or (rt < ((RR - BR) - .000000001)))
        If (rt > (RR - BR)) Then
            xb2 = xb1
            xb1 = ((Xl - xb1) / 2) + xb1
        Else
            Xl = xb1
            xb1 = xb2 + ((xb1 - xb2) / 2)
        End If
        theta = (3.141592654 / 2) + Atn(1 / (2 * AA * xb1))
```

```
        Phi = Atn(-2 * AA * xb1)
        S = RR - (xb1 + BR * Sin(theta))
        beta = Atn((AA * xb1 * xb1 + CC + BR * Cos(theta)) / (S))
        alpha = Phi - beta
        int1 = (RR - (xb1 + BR * Sin(theta))) * (RR - (xb1 + BR * Sin(theta)))
        Int2 = (AA * (xb1) ^ 2 + CC + BR * Cos(theta)) * (AA * (xb1 ^ 2) + CC +
               BR * Cos(theta))
        rt = Sqr(int1 + Int2)

    Wend
    contact = xb1

End Sub
```

Subroutine Parab

Parab calculates the x and y cuts of the parabolic lifter bar once the values of A and C have been entered by the user. The parabolic lifter bar is also plotted by this subroutine.

```
Sub parab (Ap, CP, mdp, xop, Xcp As Double)

    Dim circle1, parab1, steps, counter, rp As Double

    Xcp = Sqr(-CP / Ap)
    circle1 = 0
    rp = mdp / 2
    parab1 = 1
    steps = mdp / 1000
    counter = 0
    While parab1 > circle1
        counter = counter + steps
        parab1 = Ap * (counter ^ 2) + CP
        circle1 = Sqr(2 * counter * rp - (counter) ^ 2)
        currentx = scalewidth / 10: currenty = -scaleheight / 1.2
    Wend
    xop = counter

End Sub
```

Subroutine Slide

The subroutine uses a fourth order Runga Kutta numerical solution scheme to calculate the ball's path on the lifter from the equilibrium point until it reaches the point of departure (As described in Appendix VIII-3). The departure angle and departure velocity are calculated by this subroutine and the x and y co-ordinates of the ball are plotted as the ball moves along the lifter.

```
Sub slide (A, c, d, v, R, fc, ti, xi, xcut, xdep, tdep, vdep, thetas, BETAS, gammas,
alphas, rts As Double)

    Dim H, xnew, tnew, vnew, Kt, LT, n  As Double
    Dim x1, x2, x3, v1, v2, v3, t1, t2, t3, v4, x4, t4, ynew, xic, yic As Double
    Static K(4), L(4) As Double
    Dim xcnew, ycnew, xdot, ydot, xdot1, ydot1 As Double

    H = 3.14159 / ((180 * v) * 1)    'Time step which can be set by the programmer

    xnew = xi          'The local x value when the ball starts to slide
    tnew = ti          'The time elapsed from the ball having passed the neutral point
                        till sliding begins
    vnew = 0           ' The velocity of the ball as sliding starts
    n = 1              'n = the normal force on the liner


      While (xnew < (xcut)) And (n > 0)

        thetas = (3.14159 / 2) + Atn(1 / (2 * A * xnew))
        gammas = (Atn(-2 * A * xnew) + v * tnew)

        BETAS = Atn((R * Sin(v * tnew) - (xnew + d * Sin(thetas)) * Sin(v * tnew) +
        (A * xnew * xnew + c + d * Cos(thetas)) * Cos(v * tnew)) / (R * Cos(v *
        tnew) - (xnew + d * Sin(thetas)) * Cos(v * tnew) - (A * xnew * xnew + c + d *
        Cos(thetas)) * Sin(v * tnew)))

        alphas = gammas - BETAS

        rts = Sqr(((R * Cos(v * tnew) - (A * xnew * xnew + c + d * Cos(thetas)) *
        Sin(v * tnew) - (xnew + d * Sin(thetas)) * Cos(v * tnew)) * (R * Cos(v *
```

```
tnew) - (A * xnew * xnew + c + d * Cos(thetas)) * Sin(v * tnew) - (xnew + d *
Sin(thetas)) * Cos(v * tnew)) + (R * Sin(v * tnew) + (A * xnew * xnew + c +
d * Cos(thetas)) * Cos(v * tnew) - (xnew + d * Sin(thetas)) * Sin(v * tnew)) *
(R * Sin(v * tnew) + (A * xnew * xnew + c + d * Cos(thetas)) * Cos(v * tnew)
- (xnew + d * Sin(thetas)) * Sin(v * tnew))))

  ynew = A * (xnew ^ 2) + c

  xic = xnew + d * Sin(thetas)
  yic = ynew + d * Cos(thetas)

  xcnew = R * Cos(v * tnew) - (yic * Sin(v * tnew) + xic * Cos(v * tnew))
  ycnew = R * Sin(v * tnew) + (yic * Cos(v * tnew) - xic * Sin(v * tnew))

  currentx = (scalewidth / 3) + xcnew
  currenty = -(scaleheight / 2) + ycnew
  fillcolor = QBColor(1)
  fillstyle = 0
  Circle (currentx, currenty), d, RGB(0, 0, 255)

  x1 = xnew
  v1 = vnew
  t1 = tnew

K(1) = H * v1
L(1) = (H * Cos(gammas - (v * t1))) * (9.81 * Sin(gammas) - v ^ 2 * rts *
Cos(alphas) - fc * 9.81 * Cos(gammas) - fc * v ^ 2 * rts * Sin(alphas) - (-2 * A
* v1 * v1) / (((1 + 4 * A * A * x1 * x1) ^ (3 / 2)) * ((Cos(gammas - (v * t1)))
^ 2)))

x2 = xnew + .5 * K(1)
v2 = vnew + .5 * L(1)
t2 = tnew + .5 * H

thetas = (3.14159 / 2) + Atn(1 / (2 * A * (x2)))
gammas = (Atn(-2 * A * x2) + v * (t2))

BETAS = Atn((R * Sin(v * t2) - (x2 + d * Sin(thetas)) * Sin(v * t2) + (A * x2
^ 2 + c + d * Cos(thetas)) * Cos(v * t2)) / (R * Cos(v * t2) - (x2 + d *
Sin(thetas)) * Cos(v * t2) - (A * x2 * x2 + c + d * Cos(thetas)) * Sin(v * t2)))
alphas = gammas - BETAS

rts = Sqr(((R * Cos(v * t2) - (A * x2 * x2 + c + d * Cos(thetas)) * Sin(v * t2) -
(x2 + d * Sin(thetas)) * Cos(v * t2)) * (R * Cos(v * t2) - (A * x2 * x2 + c + d
* Cos(thetas)) * Sin(v * t2) - (x2 + d * Sin(thetas)) * Cos(v * t2)) + (R * Sin(v
* t2) + (A * x2 * x2 + c + d * Cos(thetas)) * Cos(v * t2) - (x2 + d *
Sin(thetas)) * Sin(v * t2)) * (R * Sin(v * t2) + (A * x2 * x2 + c + d *
Cos(thetas)) * Cos(v * t2) - (x2 + d * Sin(thetas)) * Sin(v * t2))))
```

```
K(2) = H * v2
L(2) = (H * Cos(gammas - (v * t2))) * (9.81 * Sin(gammas) - v * v * rts *
Cos(alphas) - fc * 9.81 * Cos(gammas) - fc * v * v * rts * Sin(alphas) - (-2 * A
* v2 * v2) / (((1 + 4 * A * A * x2 * x2) ^ (3 / 2)) * ((Cos(gammas - (v * t2)))
^ 2)))

  x3 = xnew + .5 * K(2)
  v3 = vnew + .5 * L(2)
  t3 = tnew + .5 * H

  thetas = (3.14159 / 2) + Atn(1 / (2 * A * (x3)))
  gammas = (Atn(-2 * A * x3) + v * (t3))

BETAS = Atn((R * Sin(v * t3) - (x3 + d * Sin(thetas)) * Sin(v * t3) + (A * x3
* x3 + c + d * Cos(thetas)) * Cos(v * t3)) / (R * Cos(v * t3) - (x3 + d *
Sin(thetas)) * Cos(v * t3) - (A * x3 * x3 + c + d * Cos(thetas)) * Sin(v * t3)))

alphas = gammas - BETAS

rts = Sqr(((R * Cos(v * t3) - (A * x3 * x3 + c + d * Cos(thetas)) * Sin(v * t3) -
(x3 + d * Sin(thetas)) * Cos(v * t3)) * (R * Cos(v * t3) - (A * x3 * x3 + c + d
* Cos(thetas)) * Sin(v * t3) - (x3 + d * Sin(thetas)) * Cos(v * t3)) + (R * Sin(v
* t3) + (A * x3 * x3 + c + d * Cos(thetas)) * Cos(v * t3) - (x3 + d *
Sin(thetas)) * Sin(v * t3)) * (R * Sin(v * t3) + (A * x3 * x3 + c + d *
Cos(thetas)) * Cos(v * t3) - (x3 + d * Sin(thetas)) * Sin(v * t3))))


K(3) = H * v3
L(3) = (H * Cos(gammas - (v * t3))) * (9.81 * Sin(gammas) - v * v * rts *
Cos(alphas) - fc * 9.81 * Cos(gammas) - fc * v * v * rts * Sin(alphas) - (-2 * A
* v3 * v3) / (((1 + 4 * A * A * x3 * x3) ^ (3 / 2)) * ((Cos(gammas - (v * t3)))
^ 2)))

x4 = xnew + K(3)
v4 = vnew + L(3)
t4 = tnew + H

thetas = (3.14159 / 2) + Atn(1 / (2 * A * (x4)))
gammas = (Atn(-2 * A * x4) + v * (t4))

BETAS = Atn((R * Sin(v * t4) - (x4 + d * Sin(thetas)) * Sin(v * t4) + (A * x4
* x4 + c + d * Cos(thetas)) * Cos(v * t4)) / (R * Cos(v * t4) - (x4 + d *
Sin(thetas)) * Cos(v * t4) - (A * x4 * x4 + c + d * Cos(thetas)) * Sin(v * t4)))

alphas = gammas - BETAS

rts = Sqr(((R * Cos(v * t4) - (A * x4 * x4 + c + d * Cos(thetas)) * Sin(v * t4) -
(x4 + d *Sin(thetas)) * Cos(v * t4)) * (R * Cos(v * t4) - (A * x4 * x4 + c + d *
```

```
Cos(thetas)) * Sin(v * t4) - (x4 + d * Sin(thetas)) * Cos(v * t4)) + (R * Sin(v *
t4) + (A * x4 * x4 + c + d * Cos(thetas)) * Cos(v * t4) - (x4 + d * Sin(thetas))
* Sin(v * t4)) * (R * Sin(v * t4) + (A * x4 * x4 + c + d * Cos(thetas)) * Cos(v
* t4) - (x4 + d * Sin(thetas)) * Sin(v * t4))))


K(4) = H * v4
L(4) = (H * Cos(gammas - (v * t4))) * (9.81 * Sin(gammas) - v * v * rts *
Cos(alphas) - fc * 9.81 * Cos(gammas) - fc * v * v * rts * Sin(alphas) - (-2 * A
* v4 * v4) / (((1 + 4 * A * A * x4 * x4) ^ (3 / 2)) * ((Cos(gammas - (v * t4)))
^ 2)))


Kt = (K(1) + 2 * K(2) + 2 * K(3) + K(4)) / 6
LT = (L(1) + 2 * L(2) + 2 * L(3) + L(4)) / 6


xnew = xnew + Kt
ynew = A * xnew ^ 2 + c
vnew = vnew + LT
tnew = tnew + H


n = v ^ 2 * rts * Sin(alphas) + 9.81 * Cos(gammas) + ((2 * A * (vnew ^ 2)) /
((1 + 4 * A ^ 2 * xnew ^ 2) ^ (3 / 2)))
Wend

xdep = xnew
vdep = vnew
tdep = tnew

thetas = (3.14159 / 2) + Atn(1 / (2 * A * (xdep)))

BETAS = Atn((R * Sin(v * tdep) - (xdep + d * Sin(thetas)) * Sin(v * tdep) + (A *
xdep ^ 2 + c + d * Cos(thetas)) * Cos(v * tdep)) / (R * Cos(v * tdep) - (xdep + d *
Sin(thetas)) * Cos(v * tdep) - (A * xdep ^ 2 + c + d * Cos(thetas)) * Sin(v * tdep)))

End Sub
```

Subroutine Traject

The subroutine uses the departure velocity of the ball and calculates the parabolic path of the ball from the point of departure to the point of impact on the mill shell (Appendix IX). The routine calculates the ball's impact velocity and impact angle.

```
Sub traject (Ap, CP, omegap, mradp, bradp, xdepp, tdepp, vdepp, thetap, betap,
gammap, alphap,
            rtsp, totalTime, finalvel, impangle)

    Dim cy, cx, xop, yop, ydepp, xcenp, ycenp, vrot, vtran, vxp, vyp, xpos, ypos,
        timep, deltat As Double
    Dim Nvrot, vly, vlx As Double
    Dim I As Integer

      ydepp = Ap * (xdepp ^ 2) + CP
      xop = xdepp + bradp * Sin(thetap)
      yop = ydepp + bradp * Cos(thetap)
      xcenp = mradp * Cos(omegap * tdepp) - (yop * Sin(omegap * tdepp) + xop *
              Cos(omegap * tdepp))
      ycenp = mradp * Sin(omegap * tdepp) + (yop * Cos(omegap * tdepp) - xop *
              Sin(omegap *



      vrot = omegap * rtsp
      vly = 2 * Ap * xdepp * vdepp
      vlx = vdepp
      vtran = Sqr(vly ^ 2 + vlx ^ 2)

    If betap < 0 Then
            betap = 3.14159 + betap
            vxp = -vrot * Cos(betap - (3.14159 / 2)) + vtran * Cos(3.14159 -
       gammap)
            vyp = -vrot * Sin(betap - (3.14159 / 2)) - vtran * Sin(3.14159 - gammap)
    Else
            vxp = -(vrot * Sin(betap) + vtran * Cos(gammap))
            vyp = vrot * Cos(betap) - vtran * Sin(gammap)
    End If
    timep = 0
    deltat = (Sqr((2 * mradp) / 9.81)) / 100
```

```
    While (rtsp < (mradp - bradp))
            timep = timep + deltat
            xpos = xcenp + vxp * (timep)
            ypos = ycenp + vyp * (timep) - .5 * 9.81 * (timep ^ 2)
            currentx = (scalewidth / 3) + xpos
            currenty = (-scaleheight / 2) + ypos
            Circle (currentx, currenty), bradp, RGB(0, 0, 255)
            rtsp = Sqr((xpos ^ 2) + (ypos ^ 2))
    Wend
    totalTime = tdepp + timep
    finalvel = Sqr(vxp ^ 2 + (vyp + 9.81 * timep) ^ 2)
    If ypos < 0 Then
        impangle = Atn(xpos / ypos)
    Else
        impangle = 3.141597 / 2 + Atn(ypos / -xpos)
    End If

    Print
    currentx = scalewidth * .1: currenty = -scaleheight * .8

End Sub
```

APPENDIX XII

Results from "Mill Simulator" for the Six Experimental Lifter Bars at a Mill Speed of 80 % Critical

Lifter 1

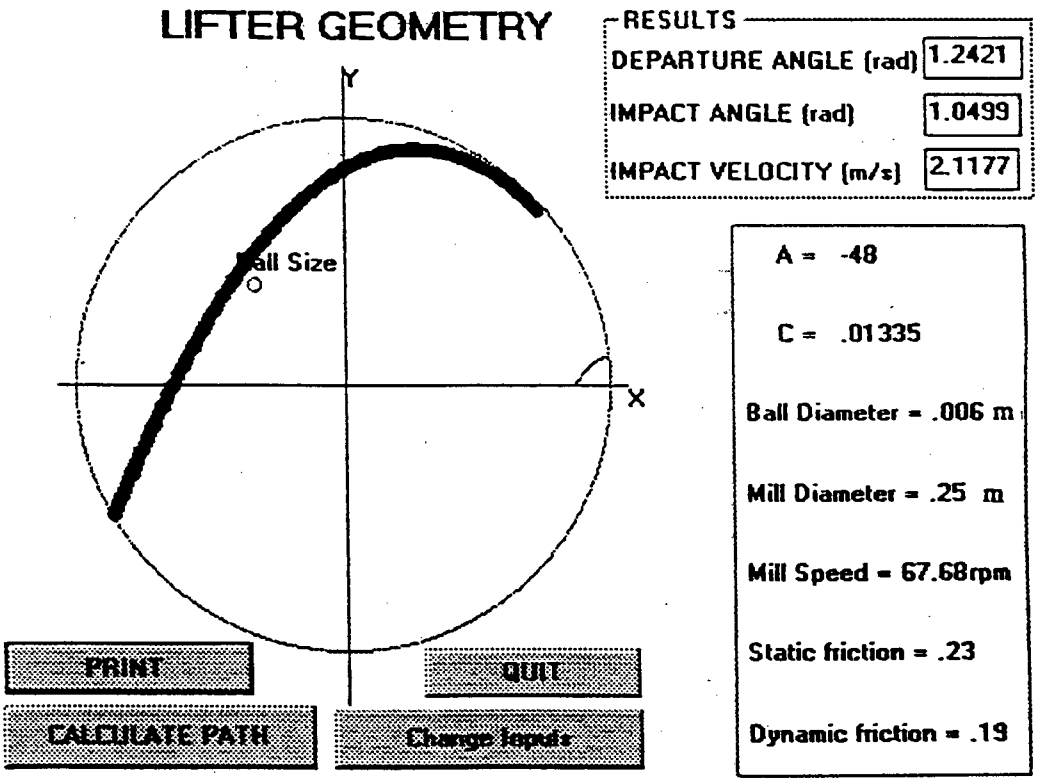

Lifter 2

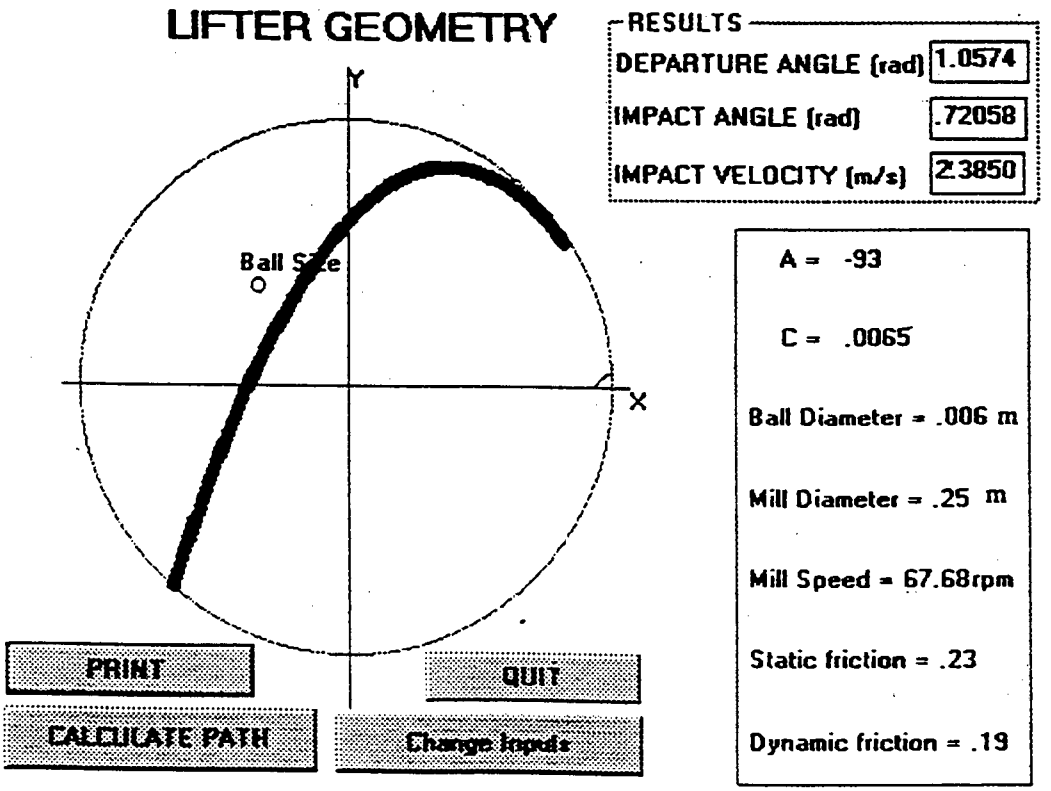

Lifter 3

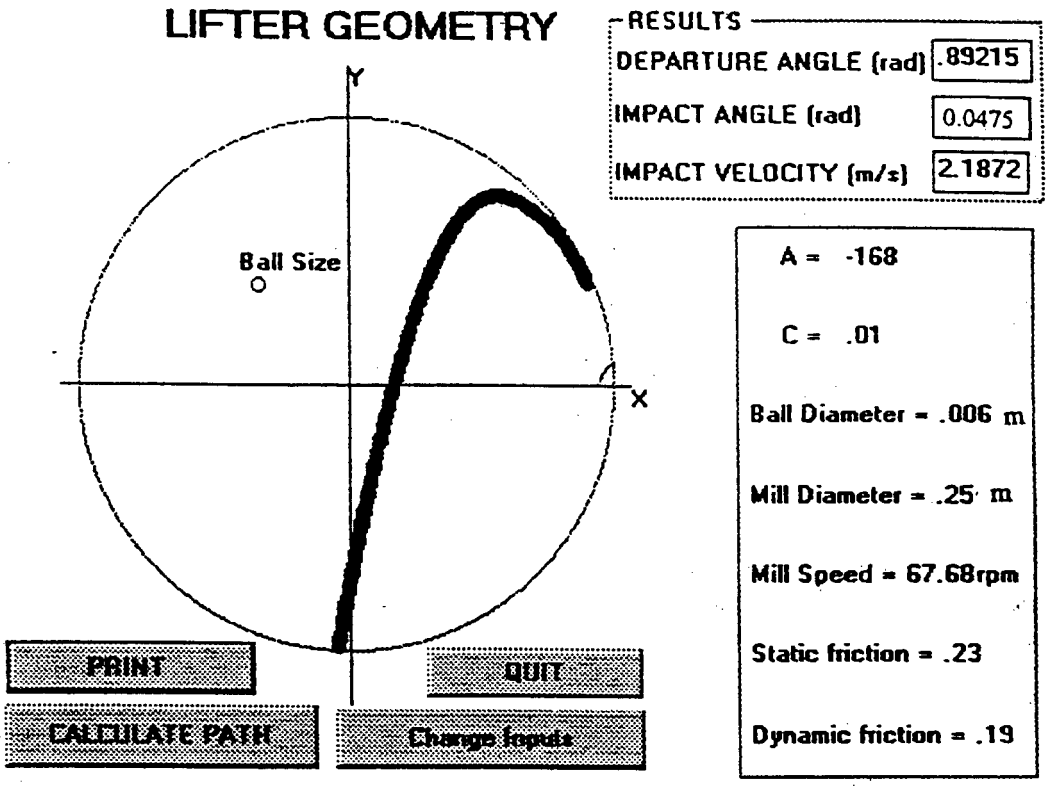

Lifter 4

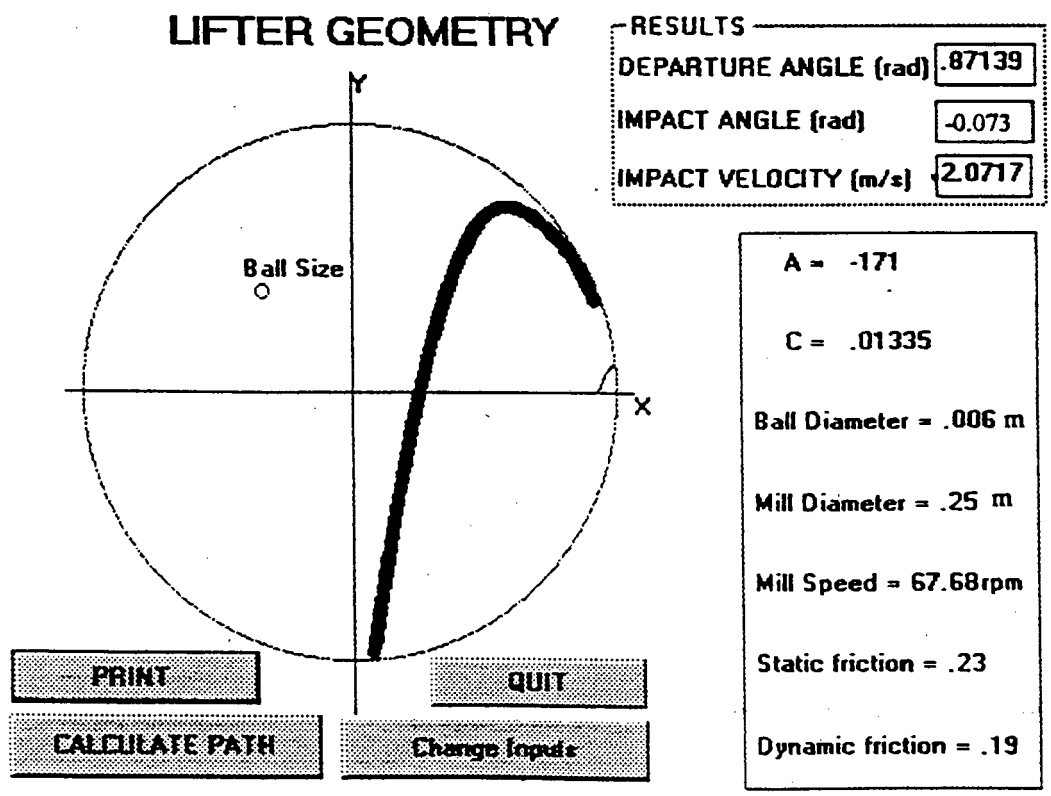

Lifter 5

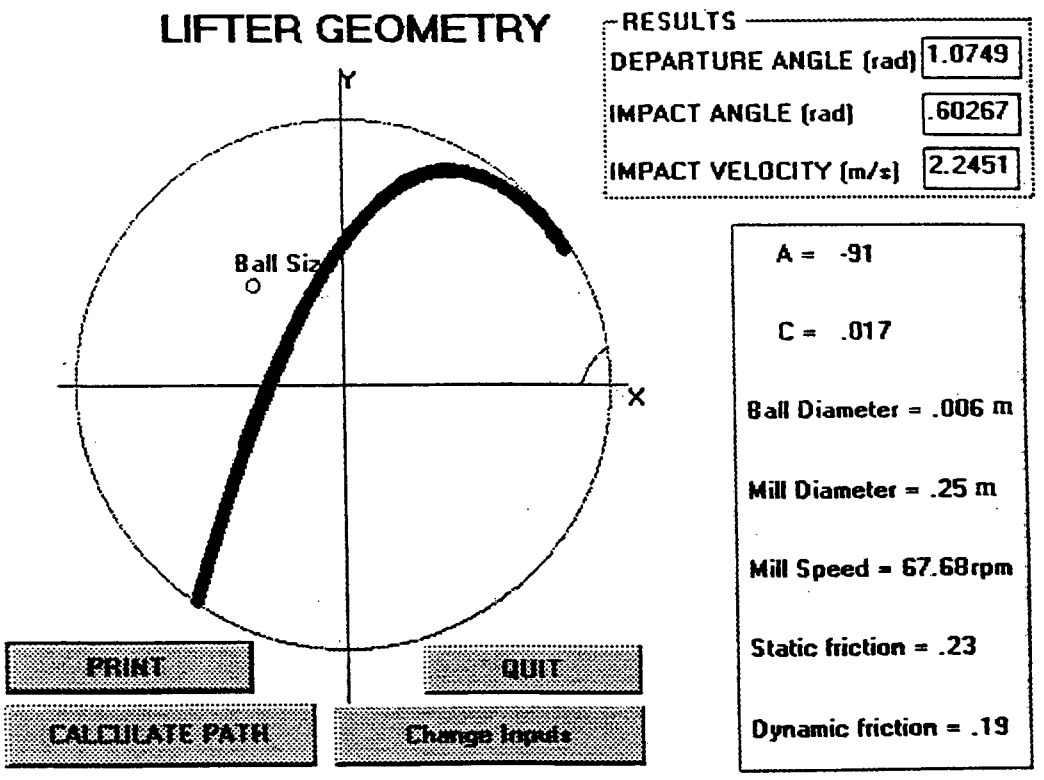

Lifter 6

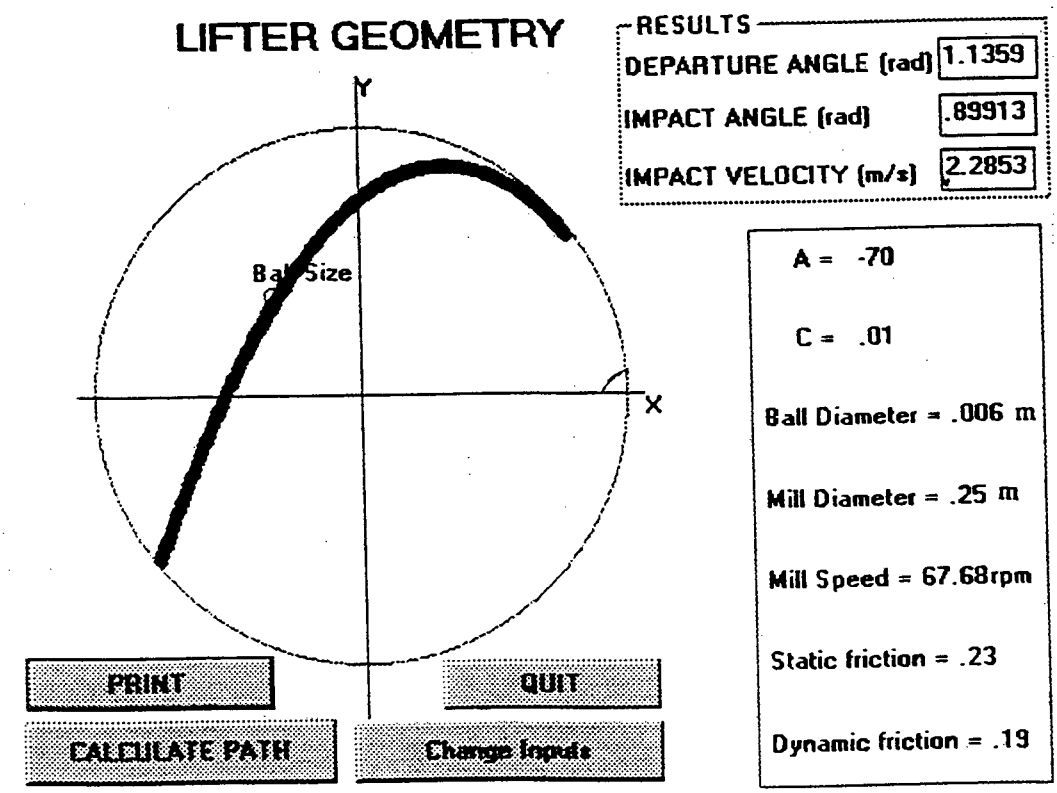

APPENDIX XIII

Determining the Effect of Lifter Height on the Charge Motion by Keeping *A* Constant and Changing C

From the definition of the parabolic lifter bar :

$$y = Ax^2 + C$$

The height will be taken to be the distance from x = 0 to where the parabola cuts the x axis. At this point y = 0 and therefore the equation can be simplified to :

$$Ax^2 + C = 0$$

The height is therefore [X(0) - X(y=0)] and this value is purely x as can be seen from figure XIII - 1.

So :

$$x = \sqrt{\frac{C}{A}}$$

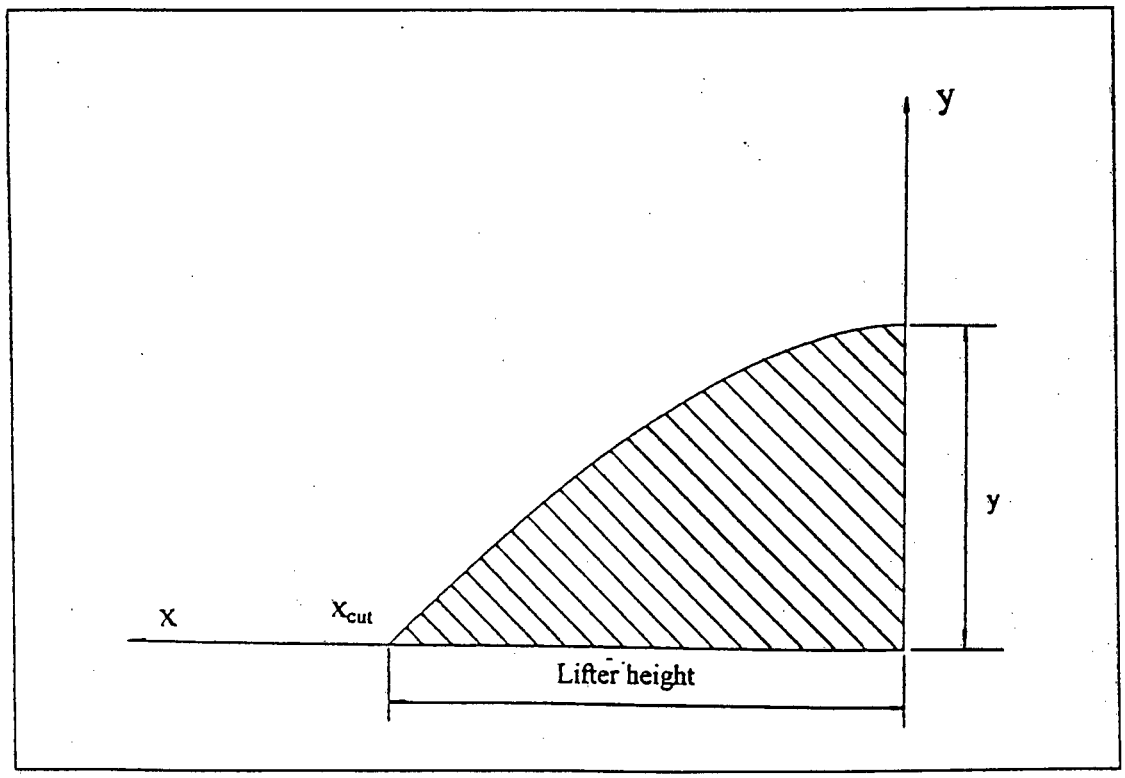

Figure XIII - 1 Determining the height of the lifter bar

APPENDIX XIV

Comparison of experimental and theoretical results

LIFTER 1

Mill Speed	THEORY		1 LAYER OF BALLS		10 % FILL		40 % FILL	
% Critical	Departure angle	Impact Angle	Departure angle	Impact Angle	Departure angle	Impact Angle	Departure angle	Impact Angle
	Degrees	Degrees	Degrees	Degrees	Degrees	Degrees	Degrees	Degrees
60 % Crit	48.41	7.51	40 to 48	-10 to 10	43 to 55	-10 to 12	65 to 83	40 to 61
70 % Crit	59.30	31.00	50 to 60	15 to 32	52 to 64	15 to 34	83 to 94	60 to 100
80 % Crit	71.16	60.16	58 to 72	45 to 65	60 to 77	46 to 69	-	-
90 % Crit	83.37	98.55	69 to 80	70 to 98	67 to 83	73 to 100	-	-
100 % Crit	90.53	150.69	76 to 92	103 to 135	80 to 100	115 to 136	-	-

LIFTER 2

Mill Speed	THEORY		1 LAYER OF BALLS		10 % FILL		40 % FILL	
% Critical	Departure angle	Impact Angle	Departure angle	Impact Angle	Departure angle	Impact Angle	Departure angle	Impact Angle
	Degrees	Degrees	Degrees	Degrees	Degrees	Degrees	Degrees	Degrees
60 % Crit	36.44	-13.75	18 to 35	-32 to -12	25 to 40	-25 to -2	48 to 58	0 to 25
70 % Crit	48.13	7.91	32 to 45	-7 to 14	37 to 48	0 to 24	58 to 74	25 to 45
80 % Crit	60.56	41.25	45 to 58	18 to 44	49 to 63	27 to 50	-	47 to 70
90 % Crit	75.97	82.91	60 to 73	49 to 86	62 to 73	55 to 87	-	90 to -
100 % Crit	90.36	144.44	74 to 87	92 to 138	75 to 85	92 to -	-	-

LIFTER 3

Mill Speed	THEORY		1 LAYER OF BALLS		10 % FILL		40 % FILL	
% Critical	Departure angle	Impact Angle	Departure angle	Impact Angle	Departure angle	Impact Angle	Departure angle	Impact Angle
	Degrees	Degrees	Degrees	Degrees	Degrees	Degrees	Degrees	Degrees
60 % Crit	24.58	-33.52	14 to 25	-45 to -30	20 to 30	-43 to -26	31 to 40	0 to 20
70 % Crit	36.44	-19.19	24 to 36	-30 to -15	30 to 40	-30 to -18	38 to 47	22 to 42
80 % Crit	51.11	2.69	35 to 50	-16 to 5	38 to 50	-14 to 11	46 to 59	45 to 60
90 % Crit	67.49	52.14	47 to 64	15 to 48	50 to 61	23 to 55	62 to 80	70 to 92
100 % Crit	87.78	126.51	65 to 82	70 to 120	60 to 74	84 to -	80 to 104	110 to -

LIFTER 4

Mill Speed	THEORY		1 LAYER OF BALLS		10 % FILL		40 % FILL	
% Critical	Departure angle	Impact Angle	Departure angle	Impact Angle	Departure angle	Impact Angle	Departure angle	Impact Angle
	Degrees	Degrees	Degrees	Degrees	Degrees	Degrees	Degrees	Degrees
60 % Crit	23.07	-39.94	13 to 23	-50 to -35	20 to 30	-45 to -30	29 to 38	-2 to 19
70 % Crit	35.12	-25.44	24 to 34	-37 to -20	30 to 40	-34 to -20	39 to 46	22 to 38
80 % Crit	49.96	-4.15	36 to 50	-20 to 0	40 to 50	-18 to 10	46 to 55	38 to 55
90 % Crit	66.69	46.75	45 to 63	10 to 45	50 to 61	20 to 50	57 to 73	58 to 73
100 % Crit	87.66	121.47	59 to 78	62 to 110	62 to 73	76 to -	74 to 92	94 to -

LIFTER 5

Mill Speed	THEORY		1 LAYER OF BALLS		10 % FILL		40 % FILL	
% Critical	Departure angle	Impact Angle	Departure angle	Impact Angle	Departure angle	Impact Angle	Departure angle	Impact Angle
	Degrees	Degrees	Degrees	Degrees	Degrees	Degrees	Degrees	Degrees
60 % Crit	35.52	-31.51	25 to 34	-40 to -30	30 to 40	-38 to -18	48 to 57	20 to 50
70 % Crit	48.36	-0.57	35 to 46	-20 to 5	39 to 51	-15 to 8	60 to 75	50 to 75
80 % Crit	61.31	34.38	48 to 59	15 to 39	52 to 62	16 to 42	-	80 to 105
90 % Crit	76.49	78.90	57 to 73	48 to 80	60 to 72	53 to 86	-	-
100 % Crit	89.38	144.39	69 to 84	90 to 130	71 to 85	95 to -	-	-

LIFTER 6

Mill Speed	THEORY		1 LAYER OF BALLS		10 % FILL		40 % FILL	
% Critical	Departure angle	Impact Angle	Departure angle	Impact Angle	Departure angle	Impact Angle	Departure angle	Impact Angle
	Degrees	Degrees	Degrees	Degrees	Degrees	Degrees	Degrees	Degrees
60 % Crit	42.23	-7.73	27 to 38	-20 to -7	35 to 47	-23 to 3	60 to 73	28 - 53
70 % Crit	53.00	19.88	37 to 51	0 to 17	46 to 60	5 to 25	72 to 84	57 to 83
80 % Crit	65.08	51.57	52 to 63	32 to 60	57 to 70	29 to 55	-	-
90 % Crit	79.41	90.36	61 to 75	68 to 95	65 to 77	70 to 97	-	-
100 % Crit	89.95	148.40	70 to 87	100 to 140	77 to 90	110 -	-	-

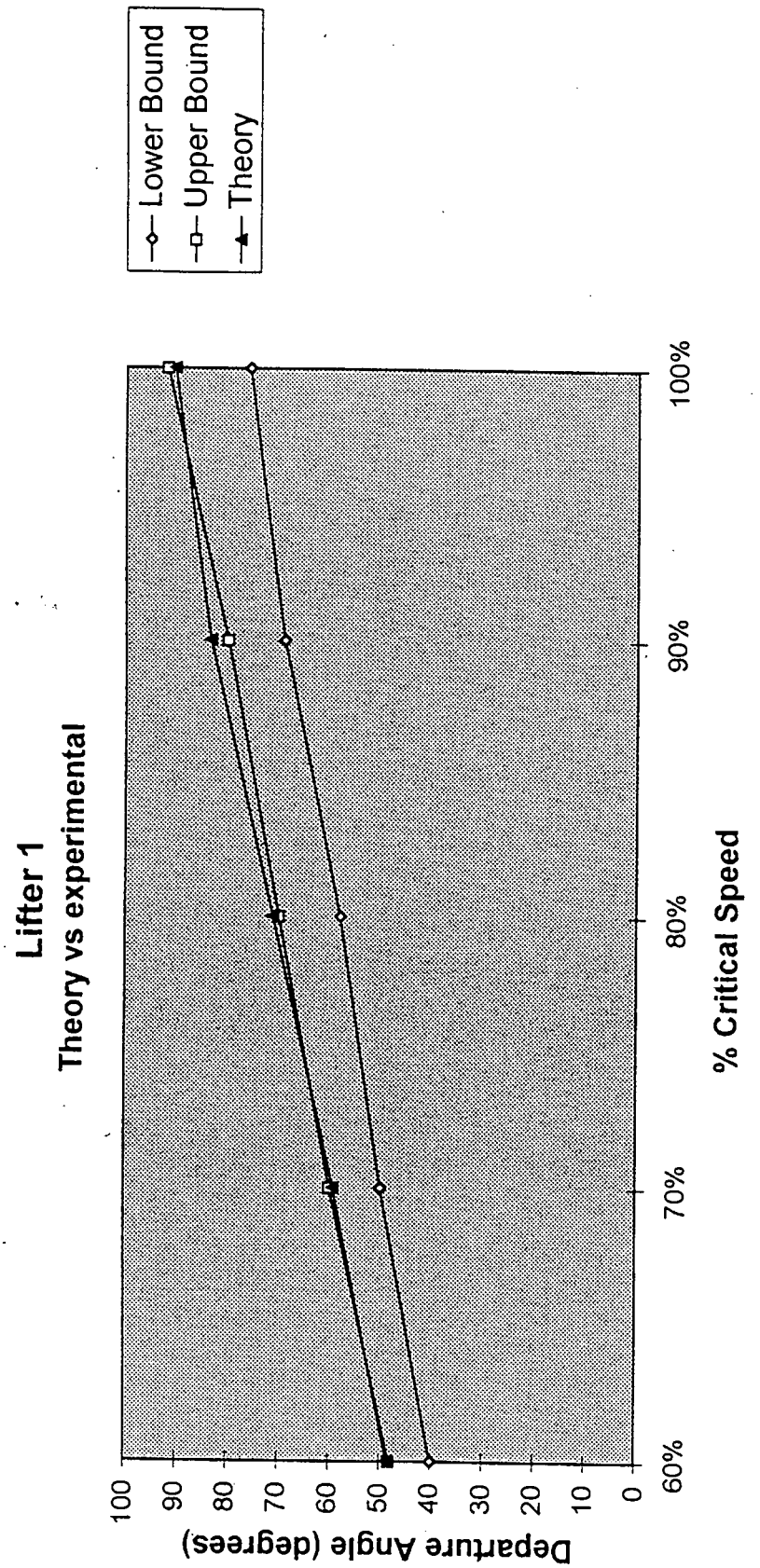
Lower Bound
Upper Bound
Theory
Lifter 1
Theory vs experimental
Departure Angle (degrees)
100
90
80
70
60
50
40
30
20
10
0
60%
70%
80%
90%
100%
% Critical Speed

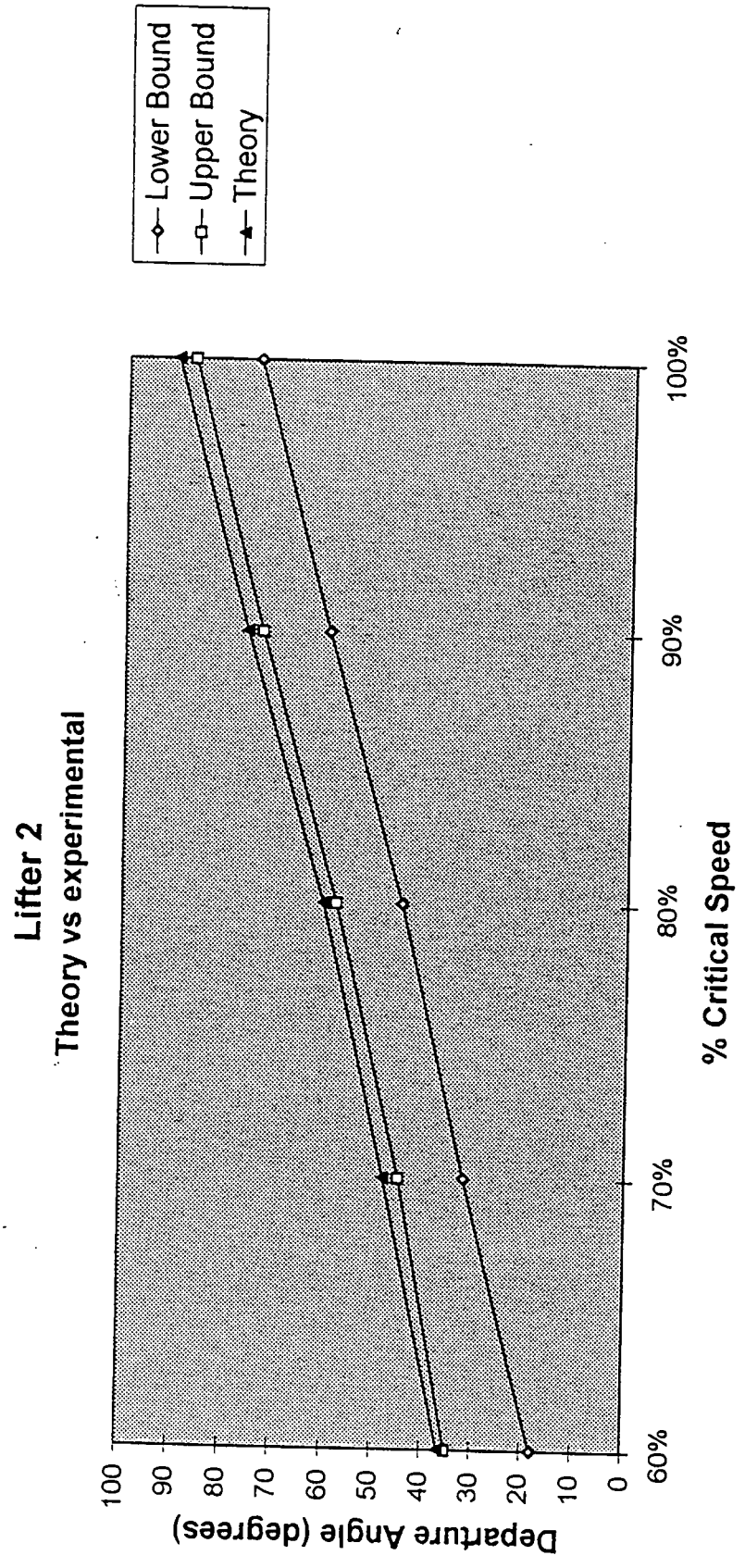
Lower Bound
Upper Bound
Theory
Lifter 2
Theory vs experimental
Departure Angle (degrees)
100
90
80
70
60
50
40
30
20
10
0
60%
70%
80%
90%
100%
% Critical Speed

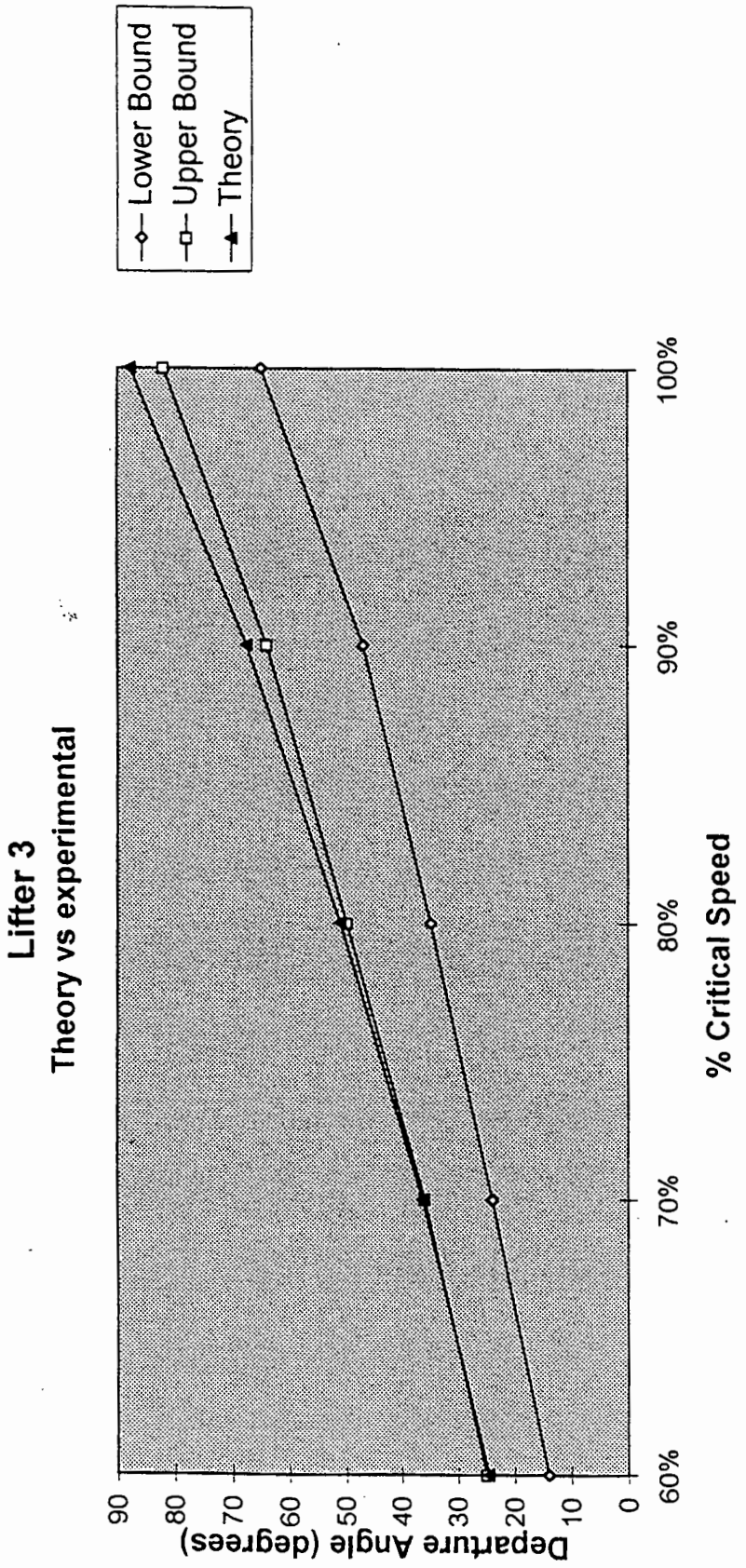
Lower Bound
Upper Bound
Theory
Lifter 3
Theory vs experimental
Departure Angle (degrees)
0
10
20
30
40
50
60
70
80
90
60%
70%
80%
90%
100%
% Critical Speed

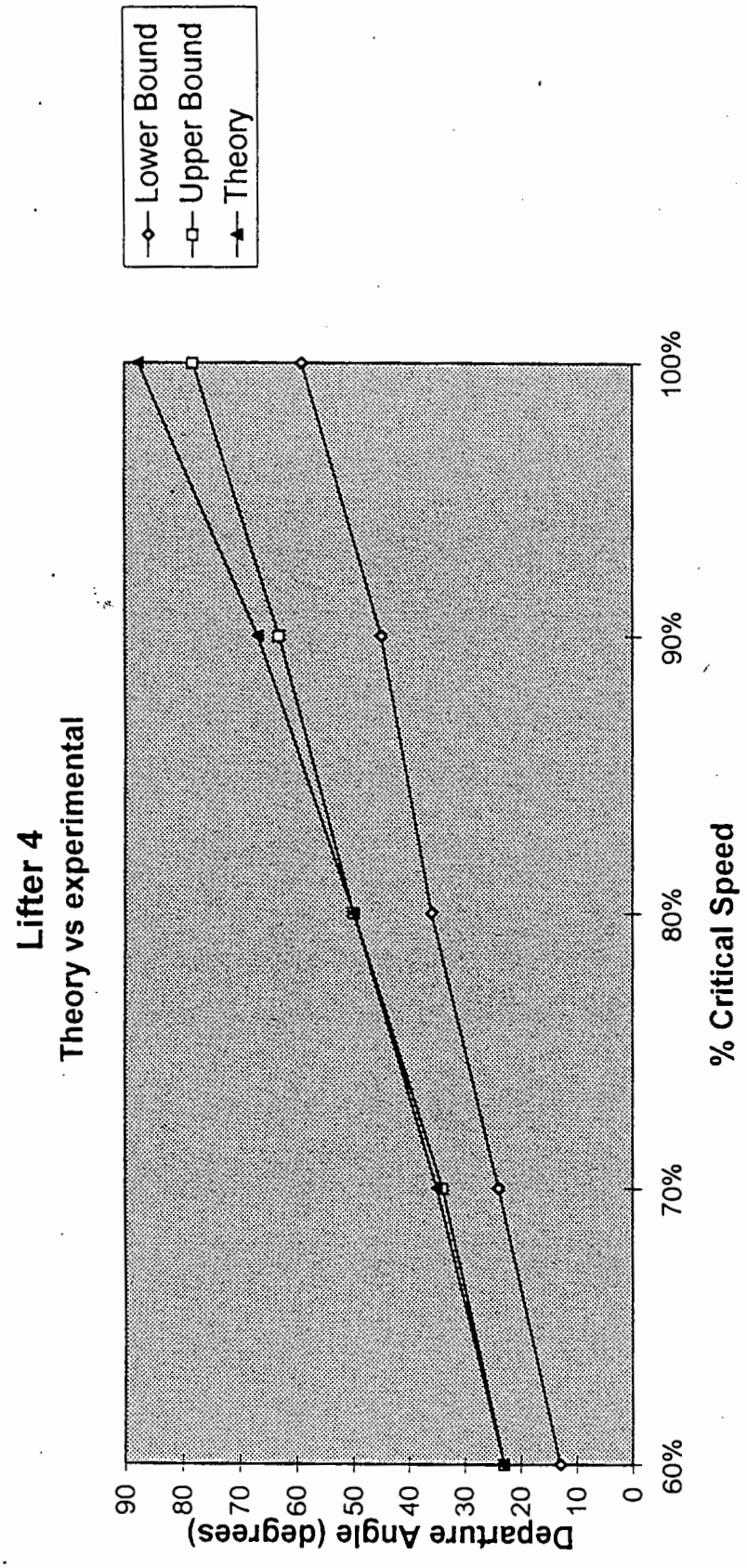
Lower Bound
Upper Bound
Theory
Lifter 4
Theory vs experimental
Departure Angle (degrees)
0
10
20
30
40
50
60
70
80
90
60%
70%
80%
90%
100%
% Critical Speed

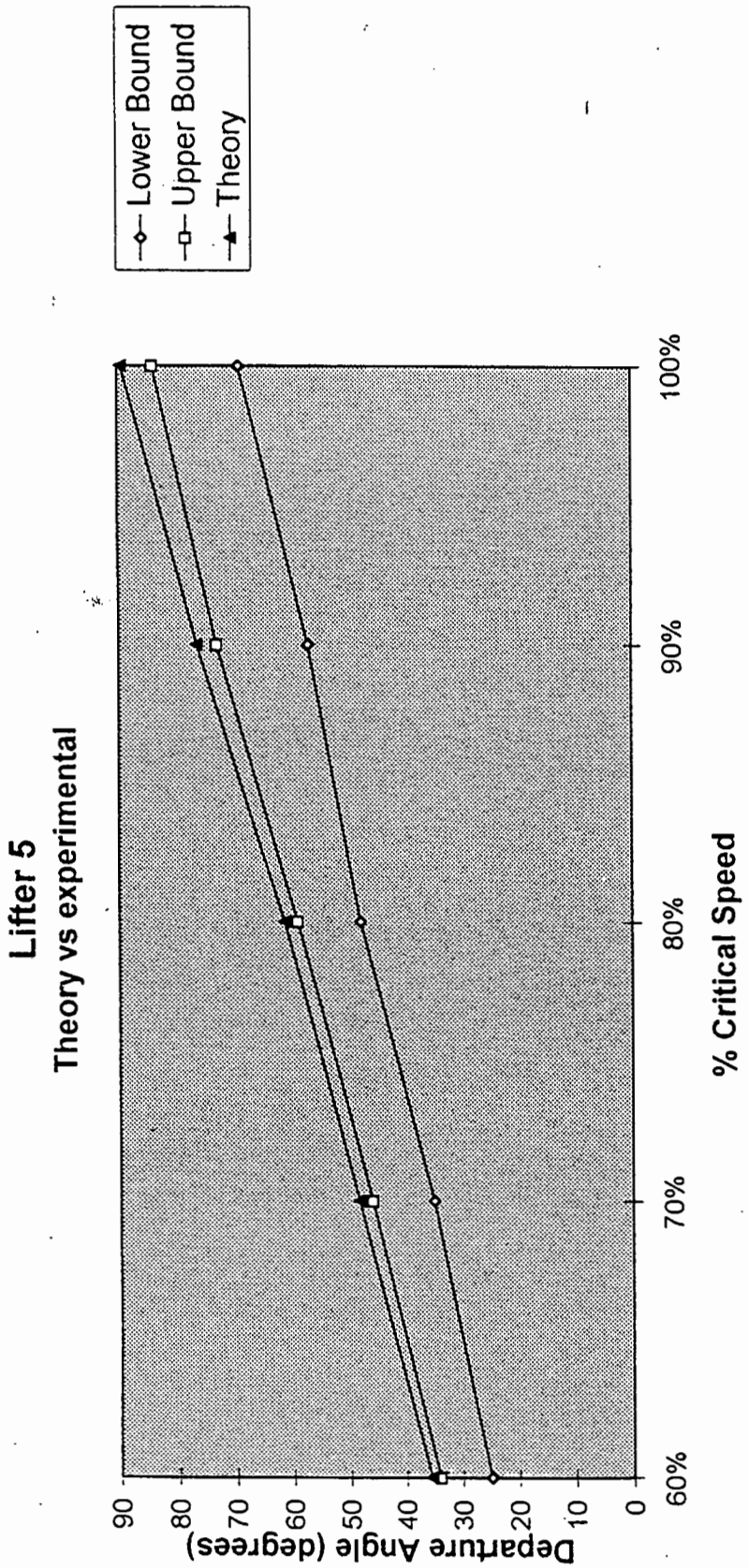
Lower Bound
Upper Bound
Theory
Lifter 5
Theory vs experimental
Departure Angle (degrees)
0
10
20
30
40
50
60
70
80
90
60%
70%
80%
90%
100%
% Critical Speed

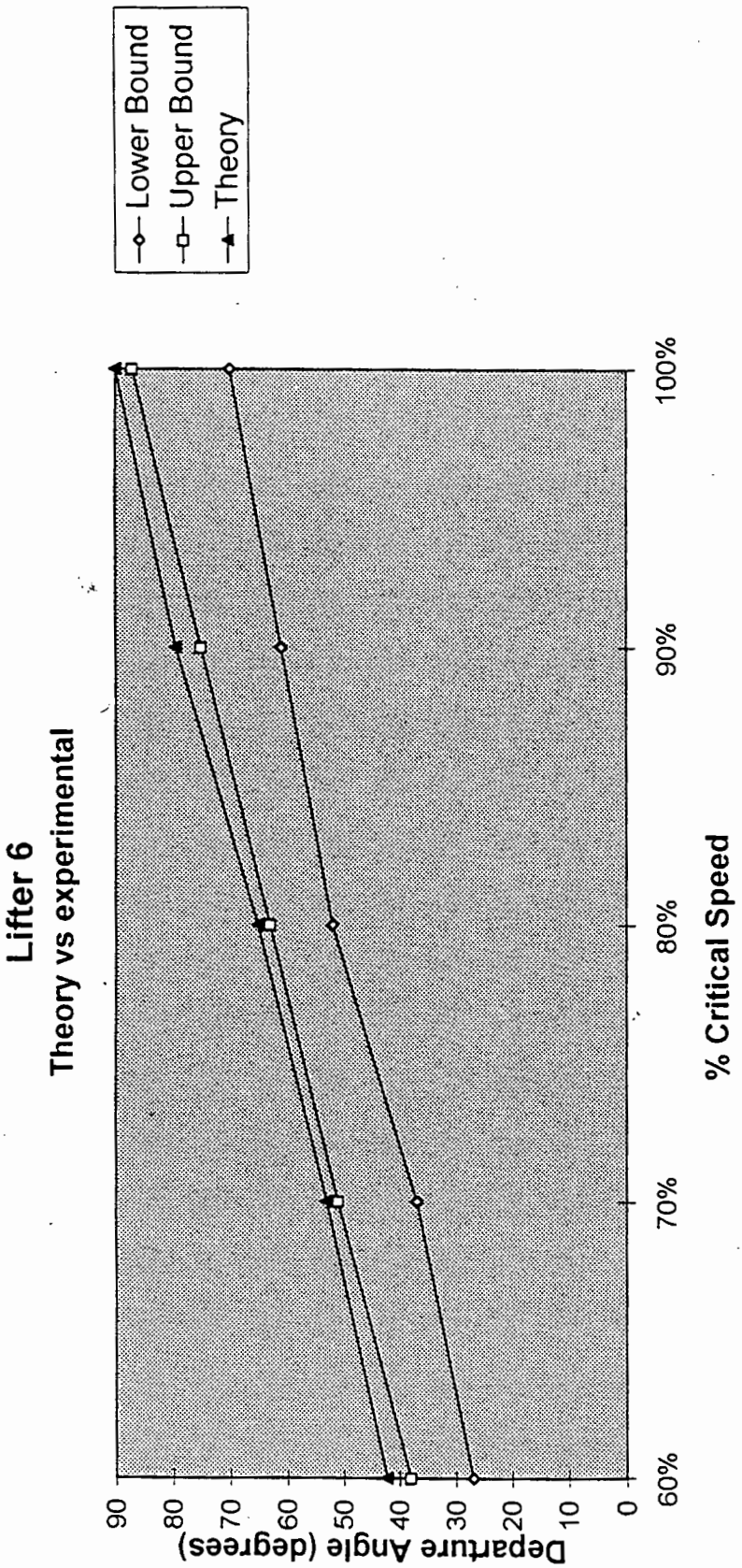
Lower Bound
Upper Bound
Theory
Lifter 6
Theory vs experimental
Departure Angle (degrees)
0
10
20
30
40
50
60
70
80
90
60%
70%
80%
90%
100%
% Critical Speed

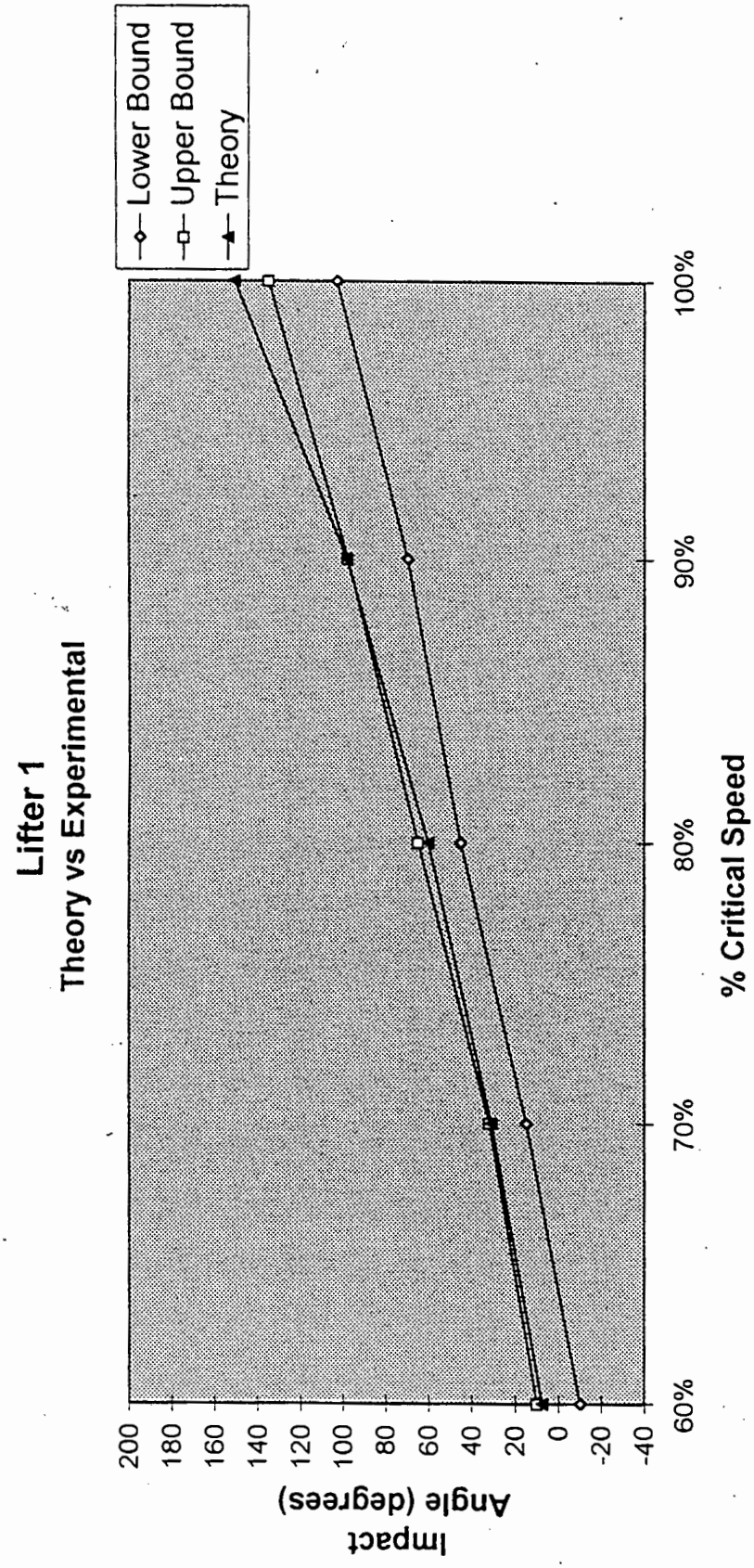
Lower Bound
Upper Bound
Theory
Lifter 1
Theory vs Experimental
Impact Angle (degrees)
200
180
160
140
120
100
80
60
40
20
0
-20
-40
60%
70%
80%
90%
100%
% Critical Speed

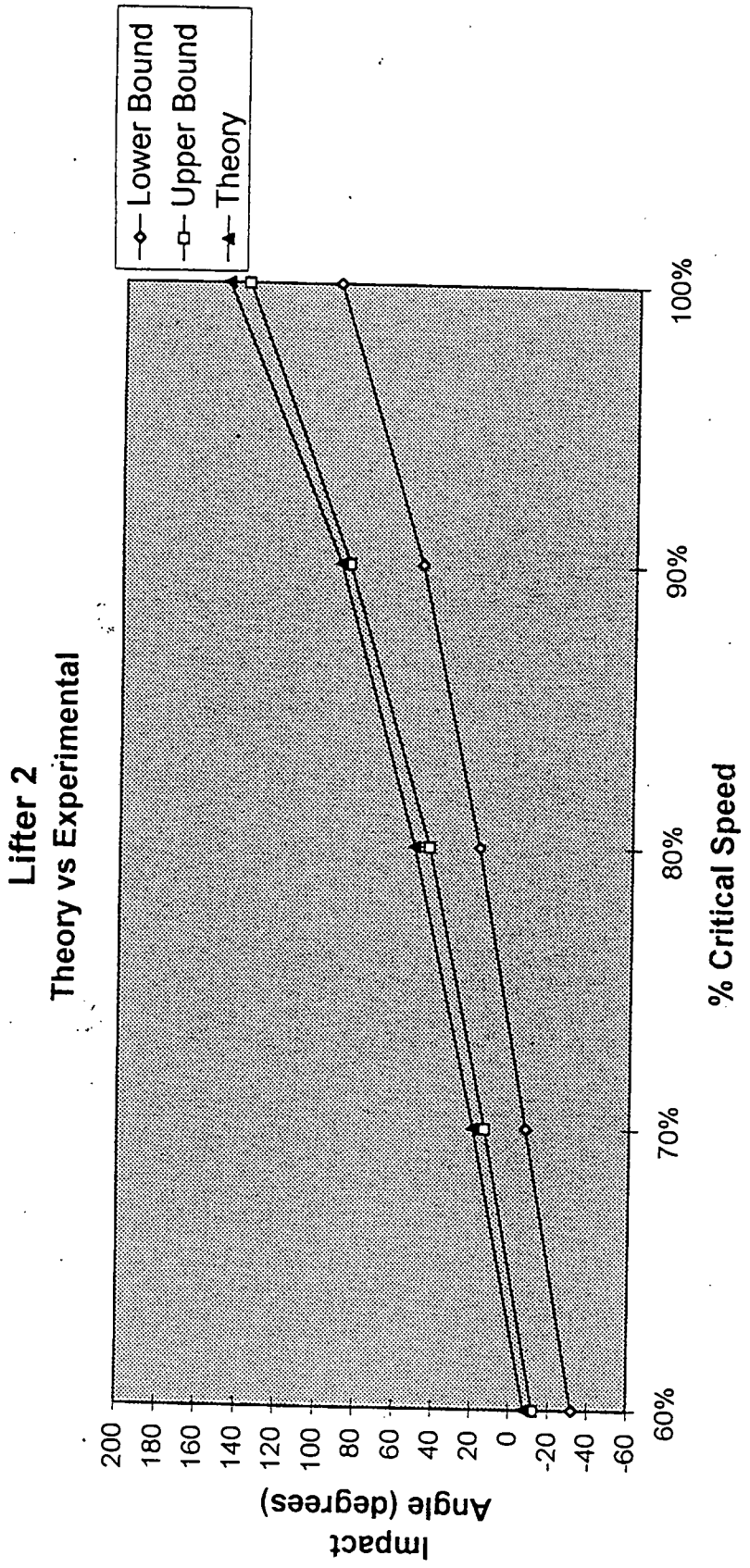
Lower Bound
Upper Bound
Theory
Lifter 2
Theory vs Experimental
Impact Angle (degrees)
200
180
160
140
120
100
80
60
40
20
0
-20
-40
-60
60%
70%
80%
90%
100%
% Critical Speed

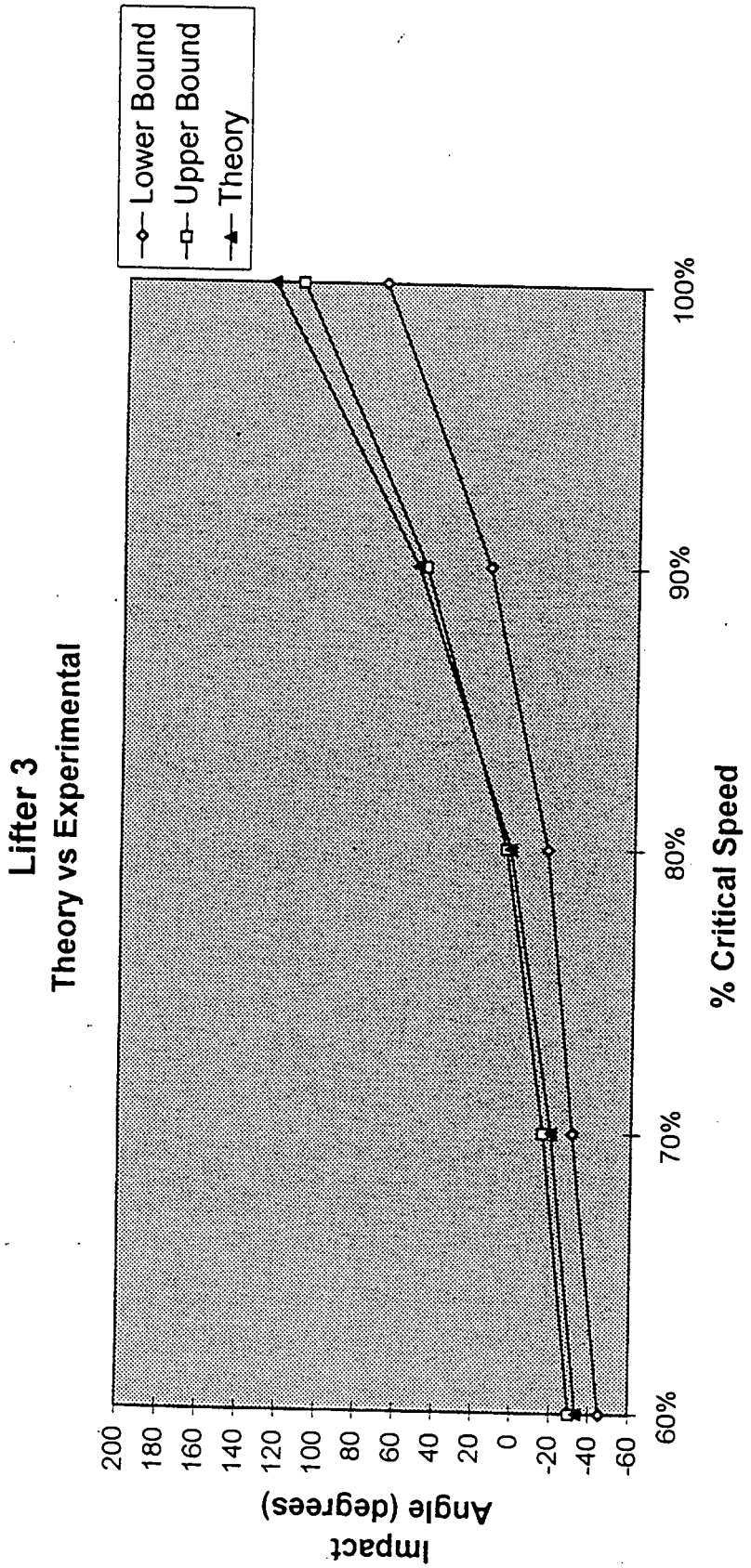
Lower Bound
Upper Bound
Theory
Lifter 3
Theory vs Experimental
Impact Angle (degrees)
200
180
160
140
120
100
80
60
40
20
0
-20
-40
-60
60%
70%
80%
90%
100%
% Critical Speed

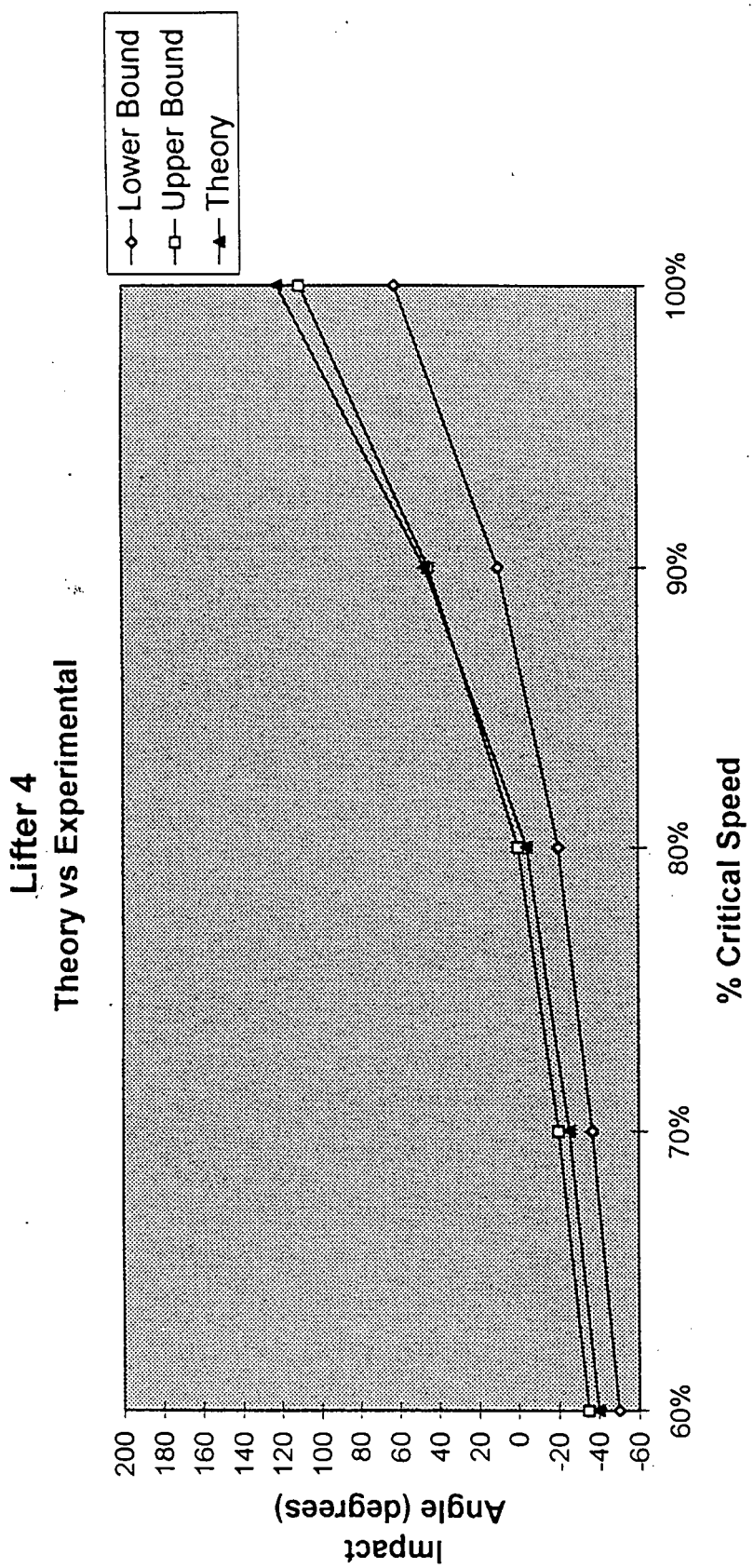
Lifter 4
Theory vs Experimental
Lower Bound
Upper Bound
Theory
Impact Angle (degrees)
200
180
160
140
120
100
80
60
40
20
0
-20
-40
-60
60%
70%
80%
90%
100%
% Critical Speed

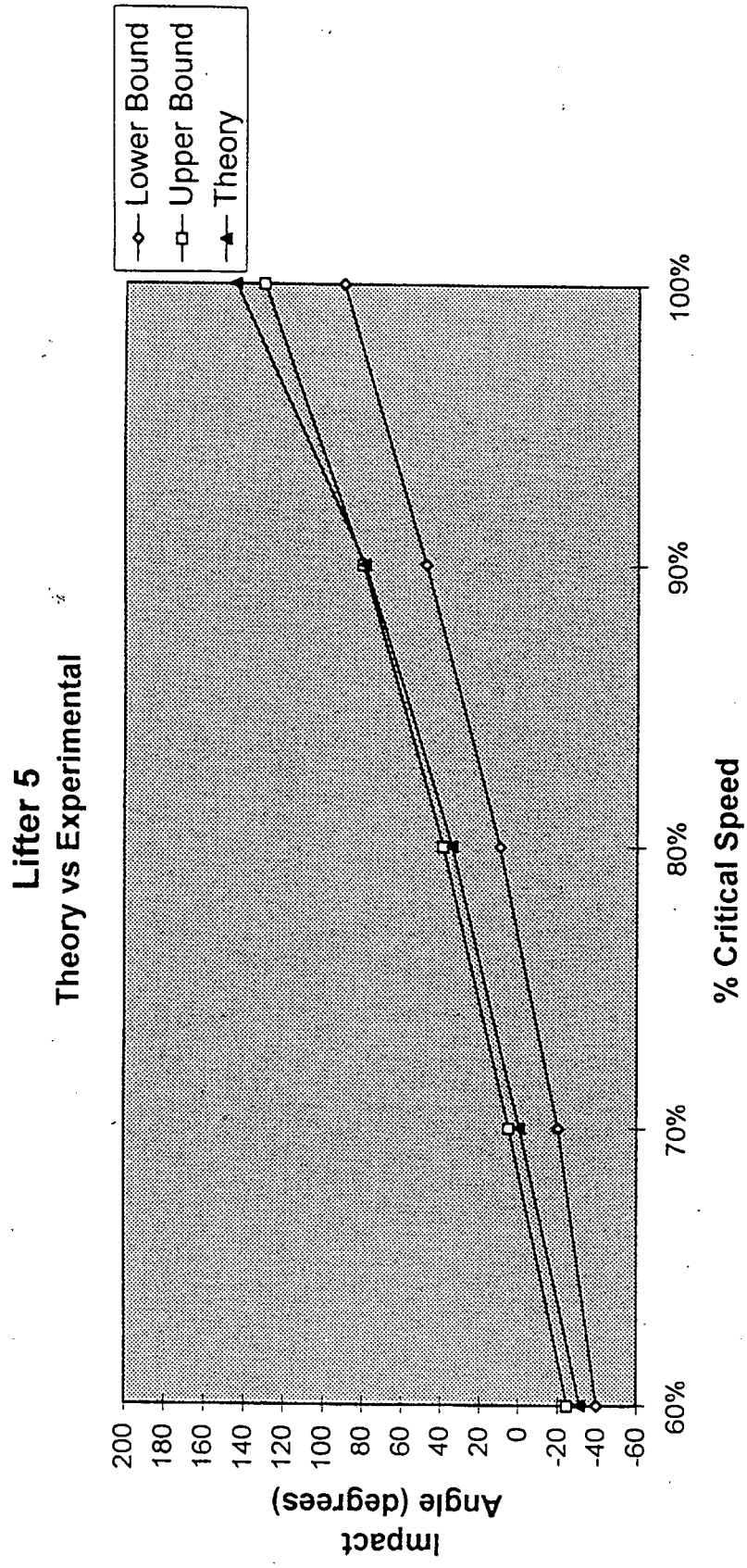
Lower Bound
Upper Bound
Theory
Lifter 5
Theory vs Experimental
Impact Angle (degrees)
200
180
160
140
120
100
80
60
40
20
0
-20
-40
-60
60%
70%
80%
90%
100%
% Critical Speed

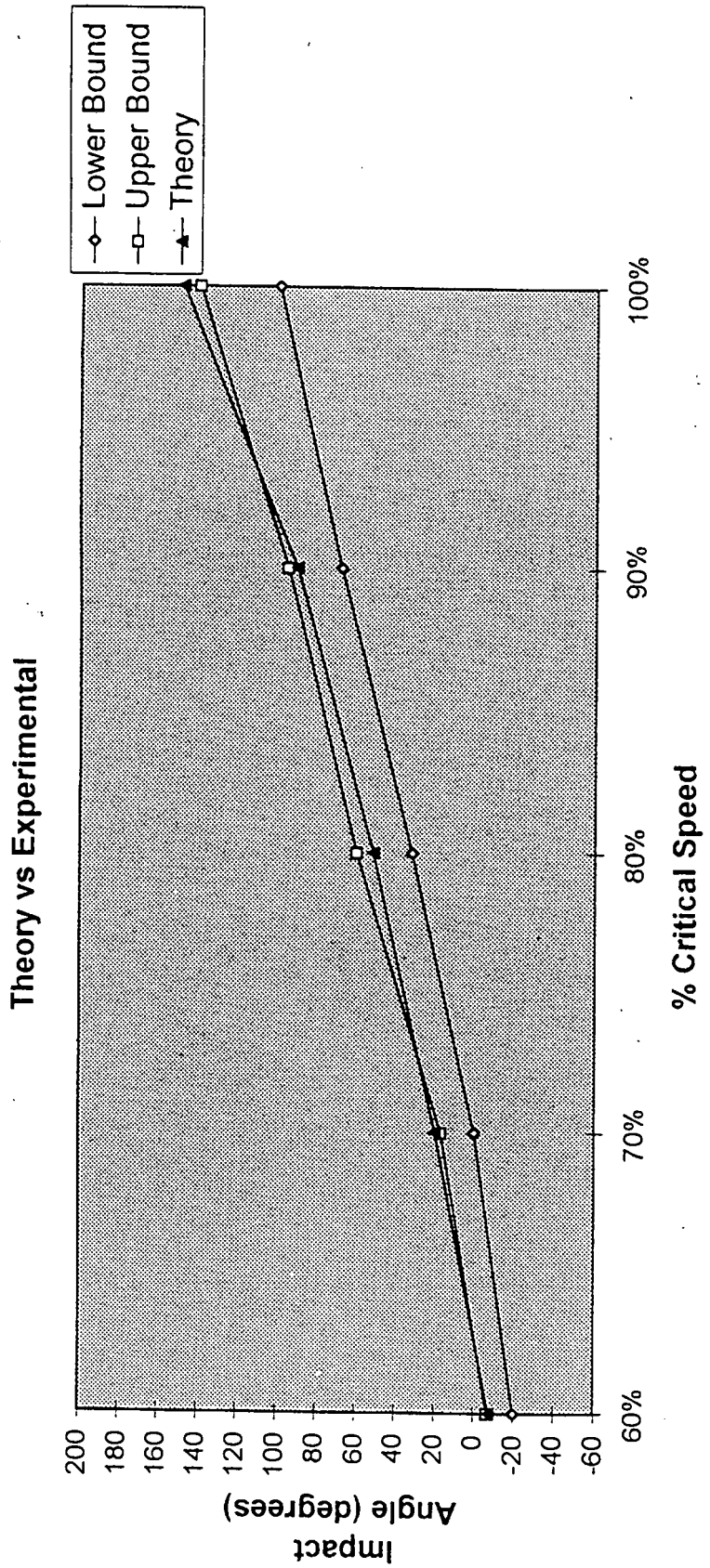
Lifter 6
Theory vs Experimental
Lower Bound
Upper Bound
Theory
Impact Angle (degrees)
200
180
160
140
120
100
80
60
40
20
0
-20
-40
-60
60%
70%
80%
90%
100%
% Critical Speed